Ultrafast nonlinear spectroscopy and control of semiconductor nanostructures: From ensembles to individual quantum states

Wolfgang Langbein

School of Physics and Astronomy, Cardiff University

- Linear and non-linear optical spectroscopy
- III-V seminconductors and nanostructures, excitonic properties, disorder
- Transient coherent spectroscopy & four-wave mixing, photon echo
- Excitons, Biexcitons and dephasing in quantum wells, wires and dots
- Rabi-oscillations in quantum dot ensembles
- Four-wave mixing of individual quantum states:
    - Photon echo formation
    - Rabi oscillations & coherent control
    - Two-dimensional four-wave mixing
    - Coherent coupling between states

Optical spectroscopy

We use electromagnetic radiation to investigate semiconductor structures

classical field of a light wave

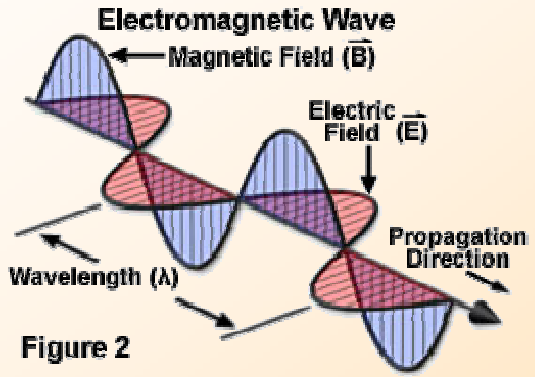

Figure 2

amplitude E_0,
wavelength λ, frequency υ
direction **k**
refractive index n
light velocity c

$$\lambda = \frac{c}{n\upsilon}$$

http://micro.magnet.fsu.edu/primer/lightandcolor/electromagintro.html

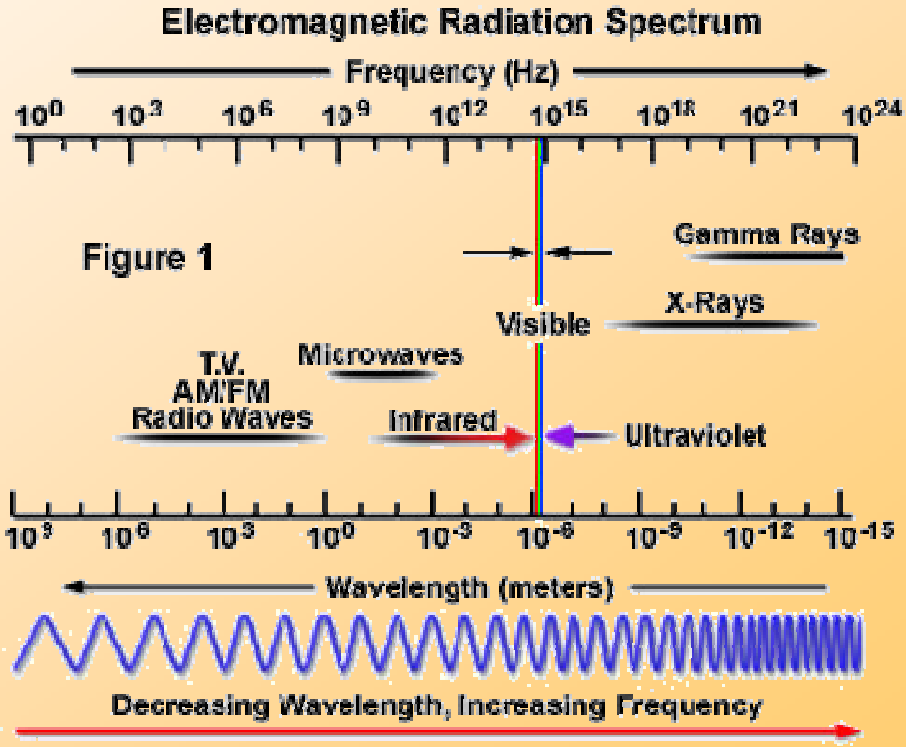

Figure 1

thermal energy kT
a room temperature

W.Langbein, Ultrafast nonlinear spectroscopy and control of semiconductor nanostructures

Linear and non-linear spectroscopy

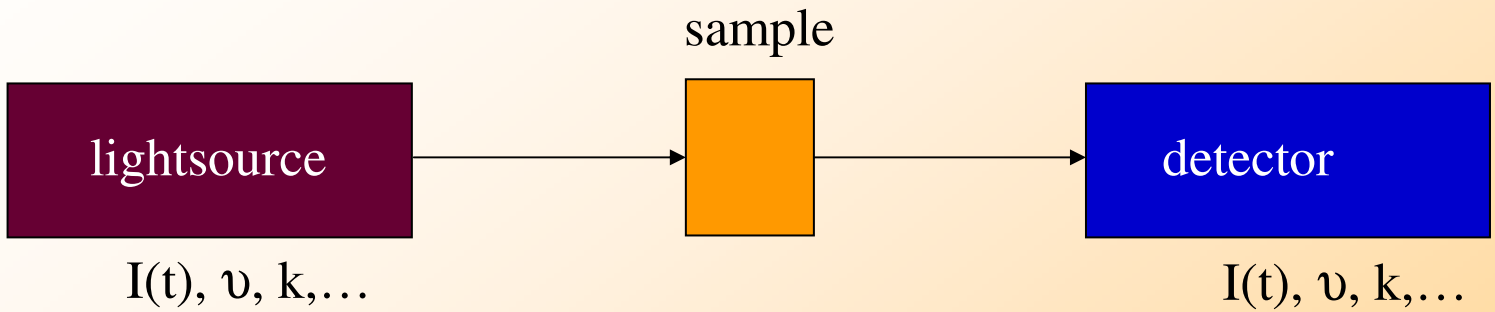

Linear Optics: detected field is proportional to the exciting field,
i.e the material polarization is $\vec{P} = \vec{\vec{\chi}}\vec{E}$

Non-linear Optics: detected field is not proportional to the exciting field.
The material polarization can be developed in orders of the exciting field E

$$\vec{P} = \vec{\vec{\chi}}\vec{E} + \vec{\vec{\chi}}^{(2)}\vec{E}^2 + \vec{\vec{\chi}}^{(3)}\vec{E}^3 + \ldots$$

Linear and non-linear optical spectroscopy

Non-linear optics: the excitation field is changing the material properties

⇒ material processing (laser-welding, laser-evaporation)
⇒ usage of light not only to measure, but also to modify the sample: very specific preparation possible

⇒ micrometer spatial resolution, femtoseconds temporal, Hz frequency (the best time standard uses nonlinear optical spectroscopy)

⇒ typical experimental configuration: pump-probe technique with one or more pump beams and one probe beam

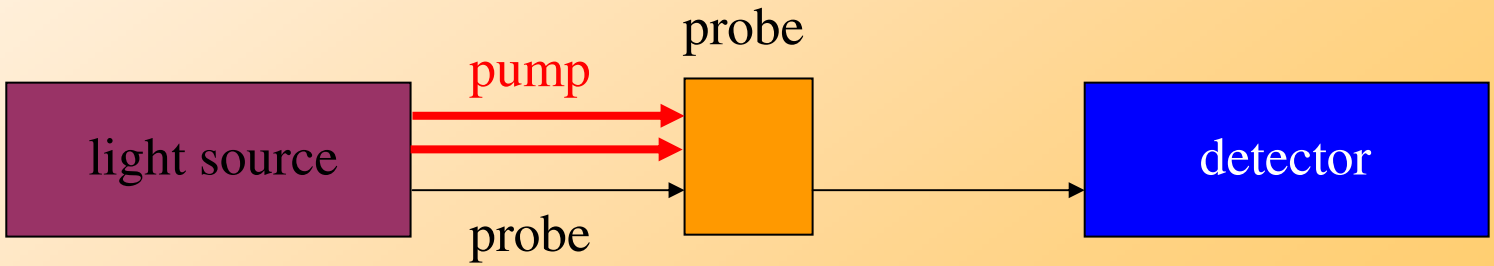

III-V Semiconductors

s-shell(2) | d-shell (10) | p-shell (6)

Group	1	2		3	4	5	6	7	8	9	10	11	12	13	14	15	16	17	18
Period														III		V			
1	1 H																		2 He
2	3 Li	4 Be												5 B	6 C	7 N	8 O	9 F	10 Ne
3	11 Na	12 Mg												13 Al	14 Si	15 P	16 S	17 Cl	18 Ar
4	19 K	20 Ca		21 Sc	22 Ti	23 V	24 Cr	25 Mn	26 Fe	27 Co	28 Ni	29 Cu	30 Zn	31 Ga	32 Ge	33 As	34 Se	35 Br	36 Kr
5	37 Rb	38 Sr		39 Y	40 Zr	41 Nb	42 Mo	43 Tc	44 Ru	45 Rh	46 Pd	47 Ag	48 Cd	49 In	50 Sn	51 Sb	52 Te	53 I	54 Xe
6	55 Cs	56 Ba	*	71 Lu	72 Hf	73 Ta	74 W	75 Re	76 Os	77 Ir	78 Pt	79 Au	80 Hg	81 Tl	82 Pb	83 Bi	84 Po	85 At	86 Rn
7	87 Fr	88 Ra	**	103 Lr	104 Rf	105 Db	106 Sg	107 Bh	108 Hs	109 Mt	110 Uun	111 Uuu	112 Uub	113 Uut	114 Uuq	115 Uup	116 Uuh	117 Uus	118 Uuo

Elements of Group III and V
i.e. 3 or 5 Electrons in the lowest not fully occupied s p shell

$[Ar].3d^{10}.4s^2.4p^1$ $[Ar].3d^{10}.4s^2.4p^3$

III - V Semiconductor (3+5=8, filling of a shell)

GaAs

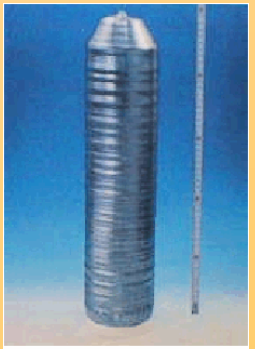

4" LEC grown crystal
(480 mm length)

others: In,Ga,Al - Sb,As,P,N

W.Langbein, Ultrafast nonlinear spectroscopy and control of semiconductor nanostructures

Zincblende type crystals: chemical binding

Topmost atomic orbitals

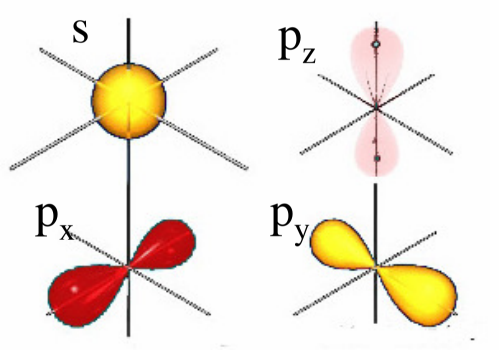

sp-3 Hybridization gives binding geometry: tetraedric

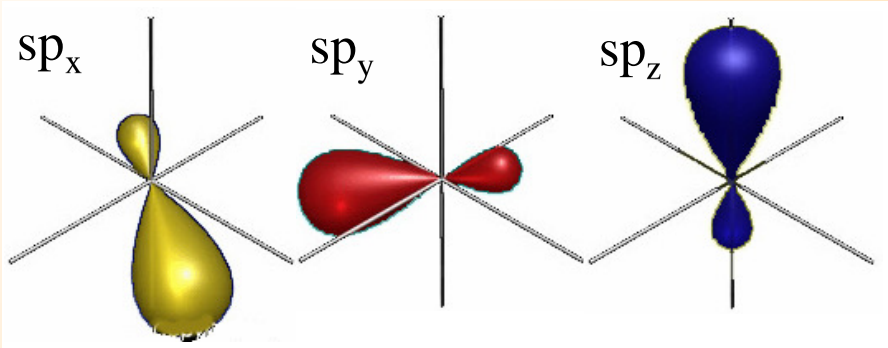

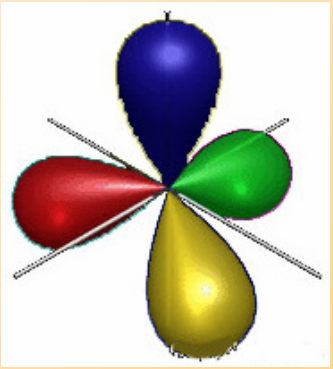

periodic arrangement of atoms Gallium : s^2p^1 Arsen : s^2p^3

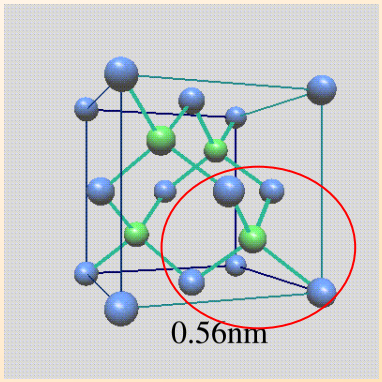

unit cell of GaAs

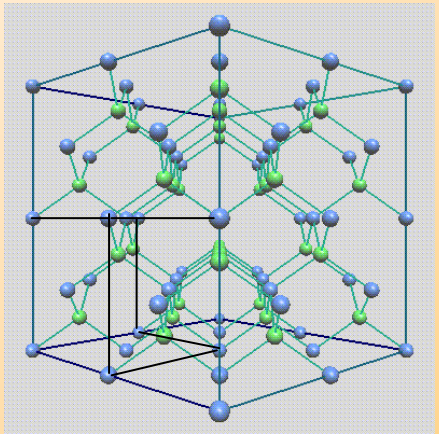

atomic levels -> energy bands

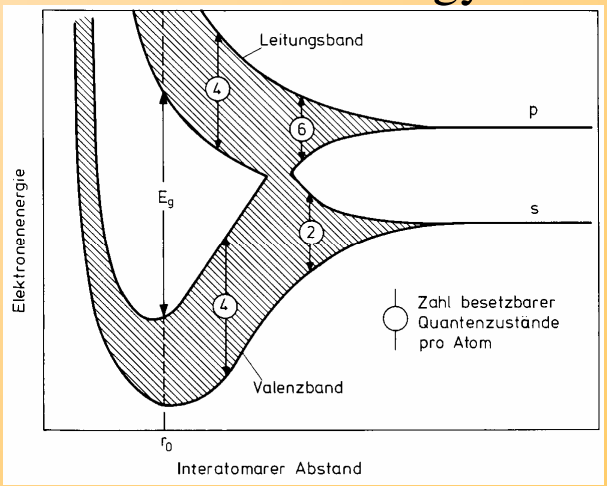

Semiconductor band structure

At **maximum / minimum** of energy bands:
Dispersion is parabolic, like for a particle with mass

electrons in the (otherwise empty) conduction band: positive mass

missing electrons (holes) in the (otherwise full) valence band: positive mass

Band gap between filled and empty states
no electronic excitations with small energy are possible
No electric conductivity

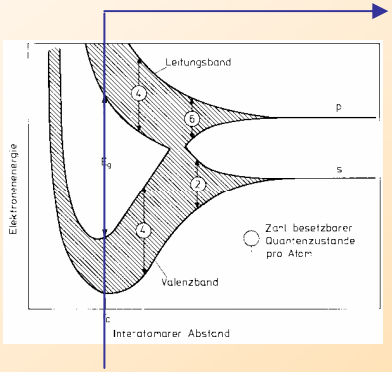

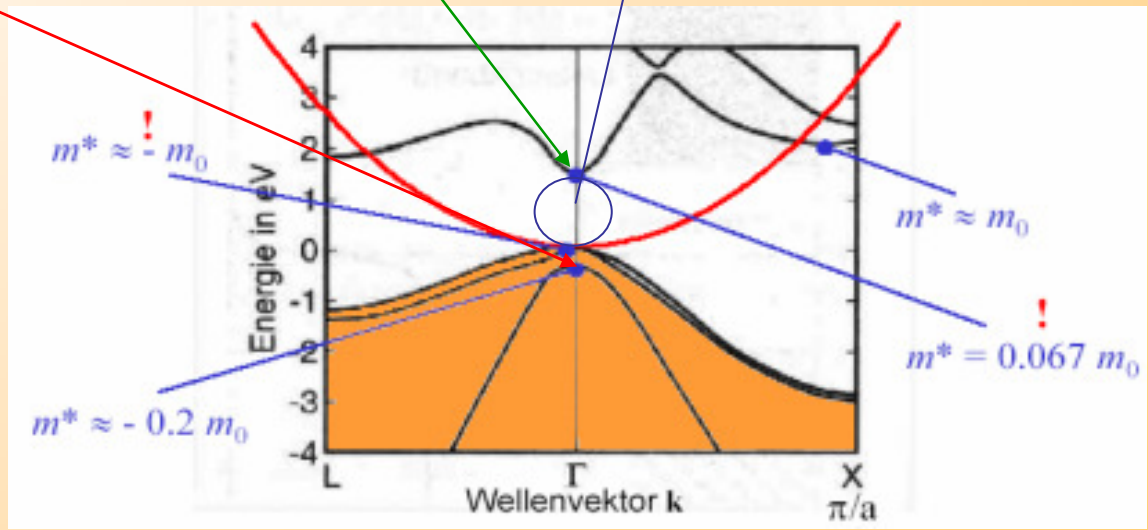

MBE growth of thin semiconductor layers

Molecular beam epitaxy:

Evaporation of element sources onto a heated substrate in ultrahigh vacuum (pressure $<10^{-13}$ atmospheres, the atom mean free path is more than a meter)

Control of the layer thickness to the lattice constant, (0.3nm)

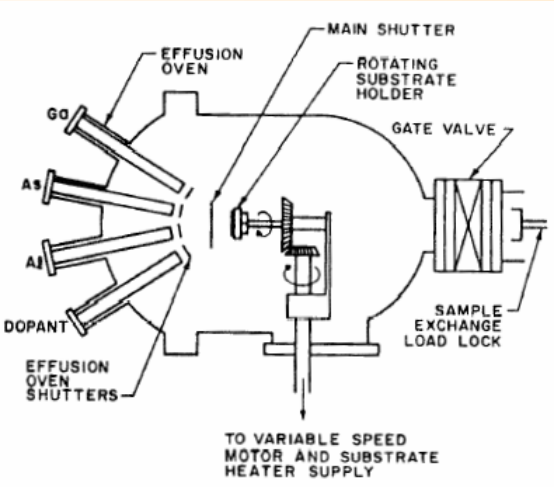

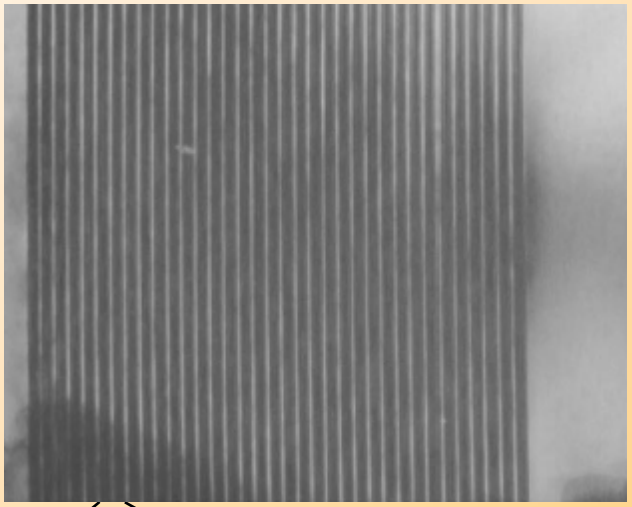

Transmission electron microscopy

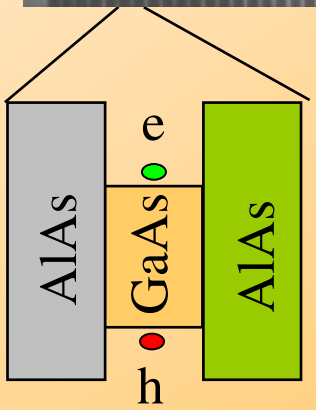

Conduction band edge

Band gap

Valence band edge

Interband transitions and excitons

Coulomb attraction between electron and hole:
Formation of a bound state (like Hydrogen atom)

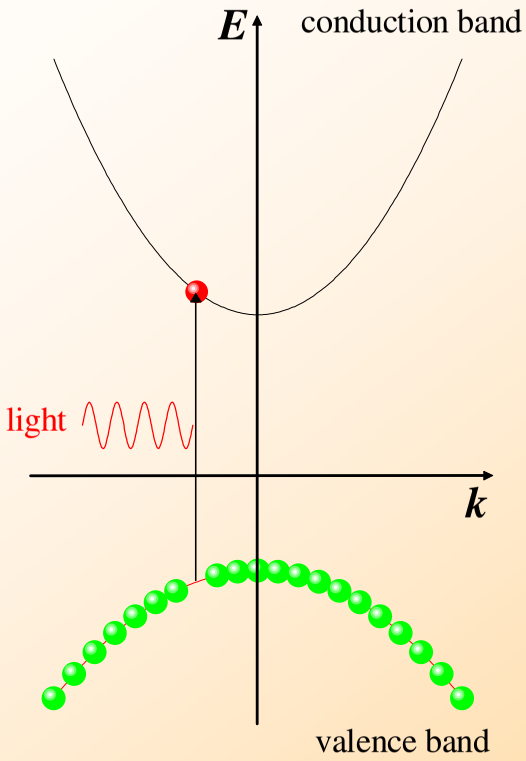

three-dimensional exciton

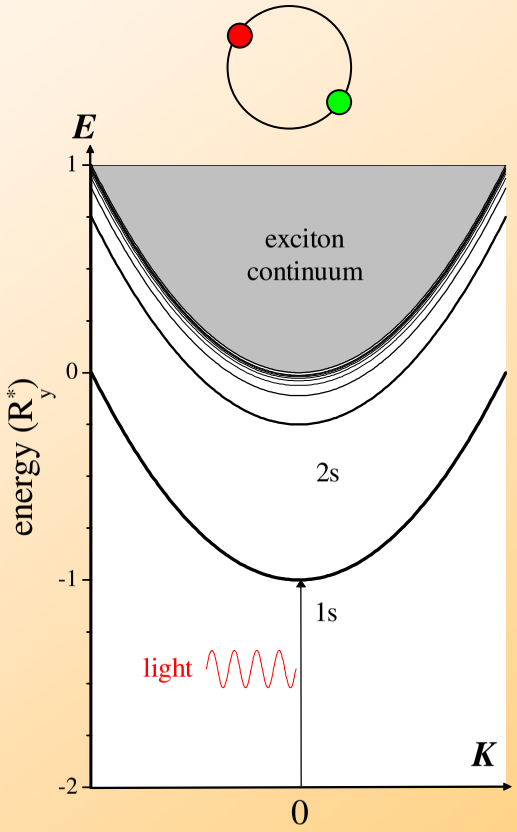

two-dimensional exciton

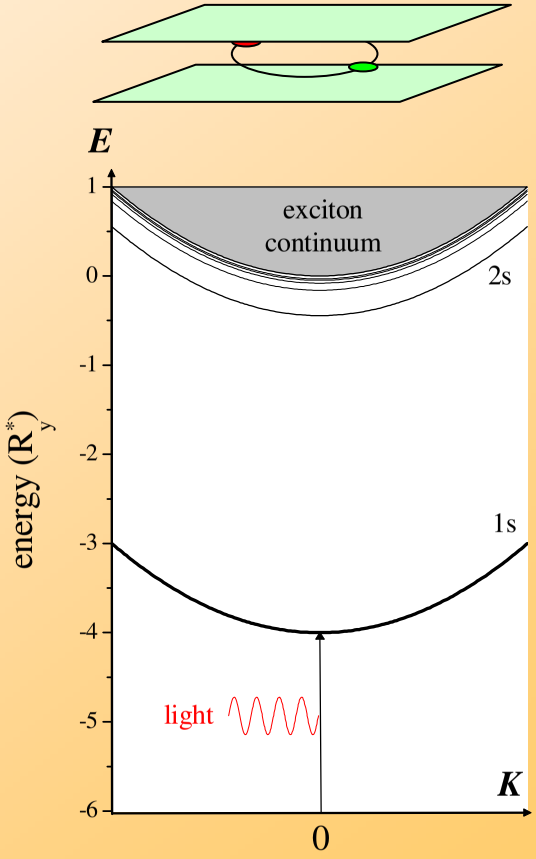

Exciton-polaritons in bulk semiconductors

Exciton and photon have 3D translational symmetry:
coupled exciton-photon states: exciton polaritons
with defined wavevector

Exciton: heavy (~electron mass), slow
Photon: massless, fast (c/n)
Exciton-polaritons:
widely variable velocity and mass

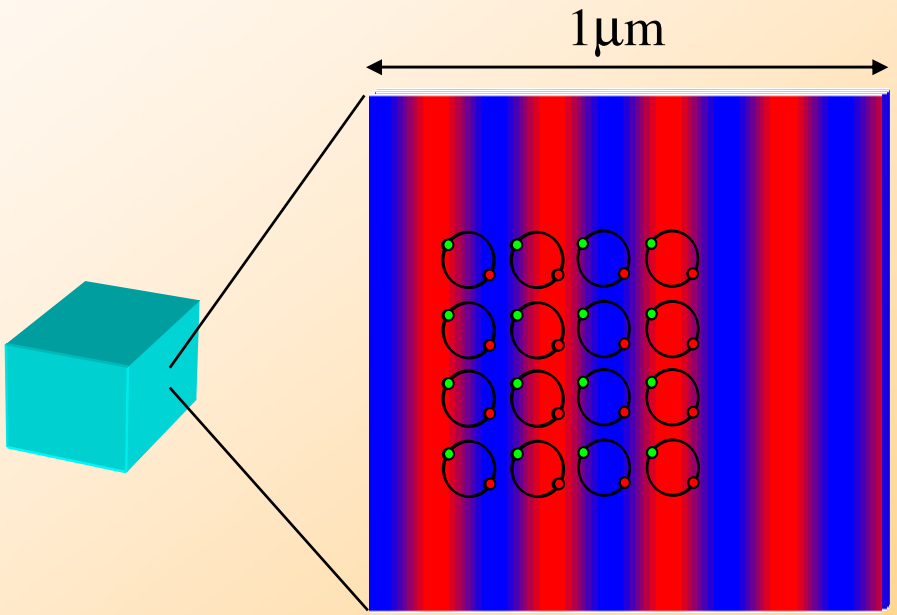

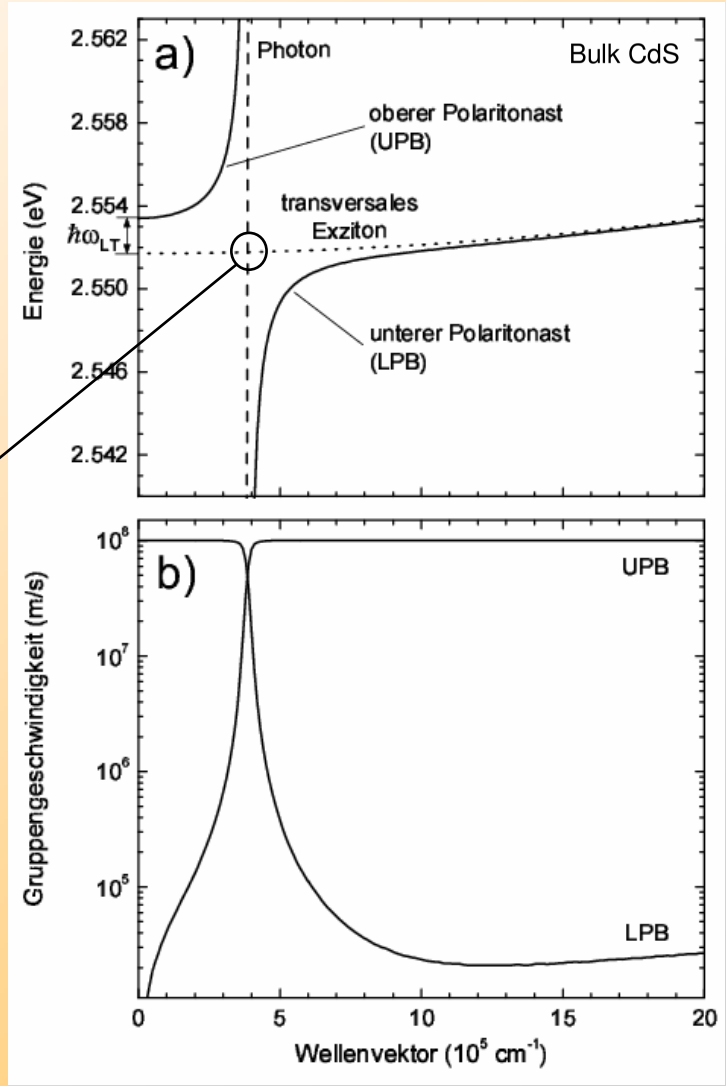

Exciton-polaritons in quantum wells

QW Exciton:
2D translational symmetry

In-plane wavevector inside light
coupling to a continuum of 3D p
radiative decay

Outside light cone ($|\mathbf{k}| > \omega c^{-1}$):
Formation of stable interface polaritons

B.Hanewinkel et al. PRB **60**,8975 (1999)

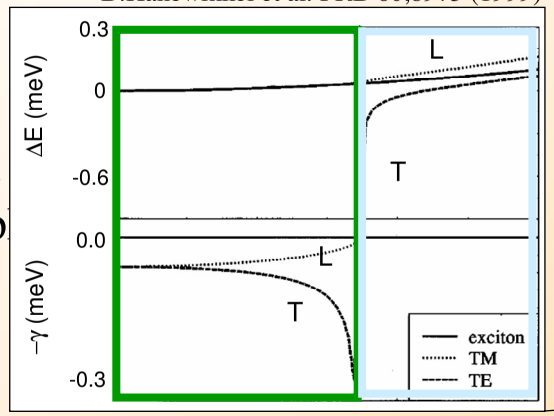

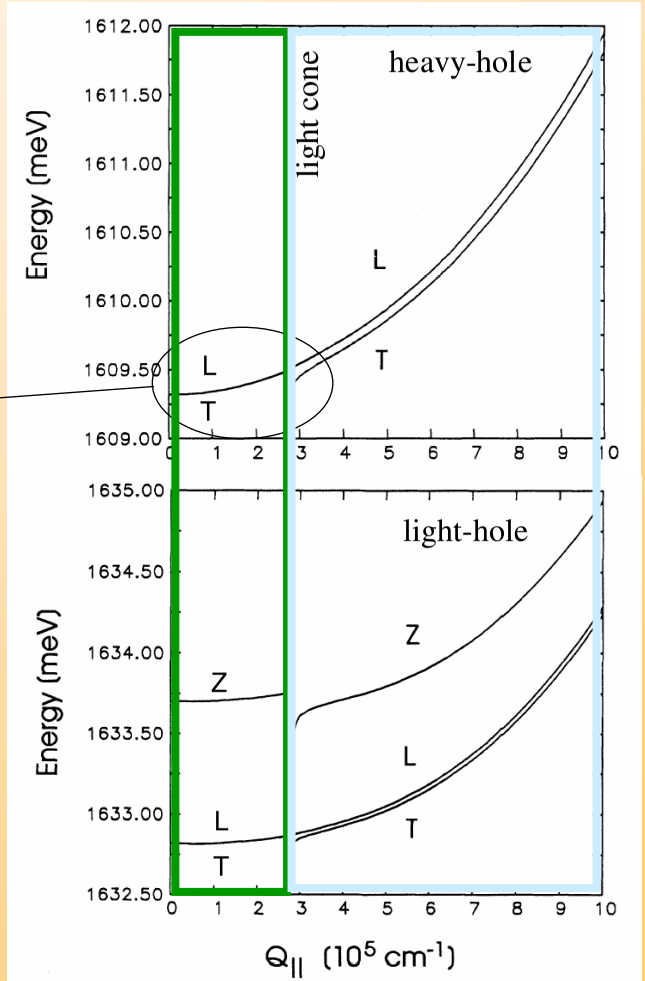

FIG. 5. LH polariton dispersion for a 50-Å QW. Resonant and localized polaritons are separated by the dashed line, which is given by $\hbar\omega = \hbar c Q_{||}/\sqrt{\epsilon_\infty}$.

S.Jorda et al. PRB 48, 1669 (1993)

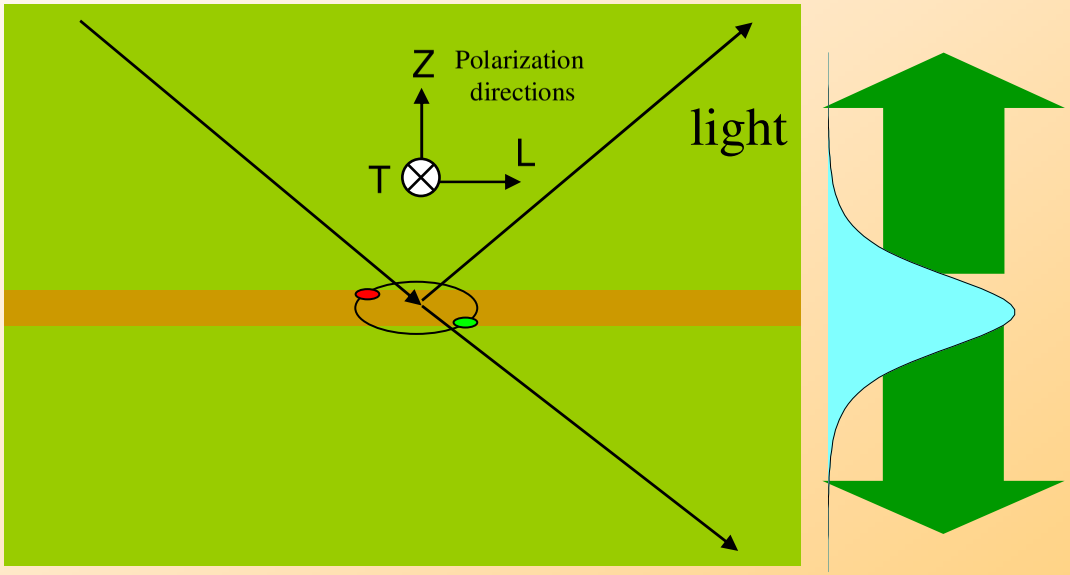

inside light cone

Disorder in quantum wells

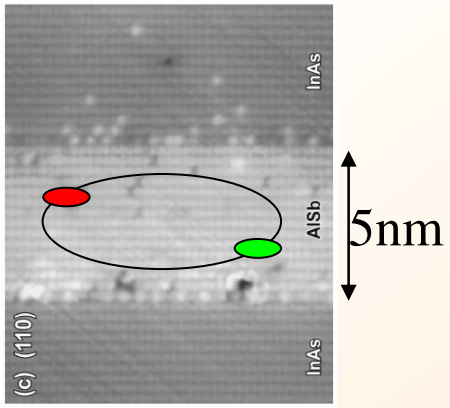

Real quantum wells:
Deviation from in-plane translational symmetry
due to interface roughness, segregation, alloy disorder:

- Formation of an effective two-dimensional disorder potential V(**R**) for the motion of the 1s exciton in the QW plane
- V is typically exceeding the coupling to the photon field, so that they are spread in k-space wider than the radiative cone

Excitons in quantum wells:

Model for a quantum-mechanical particle moving in a two-dimensional potential landscape

Advantage: excitons can be created and detected by light

Schrödinger equation for center-of-mass (COM) motion

$$H_R\psi_n(\mathbf{R}) = \left(-\frac{\hbar^2}{2M}\nabla^2_{\mathbf{R}} + V(\mathbf{R})\right)\psi_n(\mathbf{R}) = E_n\,\psi_n(\mathbf{R})$$

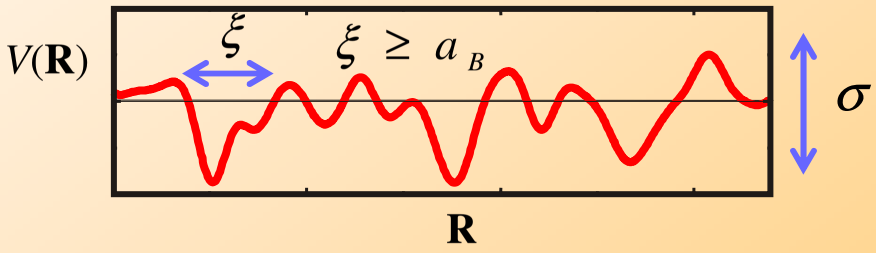

localised exciton states $\psi_\alpha(\mathbf{R})$
with eigenenergies $\hbar\omega_\alpha$

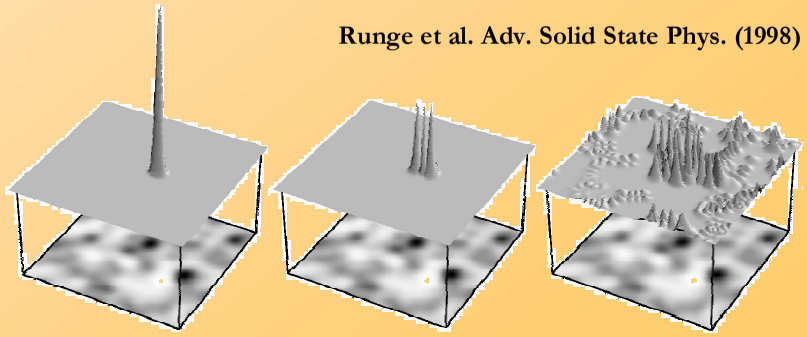

Runge et al. Adv. Solid State Phys. (1998)

Excitonic absorption in GaAs/AlGaAs quantum wells

with decreasing well width:

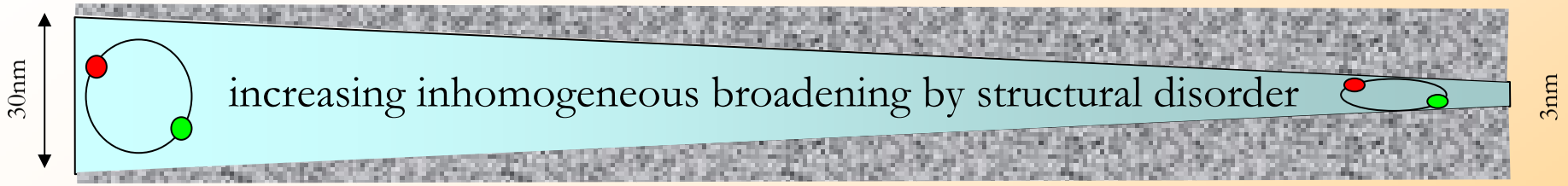

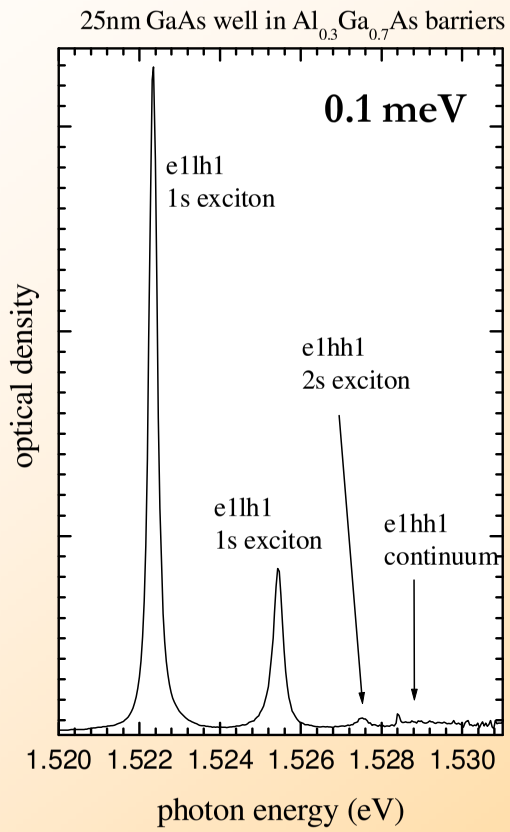

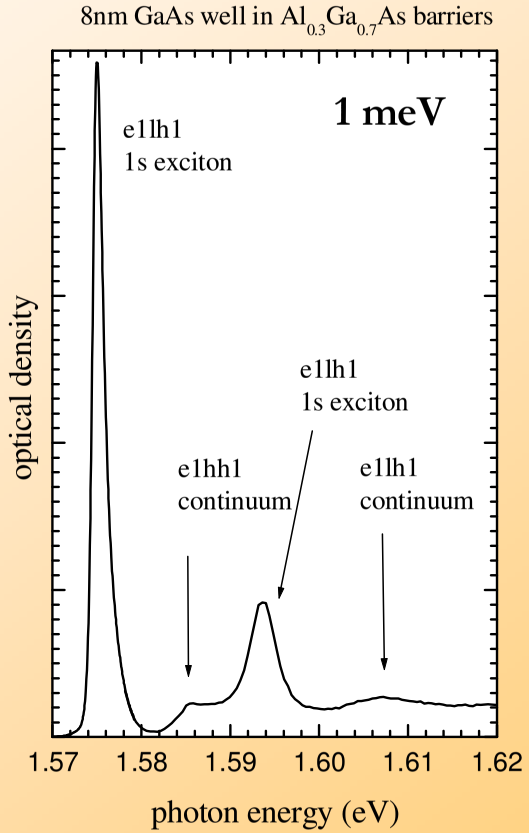

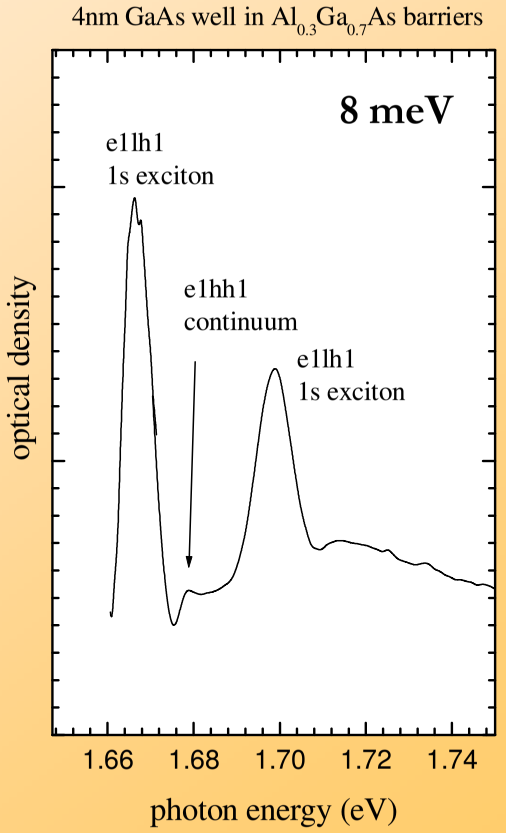

W.Langbein, Ultrafast nonlinear spectroscopy and control of semiconductor nanostructures

Transient coherent spectroscopy

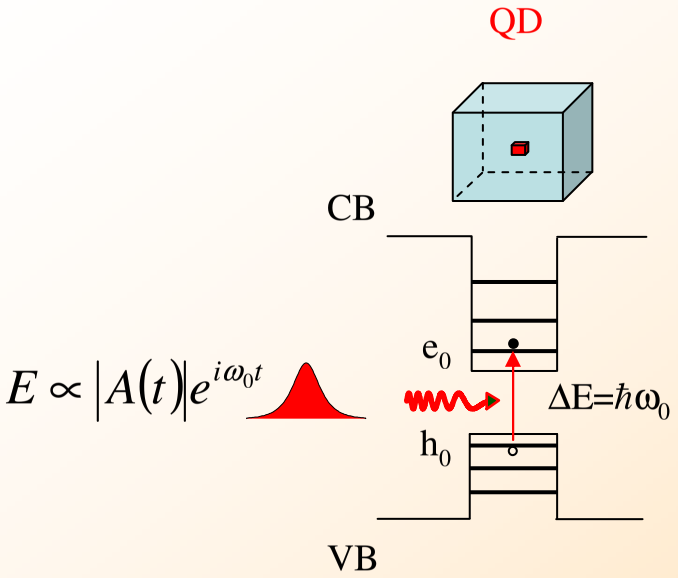

A short light pulse induces a coherent *polarization* ***P***. The average over many repeats and/or many systems is measured (even in single dot experiments)

$$\vec{P} = \sum_k P_k \langle \vec{p} \rangle_k$$ „macroscopic“ polarization

P_k: probability for the state Ψ_k $\quad \langle \vec{p} \rangle_k = \langle \Psi_k | \vec{p} | \Psi_k \rangle$

Dynamics of ***P*** is given by

- *amplitude decay* of the individual polarizations
- *mutual phase coherence* in the ensemble average.

Relaxation time approximation for ensembles of equivalent systems:

$$P \propto \exp(-t/T_2) \qquad \frac{1}{T_2} = \frac{1}{2T_1} + \frac{1}{T_2'}$$

population relaxation — pure dephasing

Inhomogeneous broadening

Non-equivalent systems: Distribution of transition frequencies

$$G(\omega_i) = \frac{1}{\sigma\sqrt{2\pi}} \exp\left\{ -\frac{(\omega_i - \omega_0)^2}{2\sigma^2} \right\}$$

$$P \propto \exp\left(-t/T_2 - \frac{1}{2} t^2 \sigma^2\right)$$

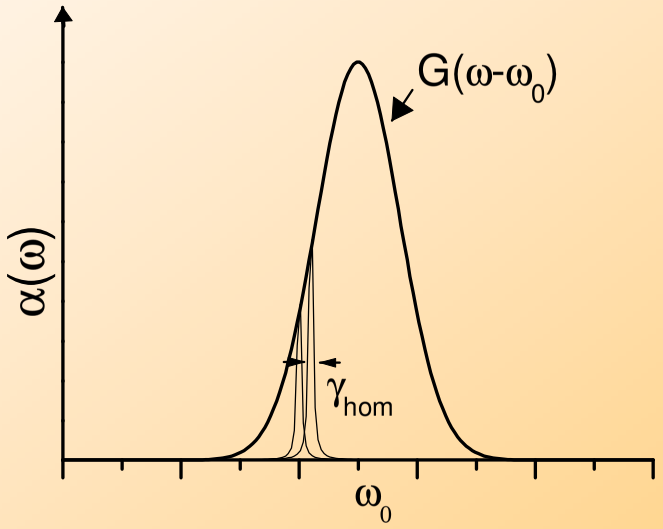

Fast decay of macroscopic polarization due to destructive interference:

$\Rightarrow$ microscopic dephasing T_2 not measurable

The way out: Consider the third-order nonlinear polarization

Four-wave mixing non-linearity

3 excitation fields E_i, 1 emitted field by third-order polarization $P^{(3)}$

$$\vec{P}^{(3)} \propto \vec{\chi}^{(3)} \vec{E}_3 \vec{E}_2 \vec{E}_1^{\,*}$$

Using excitation pulses (transient FWM) the time-ordering of the excitation fields is defined

Simplest case: 2 level system, 2x2 density matrix ρ_{ij}

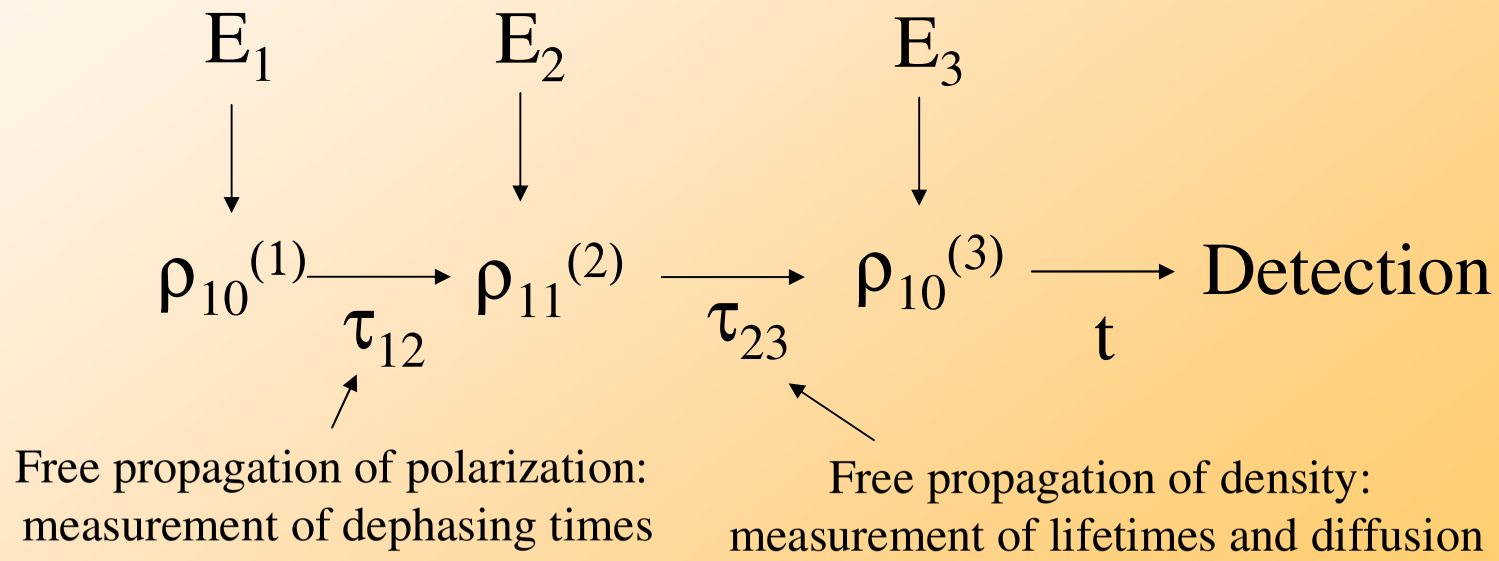

W.Langbein, Ultrafast nonlinear spectroscopy and control of semiconductor nanostructures

Detection of FWM

Self diffraction: $E_3=E_2$ (implies $\tau_{23}=0$)

$$\vec{P}^{(3)} \propto \vec{\chi}^{(3)} \vec{E}_2 \vec{E}_2 \vec{E}_1^{\,*} \qquad \vec{E} \propto \exp(i\omega t - i\vec{k}\vec{r})$$

Directional selection:

$$\vec{P}^{(3)} \propto \exp(-i(2\vec{k}_2 - \vec{k}_1)\vec{r})$$

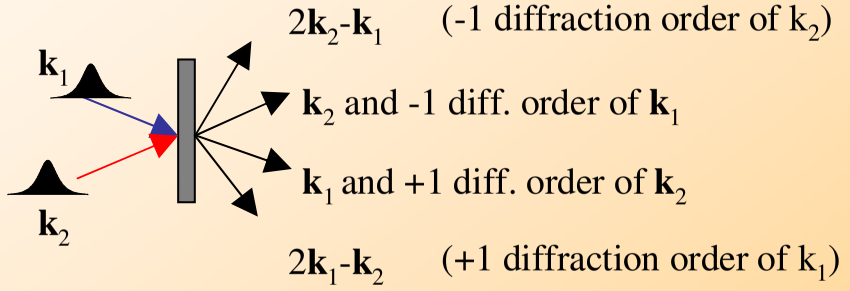

☺ Simple optical setup, measures FWM intensity, spectrally or time-resolved

☹ Uses translational invariance, which is partly broken in disordered samples:
Background due to Rayleigh scattering

☹ Uses incoherent detection: Background due to luminescence

☹ Uses non-colinear beams: phase-matching problems for thick samples,
since normally $\left|2\vec{k}_2 - \vec{k}_1\right| \neq 2\left|\vec{k}_2\right| - \left|\vec{k}_1\right|$ Solution: Specific 3 beam box-geometry

$$\vec{P}^{(3)} \propto \vec{\chi}^{(3)} \vec{E}_3 \vec{E}_2 \vec{E}_1^{\,*}$$

in-plane view:

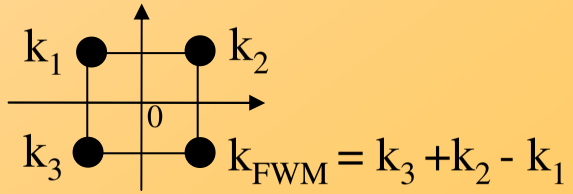

Directional selection setup: reflection geometry

For SQWs: thickness much less than wavelength, only in-plane wavevector conserved:
Reflection geometry possible (good for absorptive substrates, like GaAs for GaAs QWs)

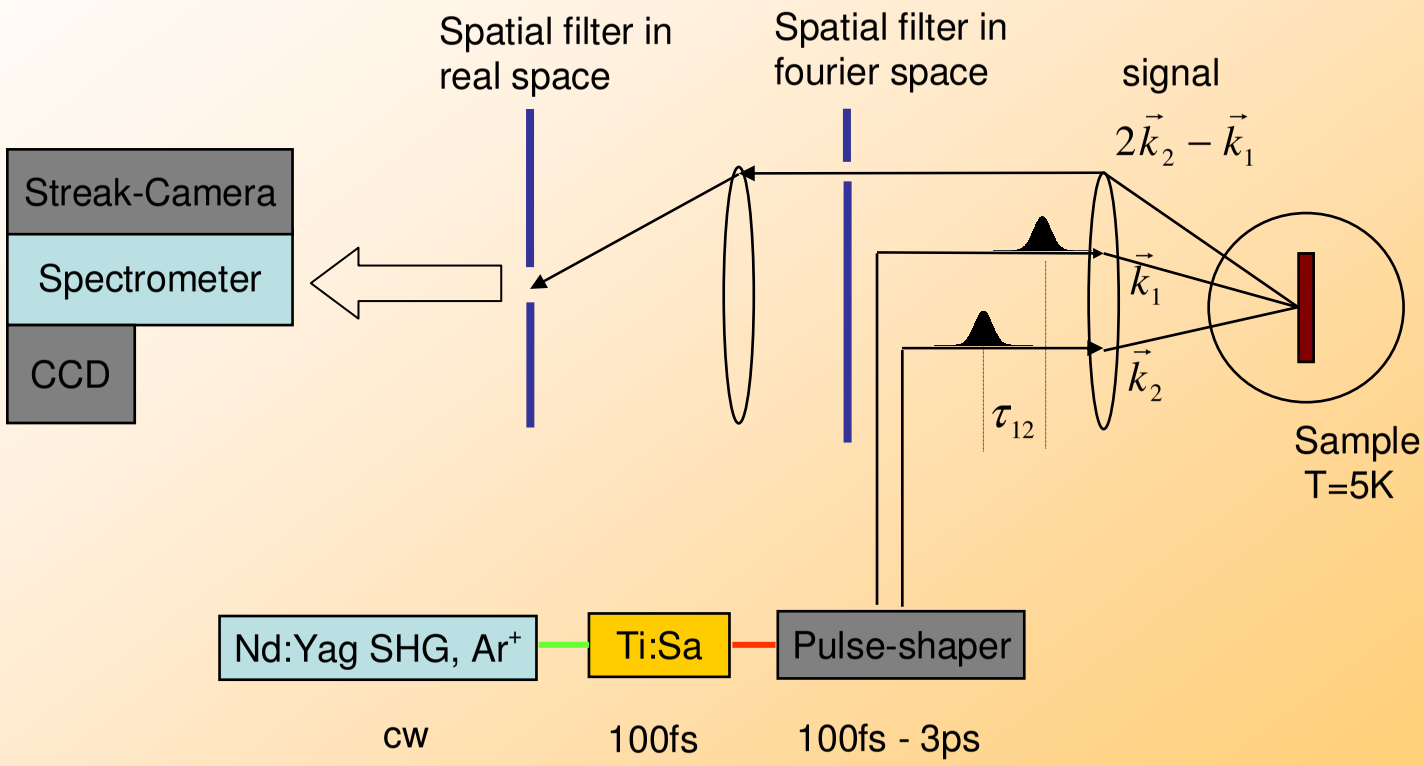

Detection of FWM

$$\vec{P}^{(3)} \propto \vec{\chi}^{(3)} \vec{E}_2 \vec{E}_2 \vec{E}_1^{\,*}$$

$$\vec{E} \propto \exp(i\omega t - i\vec{k}\vec{r})$$

Frequency selection: $\vec{P}^{(3)} \propto \exp(i(2\omega_2 - \omega_1)t)$

K. Hall *et al.*, Optics Lett.**17**, 874 (1992); A. Mecozzi *et al.* Optics Lett. **21**, 1017 (1996)

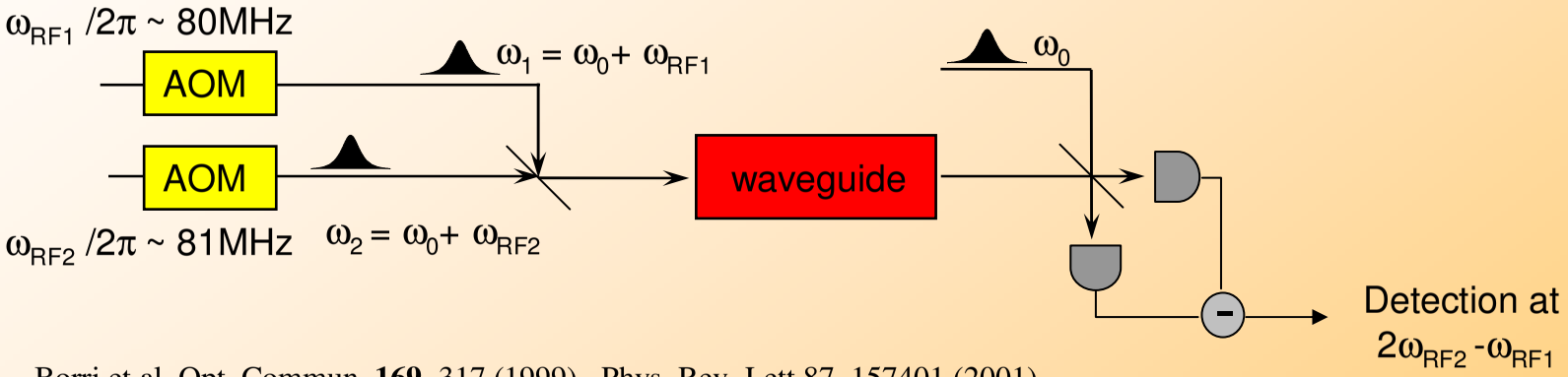

Borri et al. Opt. Commun. **169**, 317 (1999), Phys. Rev. Lett.87, 157401 (2001)

☺ Uses time-invariance, which applies also to disordered samples
☺ Can be used in colinear geometry with perfect phase matching (waveguides)
☹ Colinear geometry: excitation pulses create classical noise & detector saturation
☺ Balanced detection reduces classical noise due non-FWM intensities
☺ Coherent (heterodyne) detection rejects incoherent background (luminescence)
☹ Single chanel detection inefficient for complex FWM signals needing spectral or time-resolution

Photon echo by phase conjugation

$\vec{P}^{(3)} \propto \vec{\chi}^{(3)} \vec{E}_2 \vec{E}_2 \vec{E}_1^{\,*}$

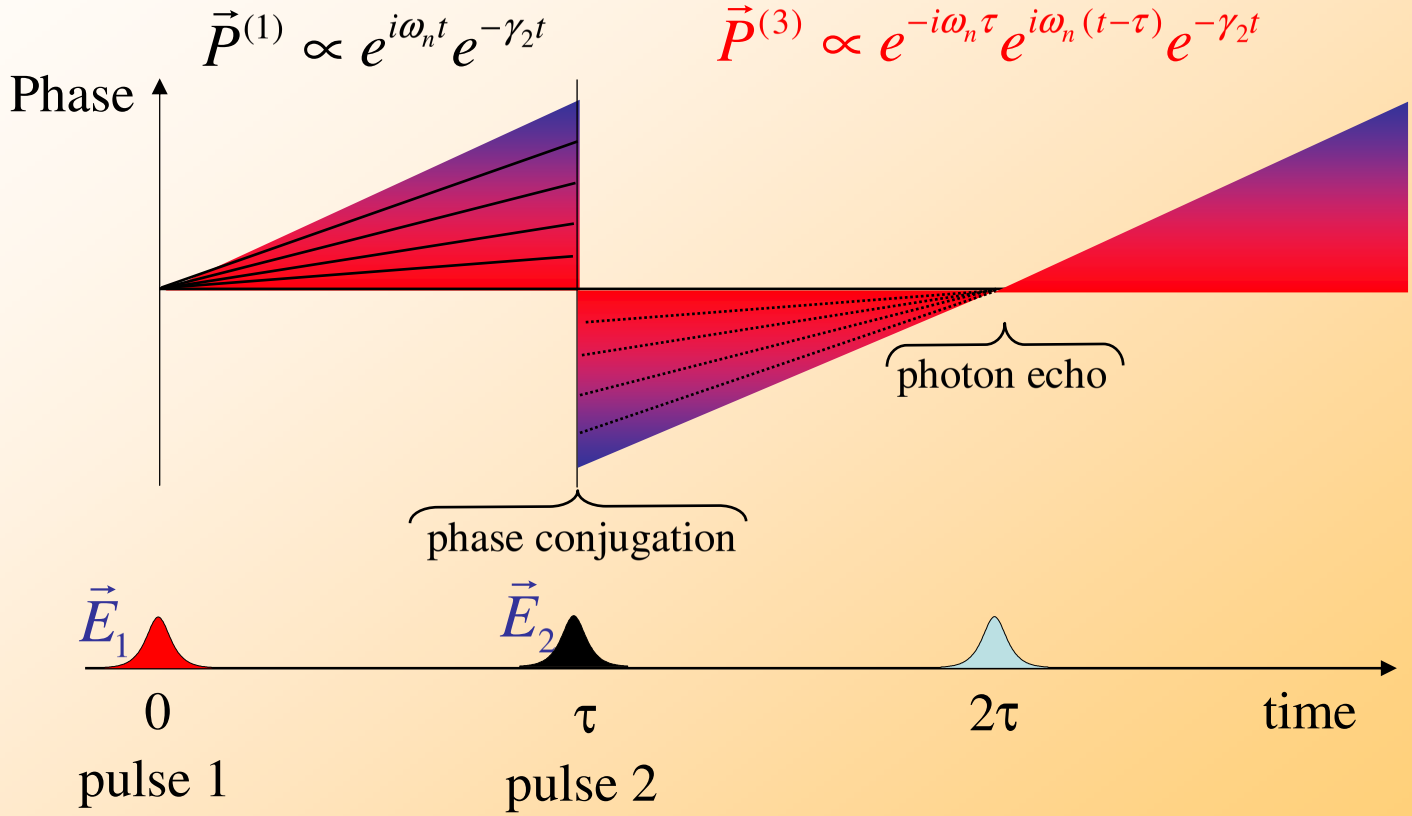

Rephasing of all polarizations at t=2τ so that the macroscopic polarization is

- independent of inhomogeneous broadening
- only sensitive to microscopic dephasing
- insensitive to slow spectral diffusion

Measured FWM signal from an ensemble of InGaAs quantum dots in a waveguide

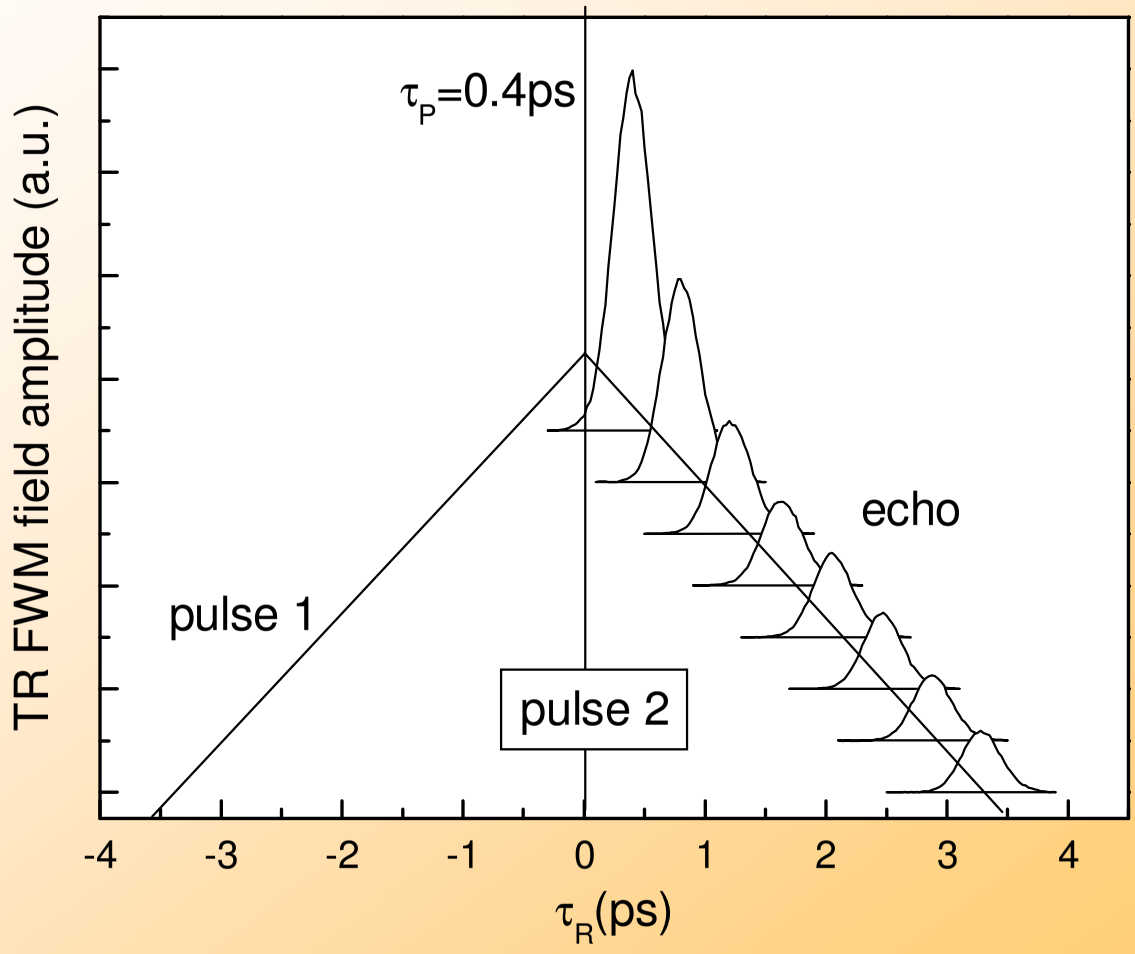

W.Langbein, Ultrafast nonlinear spectroscopy and control of semiconductor nanostructures

Free polarization decay and photon echo

Ensemble of two-level systems with variance σ of inhomogeneous broadening, polarization decay time T_2, homogeneous broadening $\gamma = \frac{2\hbar}{T_2}$

Time-resolved

Time-integrated

Homogeneous case: σ=0: Free Polarization Decay

$$I^{(3)}_{eid}(t) \propto (t-\tau)e^{-2t/T_2}\Theta(t-\tau)$$

$$I^{(3)}_{psf}(t) \propto e^{-2t/T_2}\Theta(t-\tau)$$

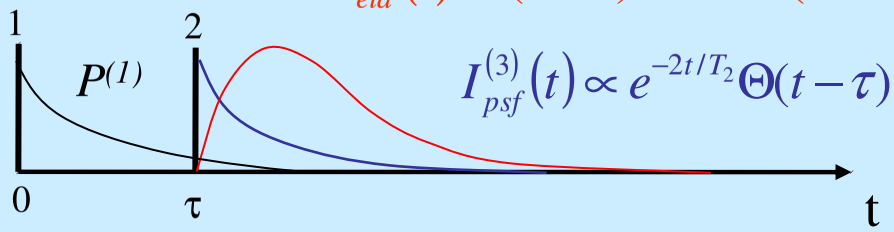

$$I^{(3)}_{\mathrm{hom}}(\tau) \propto e^{-2\tau/T_2}\Theta(\tau)$$

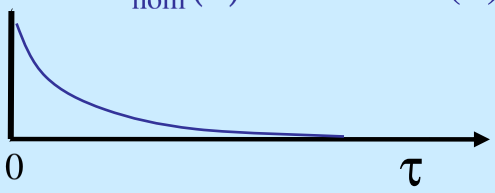

Inhomogeneous case: σ >> γ: Photon Echo

$$I^{(3)}_{inh}(t) \propto e^{-2t/T_2}e^{-\sigma^2(t-2\tau)^2}$$

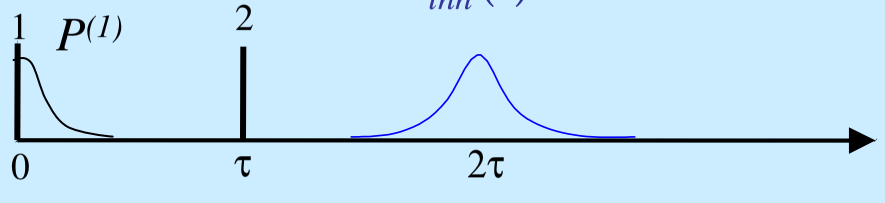

$$I^{(3)}_{inh}(\tau) \xrightarrow[\tau >> 1/\sigma]{} e^{-4\tau/T_2}$$

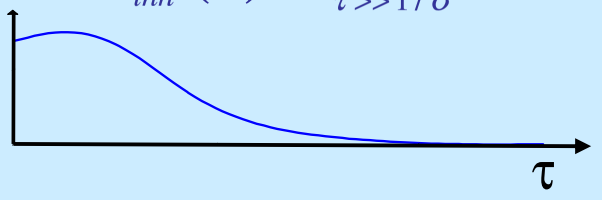

FWM versus inhomogenoeus broadening

Borri et al., Phys. Rev. B **63**, 035307 (2001)

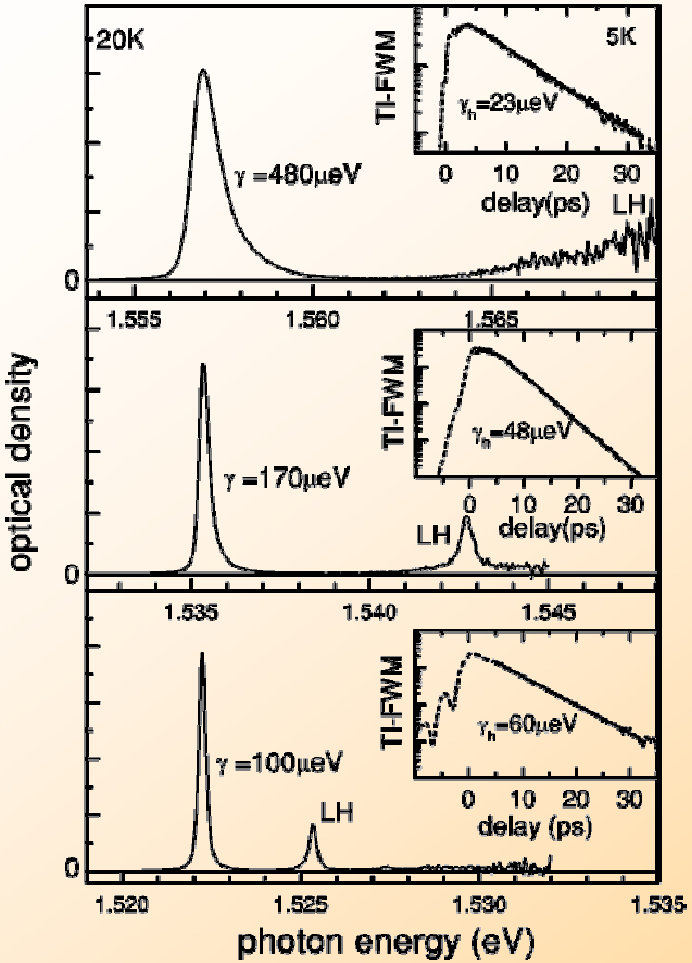

FIG. 1. Absorption profile, as deduced from the photoluminescence spectrum at 20 K corrected by a Boltzmann population factor, for a 25 nm (bottom), a 15 nm (middle), and a 10 nm (top) GaAs/$Al_{0.3}Ga_{0.7}As$ single quantum well. In the insets, four-wave mixing (FWM) traces at 5 K are given with the corresponding fits of the homogeneous broadening.

For a Gaussian broadening of FWHM $\Gamma = \sigma\sqrt{8\ln(2)}$

$$I_{\text{TI-FWM}}(\omega,\tau_{12}) \propto \left| \exp\left(-\gamma\tau_{12} - 4\ln 2 \frac{(\omega_X-\omega)^2-(\gamma/2)^2}{\Gamma^2} \right) \times \operatorname{erfc}\left[2\sqrt{\ln 2}\left(\frac{\gamma}{2\Gamma} - \frac{\Gamma\tau_{12}}{8\ln 2} + i\frac{\omega_X-\omega}{\Gamma} \right) \right] \right|^2 .$$

Erland et al., Phys. Rev. B **50**, 15047 (1994), Borri et al., Phys. Rev. B **59**, 2215 (1999)

- Spectrally resolved FWM has a width of $\Gamma/\sqrt{2}$
- Initial intensity rise with delay time until echo is fully developed

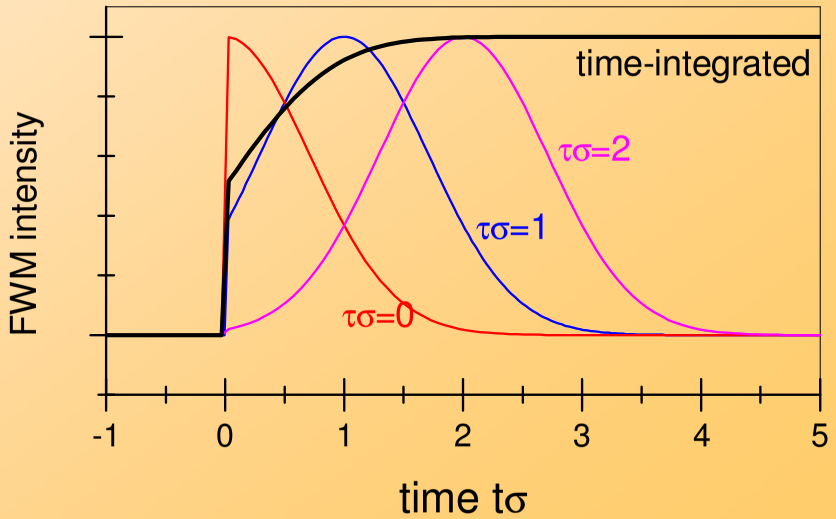

W.Langbein, Ultrafast nonlinear spectroscopy and control of semiconductor nanostructures

Time-resolved FWM intensity versus inhomogeneous broadening

Circularly polarized excitation & detection polarization to avoid signal from bound biexcitons
Streak camera detection, logarithmic color scale over 2 orders of magnitude

FWM dominated by EID:
delayed maximum
Influence of echo for
large delay times

$\sigma \gg \gamma_{hom}$

$\sigma \sim \gamma_{hom}$

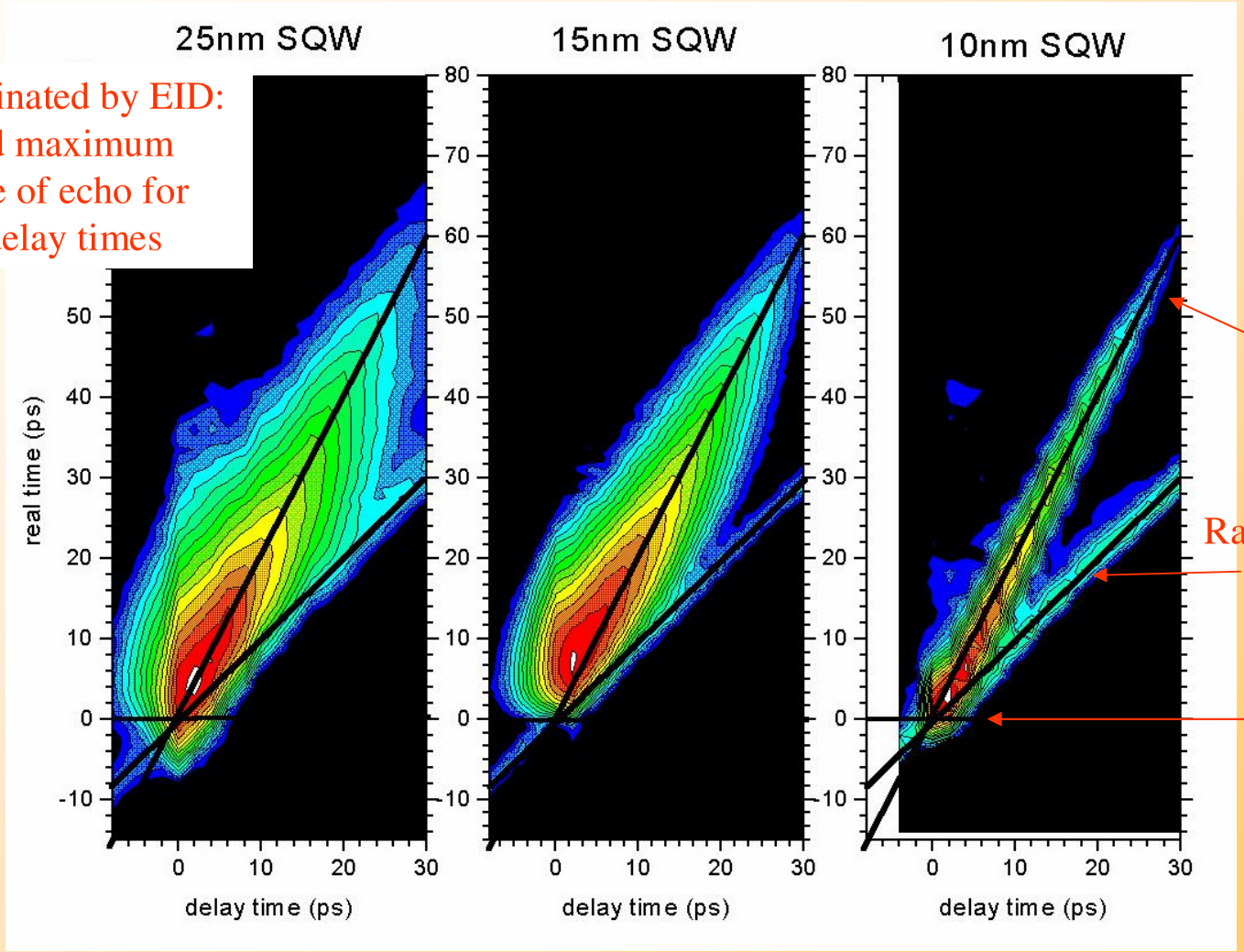

photon
echo

Rayleigh scattering
of pulse 2

pulse 1

W.Langbein, Ultrafast nonlinear spectroscopy and control of semiconductor nanostructures

FWM on the exciton-biexciton system

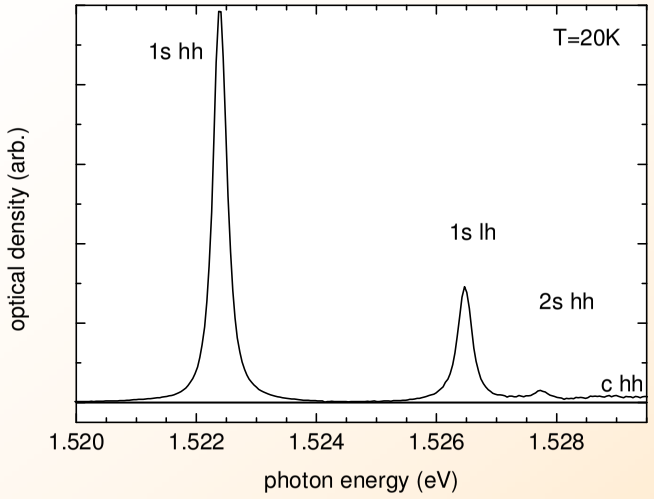

Sample:
25nm GaAs SQW

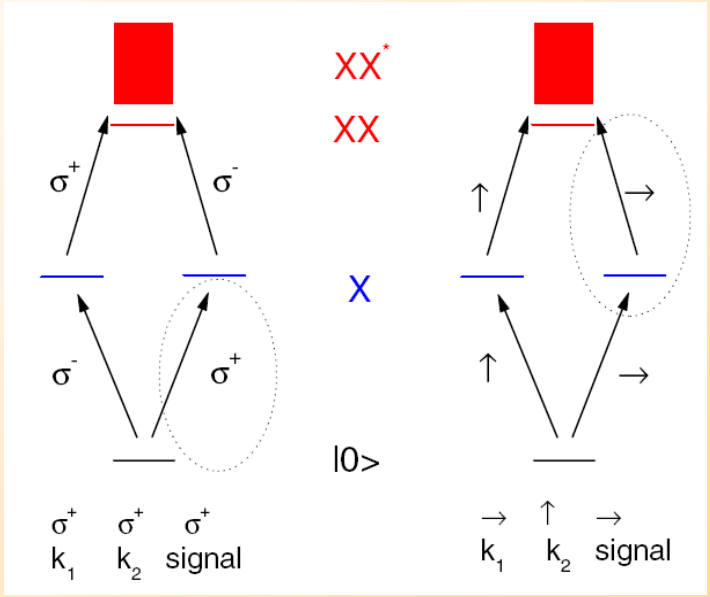

5-level model

Fig. 1. Schematic representation of the five-level system and the optical transitions for a circular (left) and linear polarized (right) exciton basis. The transitions emitting the FWM signal $P^{(3)}$ in $2\mathbf{k}_2 - \mathbf{k}_1$ direction are encircled

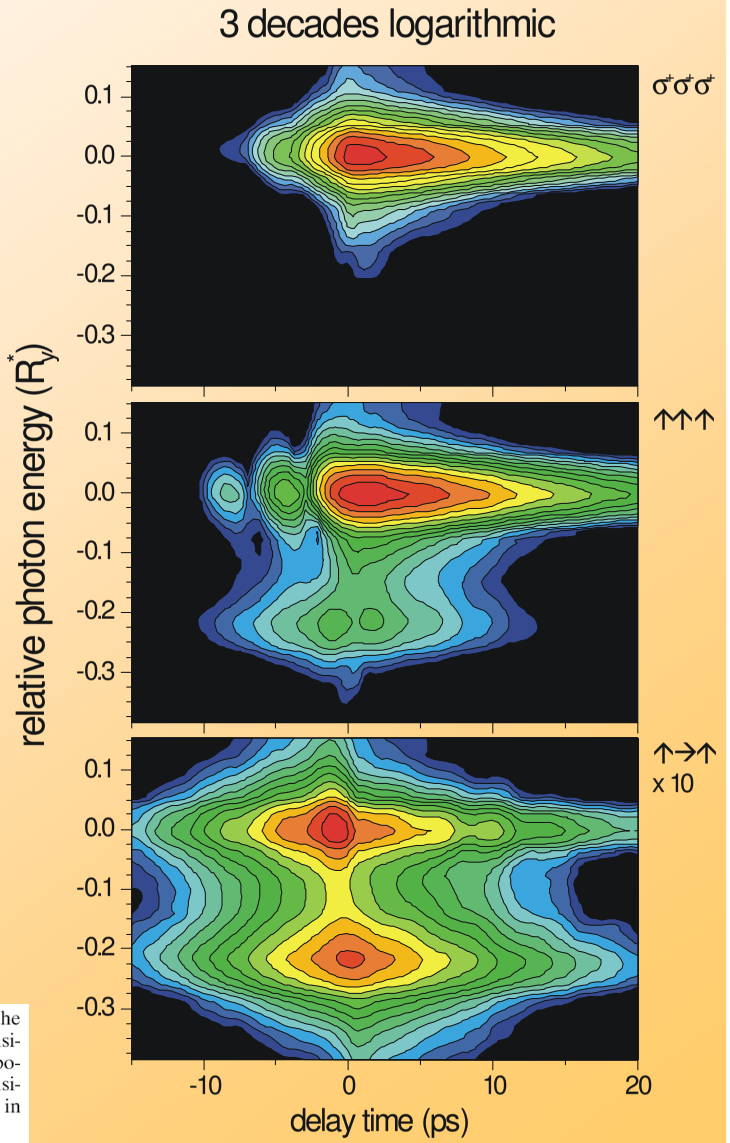

W.Langbein, Ultrafast nonlinear spectroscopy and control of semiconductor nanostructures

Polarization decay in the exciton-biexciton system

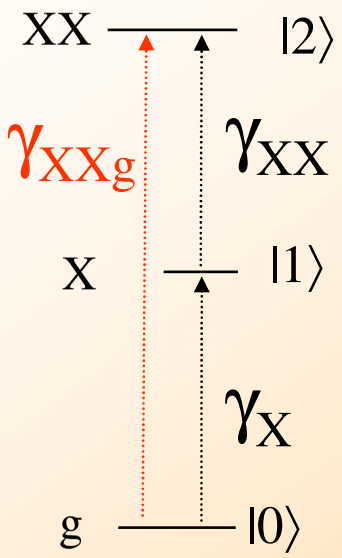

negative delay time, E_2 before E_1

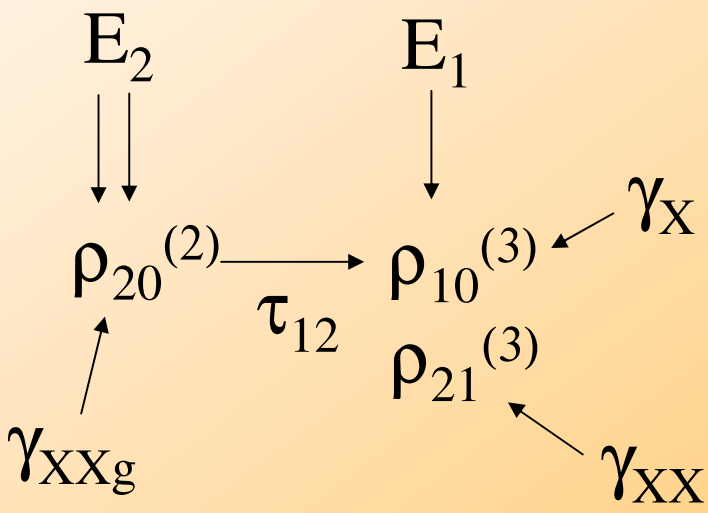

γ_{XXg}: measured in decay of FWM intensity for negative delay times

γ_X: measured in decay of FWM intensity for positive delay times

γ_{XX}: measured in FWM spectrum

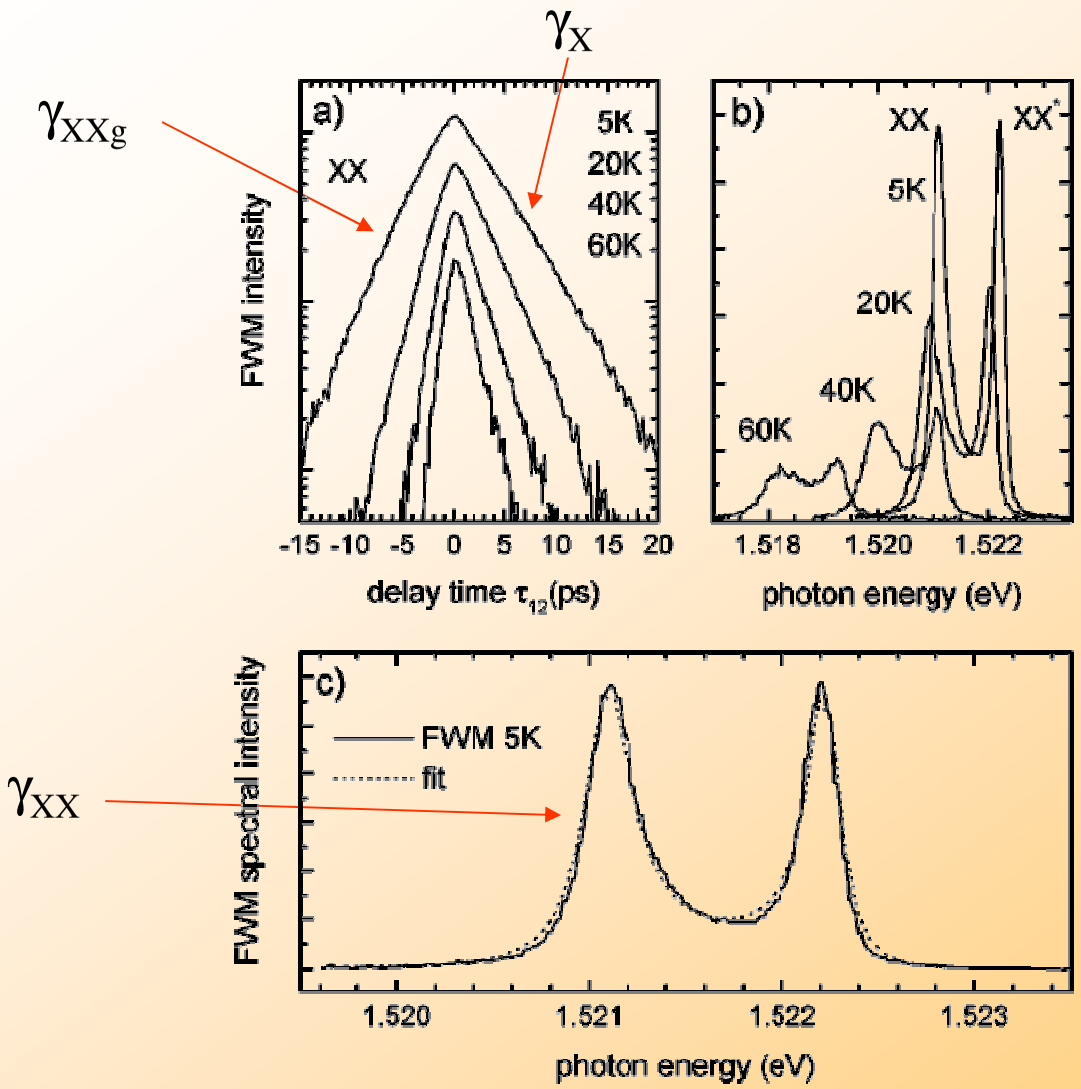

FIG. 2. (a),(b) Temperature dependency of the four-wave mixing signal for ($\uparrow \rightarrow$) configuration. (a) Delay-time traces detected at the exciton-biexciton transition. (b) Spectra for $\tau_{12}=1$ ps. (c) Four-wave mixing spectrum at $\tau_{12}=1$ ps, and 5 K lattice temperature, together with a fit using Eq. (1).

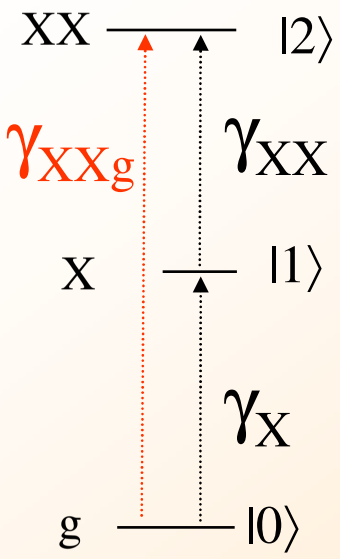

Relation between decay rates gives information about the correlation *R* between the scattering processes of excitons and biexcitons

$$\gamma_{XX} = \gamma_X + \gamma_{XXg} - 2R\sqrt{\gamma_X \gamma_{XXg}}, \quad |R| \leqslant 1.$$

Decay rates are expected to be due to

• radiative decay: should be uncorrelated since emitted photons have different energies

• phonon absorption: uncorrellated since exciton and biexciton dispersions are different, but scattering into the biexciton continuum allows equal modes to couple

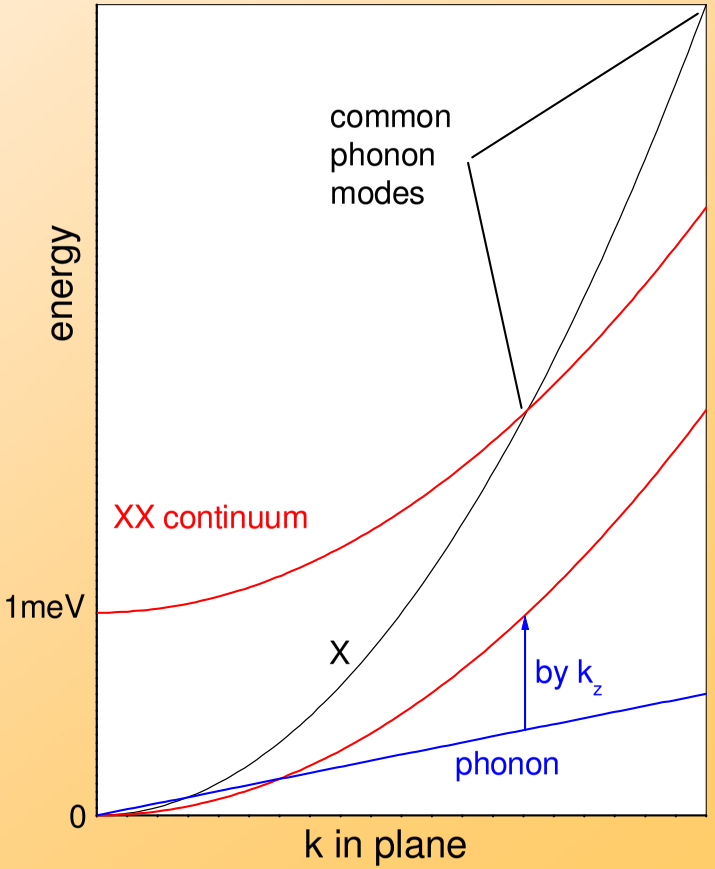

W.Langbein, Ultrafast nonlinear spectroscopy and control of semiconductor nanostructures

Exciton-biexciton dephasing: experimental results

- At low temperature scattering is uncorrelated: expected since dominated by radiative decay

- with increasing temperature scattering gets partially correlated (kT>>biexciton binding), as expected from the scattering into the XX continuum

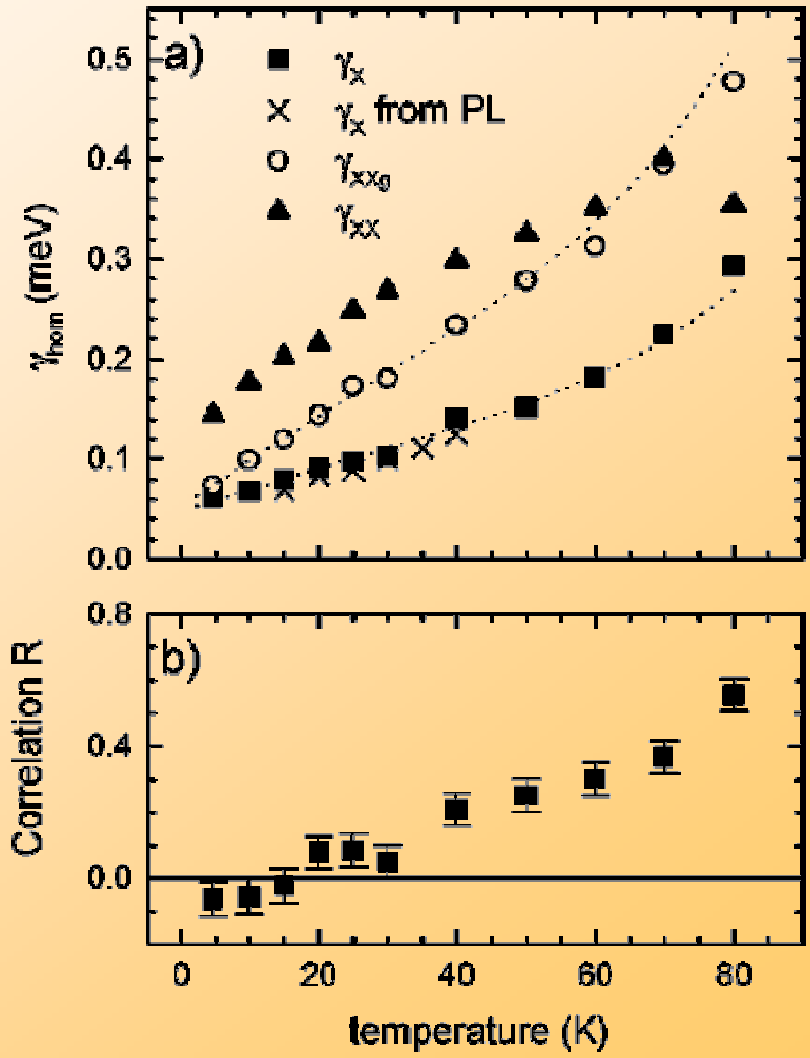

Exciton-exciton interaction effects in FWM

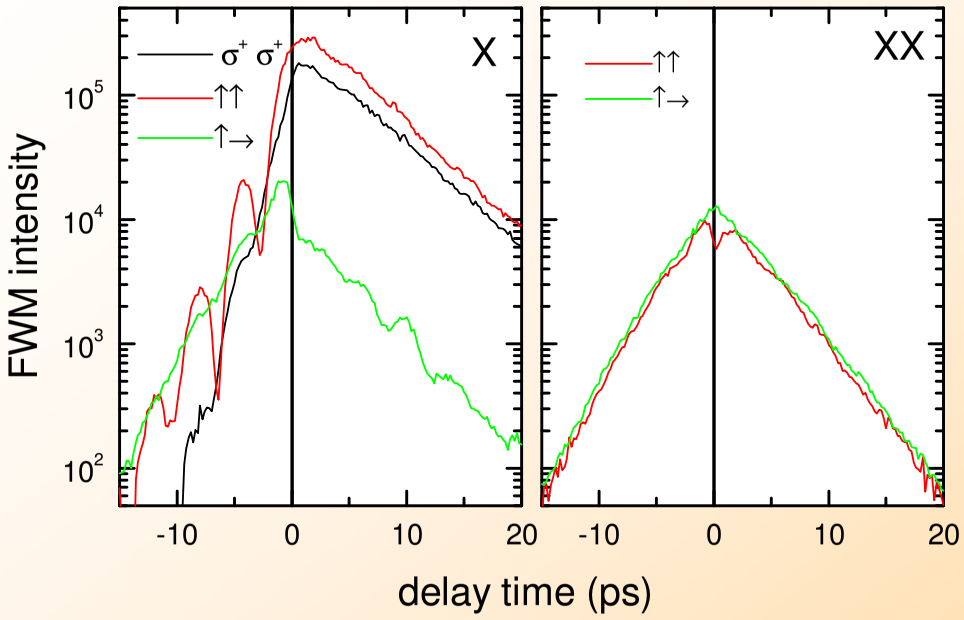

Excitation-induced dephasing (EID):

(↑↑),(σ+σ+): X signal-enhancement

(↑↑),t<0: beats with BIF at X

Biexciton-formation (BIF):

(↑↑), (↑→): signal at XX

(↑↑),t<0: beats with EID and LFC at X

(↑→),t<0: beats with LFC at X

Local Field Correction (LFC):

X signal-enhancement

(↑↑),(↑→), t<0: beats with BIF at X

Theoretical Modeling:

5-level system + EID + LFC

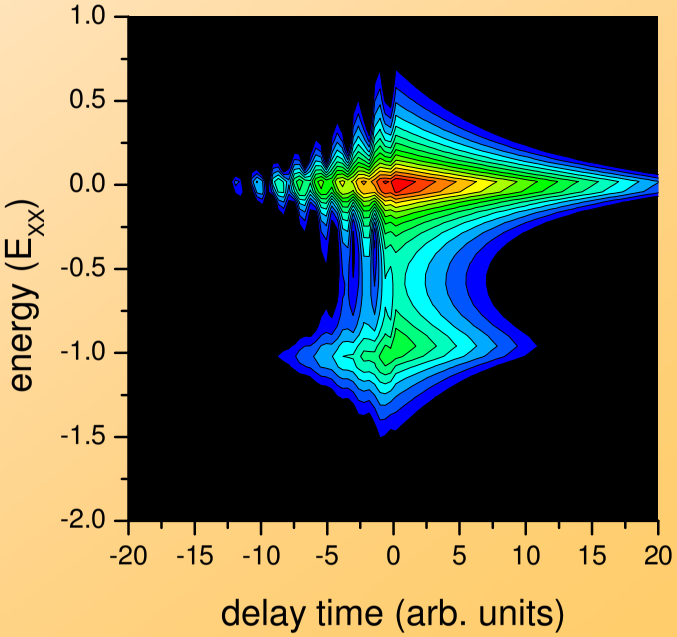

W.Langbein, Ultrafast nonlinear spectroscopy and control of semiconductor nanostructures

Localization enhanced biexciton binding in $Al_xGa_{1-x}As$

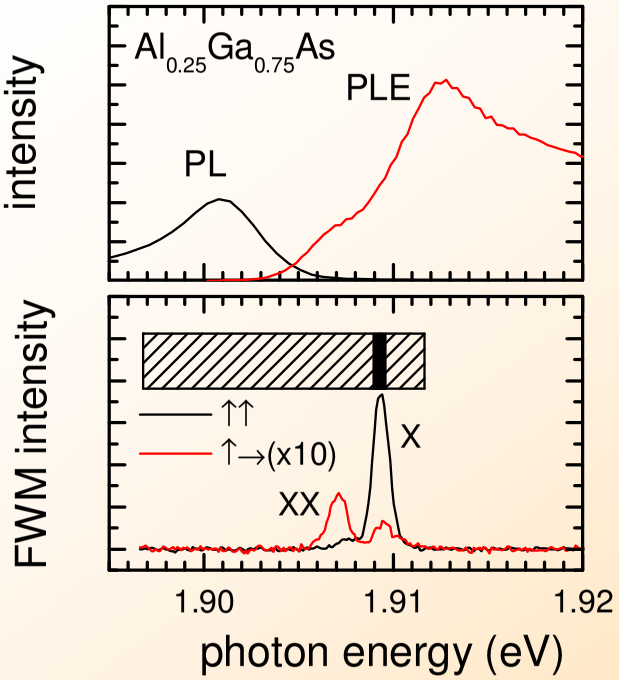

Langbein & Hvam, Phys. Rev. B **59**, 15405 (1999)

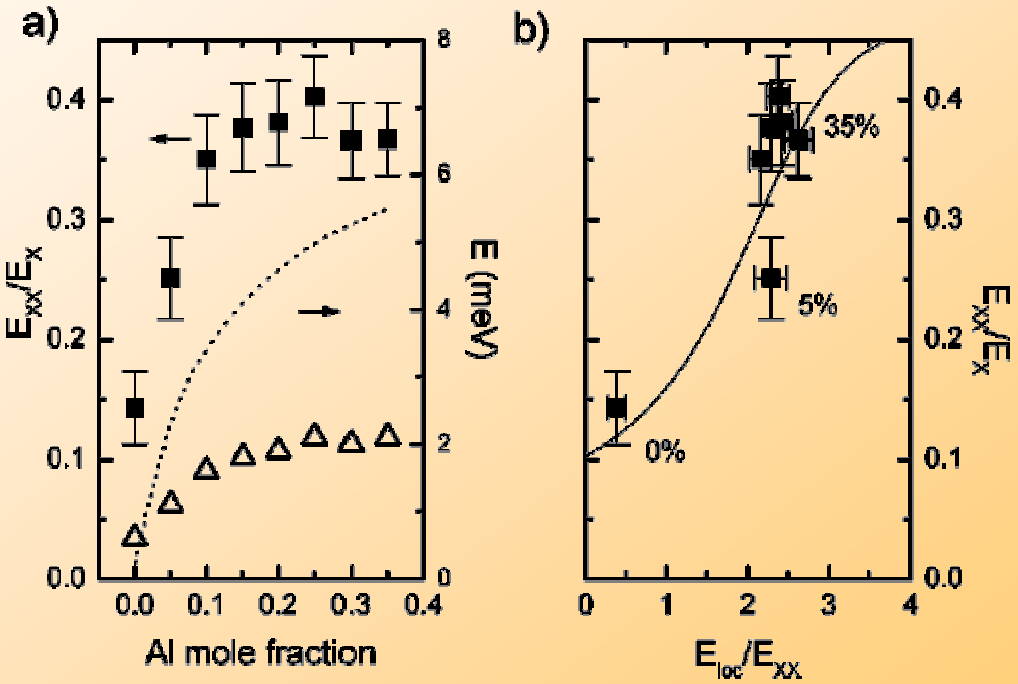

Biexciton binding energy E_{XX} increases from 0.5meV to 2meV with increasing disorder. Binding energy ratio beween biexciton and exciton E_{XX}/E_X increases from 0.13 to 0.37 when the inhomogeneous broadening E_{loc} gets larger than E_{XX}

FIG. 1. (a) Biexciton binding energy E_{XX} (triangles), photoluminescence linewidth $E_{\rm loc}$ (dotted line), and ratio E_{XX}/E_X (squares) for the $Al_xGa_{1-x}As$ mixed crystal samples as a function of the Al mole fraction x. (b) E_{XX}/E_X as a function of the localization ratio $E_{\rm loc}/E_{XX}$. Line: calculated dependence [Eq. (5)] for $n=3$, $E_{\rm loc}=4\hbar\omega_{\rm loc}$, $\alpha=0.312$, $\beta=2.4$, and $\sigma=0.2$.

Binding energy of localized biexcitons

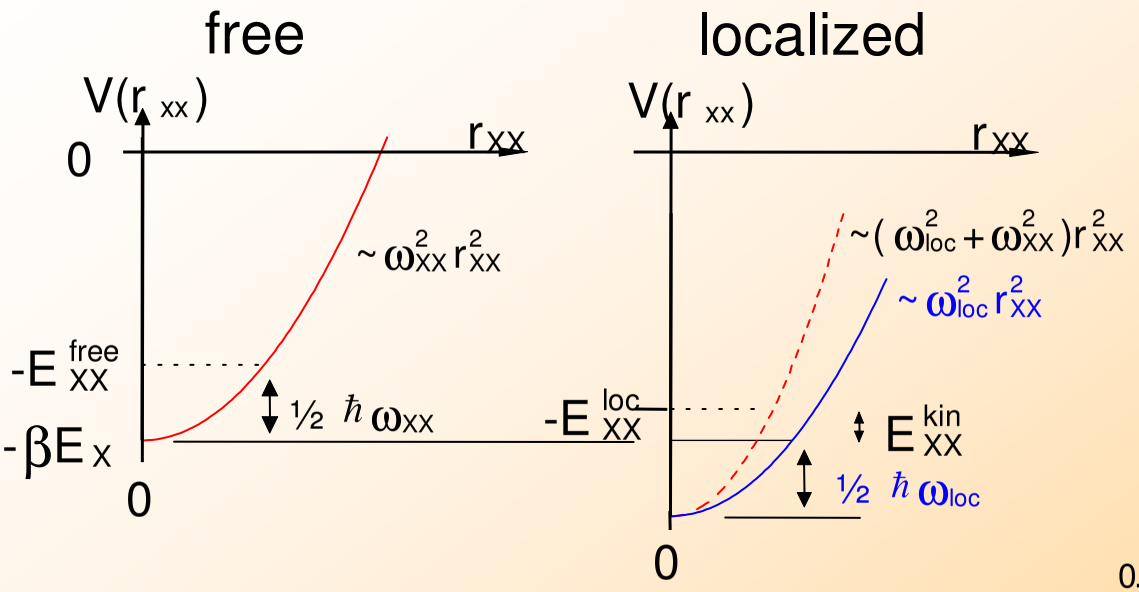

Enhancement of the binding energy
by the quenching
of the binding-induced kinetic energy

E_{XX}^{kin}

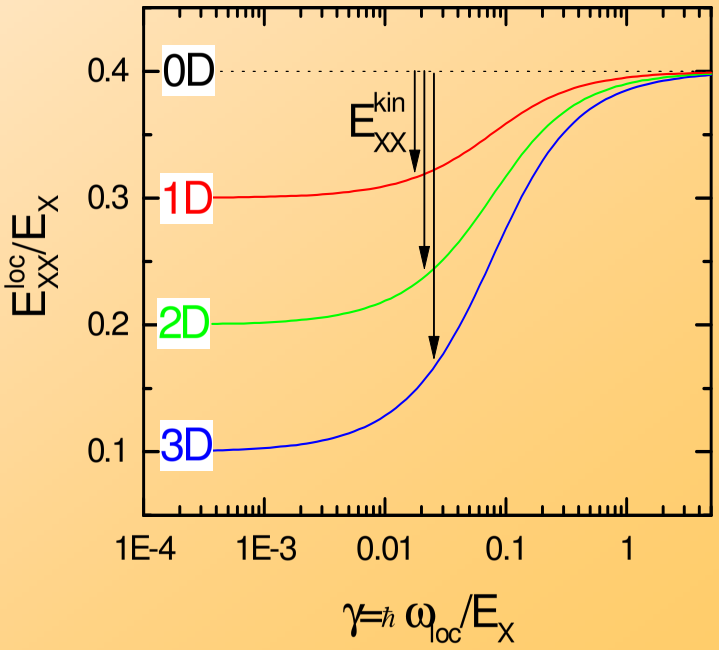

Localization enhanced biexciton binding in GaAs QW

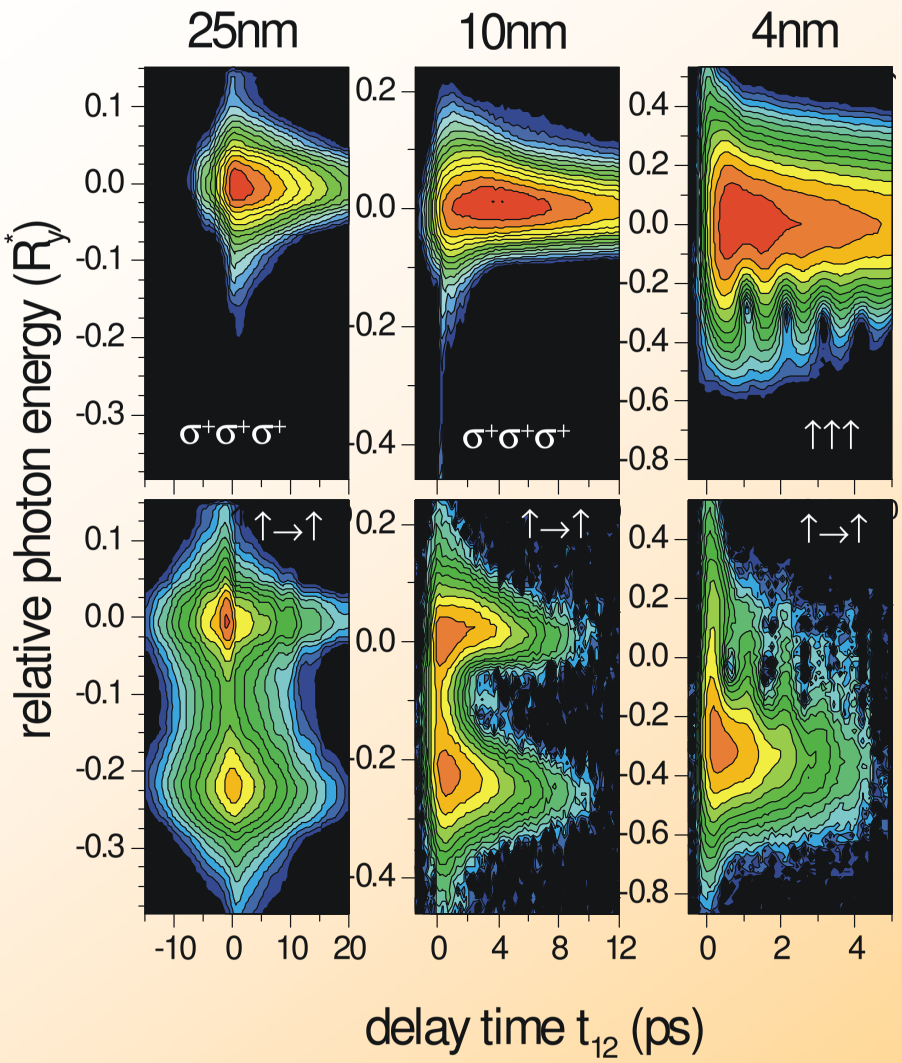

The biexciton binding energy -E_{XX} increases with increasing localization due to a quenching of the binding-induced kinetic energy.

The biexcitonic continuum edge (XX^*) is quantized to higher energies and reduced in oscillator strength by the localization.

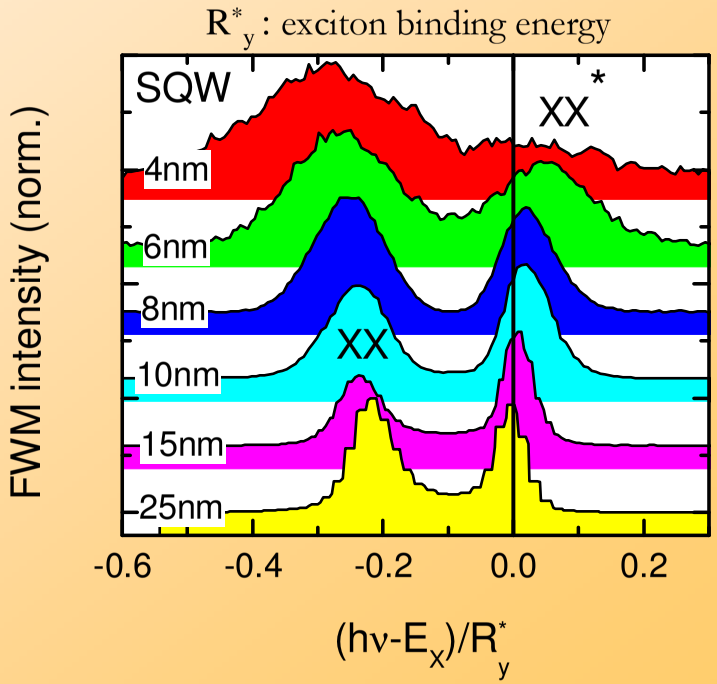

W.Langbein, Ultrafast nonlinear spectroscopy and control of semiconductor nanostructures

Localization enhanced biexciton binding in GaAs QWs

Binding energy ratio beween biexciton and exciton E_{XX}/E_X increases from 0.2 to 0.32 when the inhomogeneous broadening E_{loc} gets larger than the biexciton binding E_{XX}

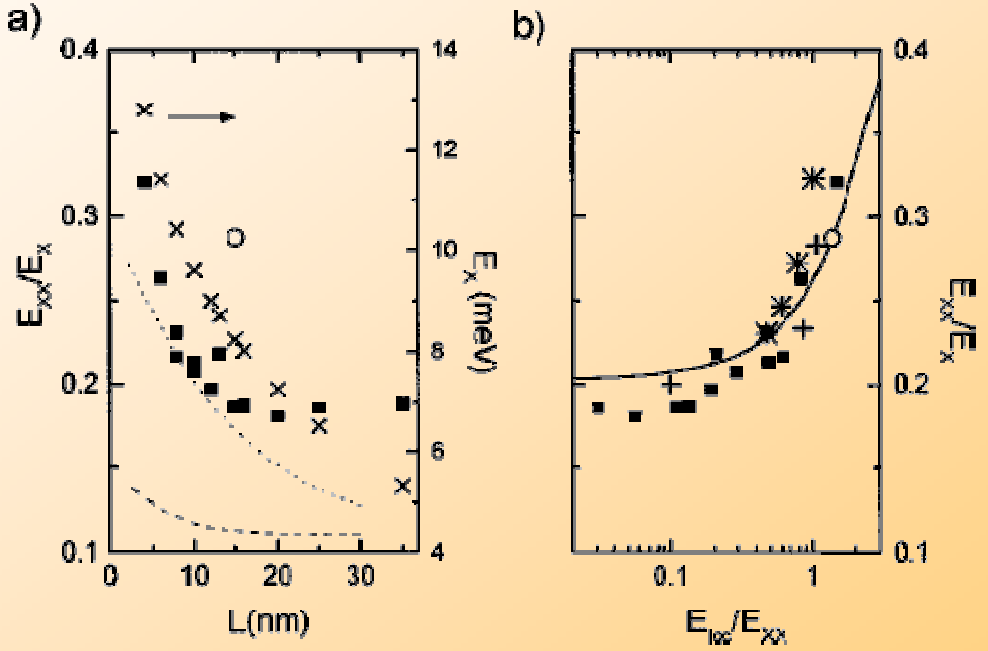

FIG. 3. Experimental and calculated data for quasi-2D samples. (a) Symbols: experimental data for GaAs/$Al_{0.3}Ga_{0.7}As$ QWs as a function of the well thickness L. Crosses: Exciton binding energy; squares: experimental ratio E_{XX}/E_X. Cicle: E_{XX}/E_X for an $Al_{0.1}Ga_{0.9}As/Al_{0.3}Ga_{0.7}As$ QW. Lines are calculations (Refs. 30, 35 and 36). (b) E_{XX}/E_X versus localization strength E_{loc}/E_{XX} for different quasi-2D material systems: Open diamonds: this work; filled squares: GaAs/$Al_xGa_{1-x}As$ QWs; crosses: ZnSe/$Zn_xMg_{1-x}S_ySe_{1-y}$ (Refs. 25, 37, and 38); stars: $In_{1-x}Ga_xAs$/GaAs (Ref. 39). Line: calculated with Eq. (5) for $n=2$, other parameters as in Fig. 1.

Inhomogeneous broadening of biexciton binding

Testing the biexciton binding energy distribution within the exciton ensemble using a spectrally selective excitation of the first-order polarization (k_1)

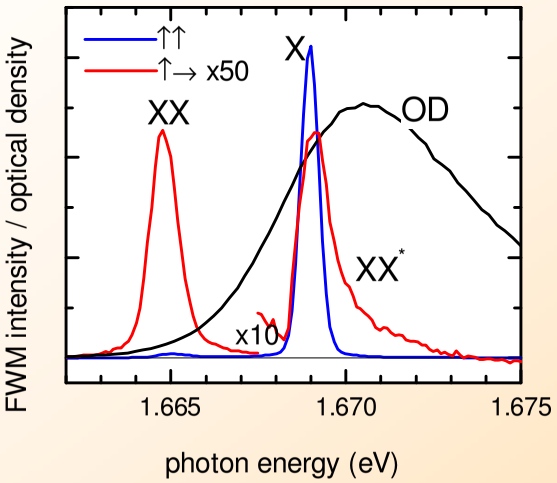

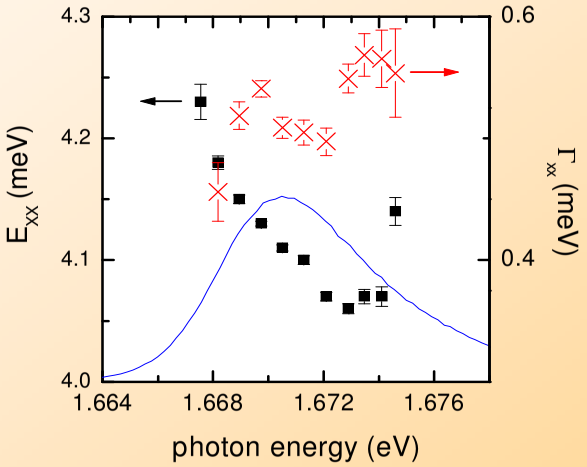

The inhomogeneous broadening of the biexcitonic binding energies lead to a fast decay of the X-XX and X-XX* photon-echo signal (rephasing is not complete)

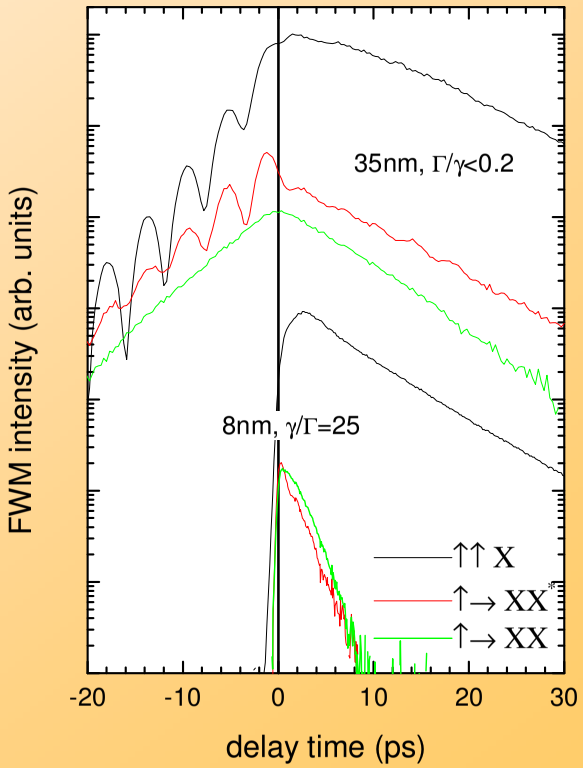

Biexciton binding energy is
⇒ inhomogeneously broadened for each exciton energy
⇒ increasing with decreasing exciton energy
(stronger localization)

T-shaped quantum wires

Growth Technique :
Cleaved Edge Overgrowth

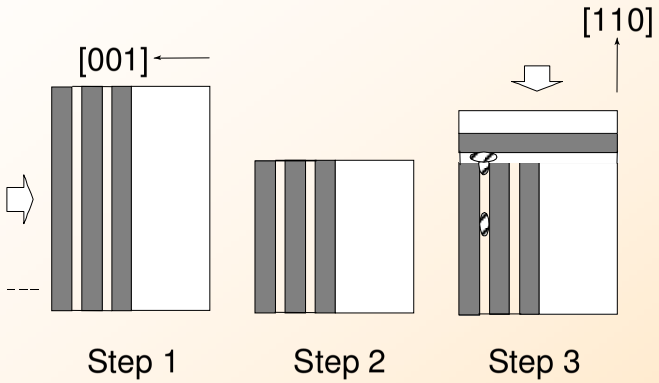

Confined states of an optimized structure with a 3nm overgrown GaAs QW

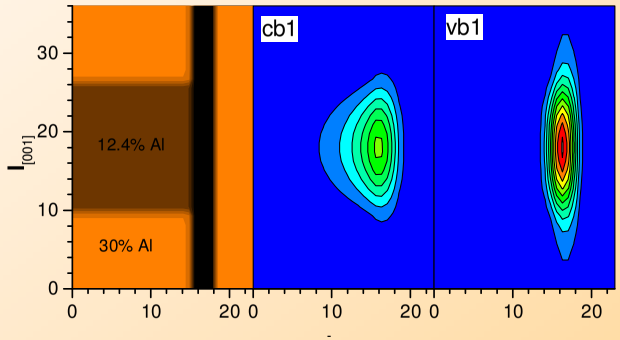

Investigated 6.6 x 24 nm T-wire:

50 period [001] MQW, thickness 2.5mm
24nm $Al_{0.03}Ga_{0.07}As$ well, 26nm $Al_{0.3}Ga_{0.7}As$ barrier
Overgrown by **6.6nm GaAs well**

20 meV confinement
3.4 meV inhomogeneous broadening

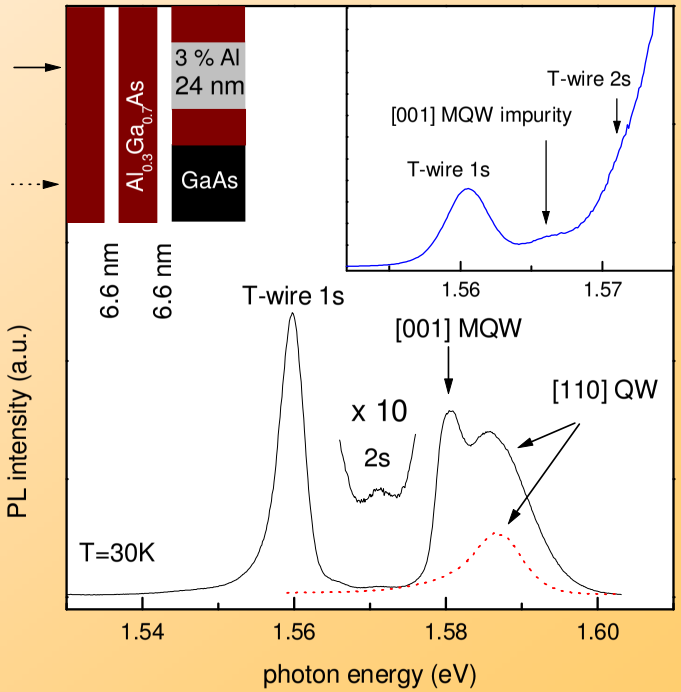

FWM on T-shaped quantum wires

Langbein et al., Phys. Rev. B **60**, 16667 (1999)

Exciton localization:

Stokes-shift between absorption

and PL at low temperatures.

Strongly varying homogeneous linewidth

within the inhomogeneous broadening:

phonon-assisted relaxation

Exciton binding energy:

Excitation of exciton series up to the continuum edge:

high-energy side-line, quantum beats

$\Rightarrow$ Identification of the 1s-2s beating with

$E_{1s\text{-}2s}$=10.5±0.4meV

From fractional-dimensional model:

E_X = 11.9 ±0.4 meV

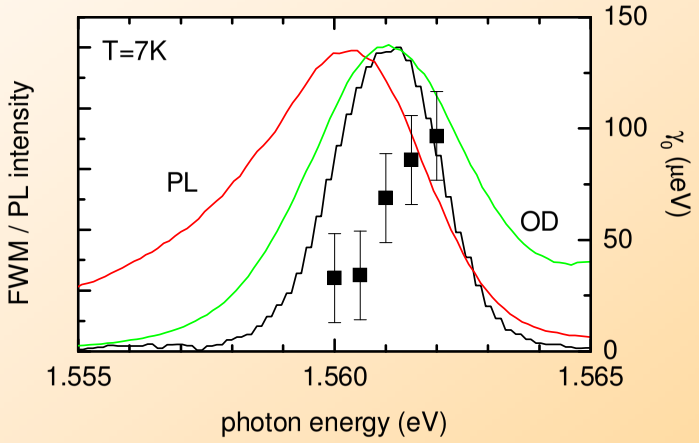

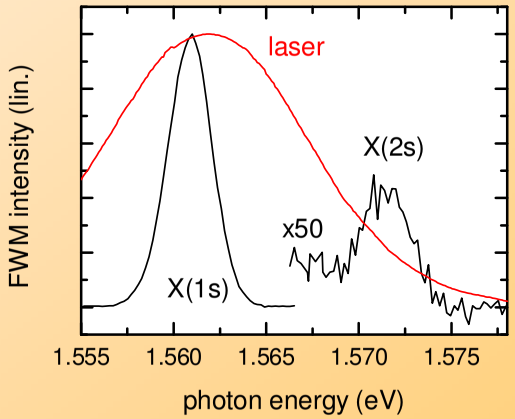

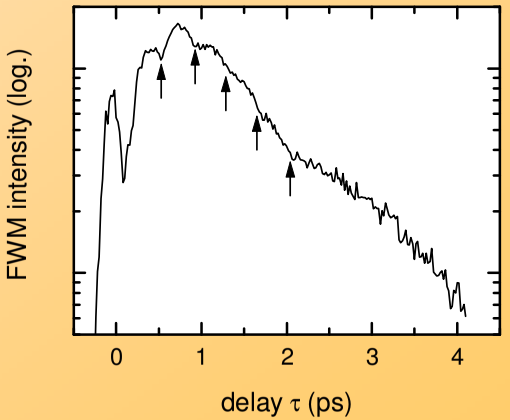

$In_xGa_{1-x}As/GaAs$ self-organized quantum dots

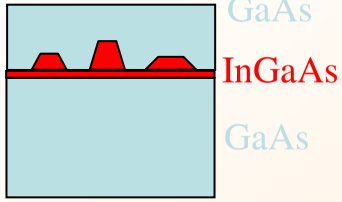

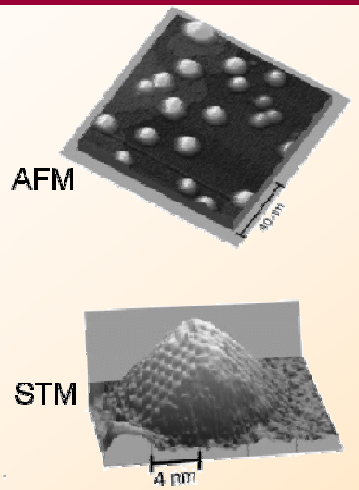

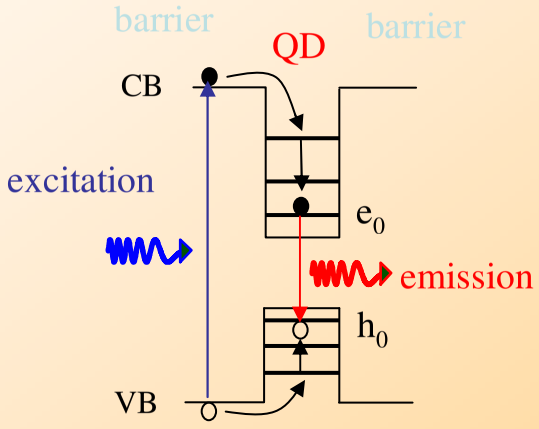

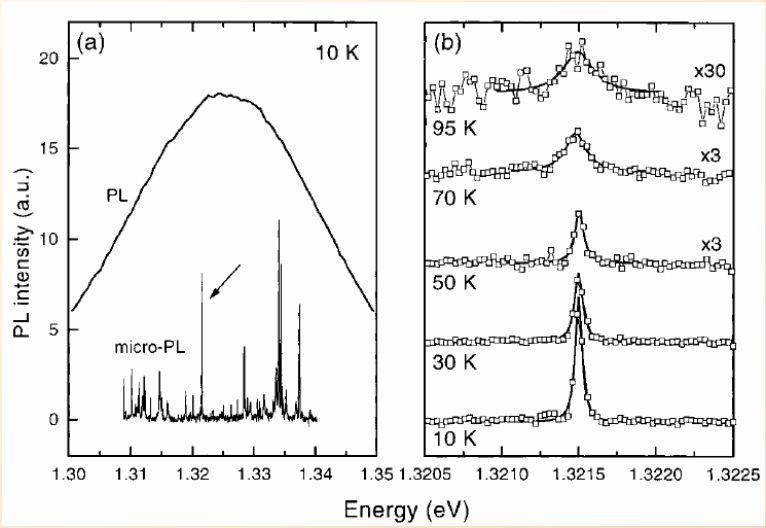

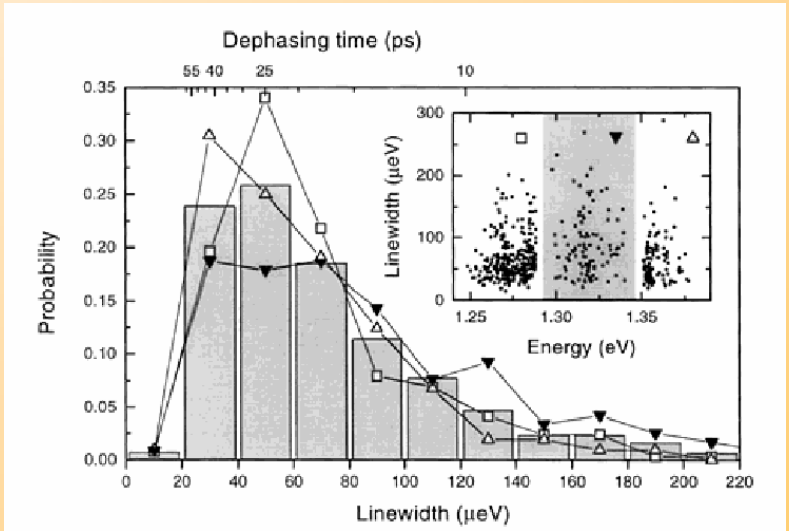

K. Leosson, J.R.Jensen, J.M.Hvam and W. Langbein, phys. stat. sol. **221**, 49 (2000)

Linewidth of ~50μeV (25ps dephasing time) but γ_{rad}~0.66μeV (1ns lifetime)

Annealed InAs QDs

Systematic study of confinement-dependent effects: Rapid thermal annealing

S. Fafard and C. Ni. Allen, Appl. Phys. Lett. **75**, 2374 (1999)

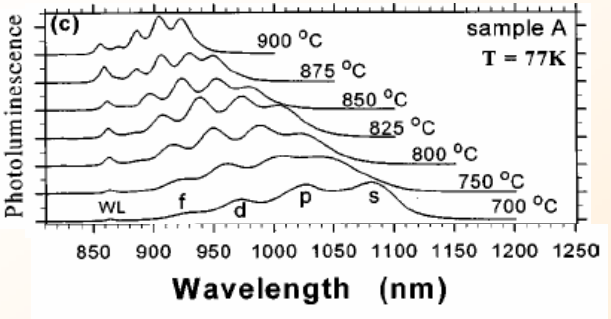

Thermally activated In-diffusion changes confinement potential

Vertical confinement larger than in-plane confinement ⇒
In-plane confinement determined by the potential created by the confinement energy in growth direction

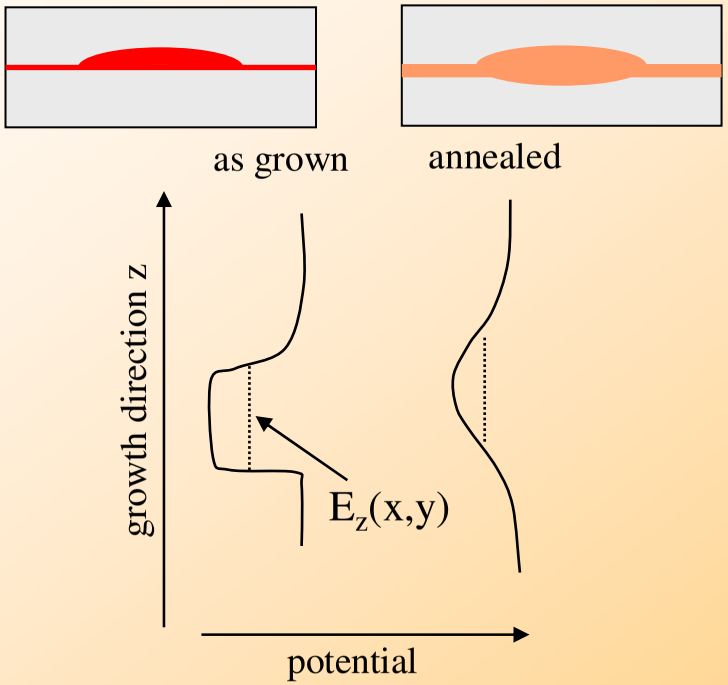

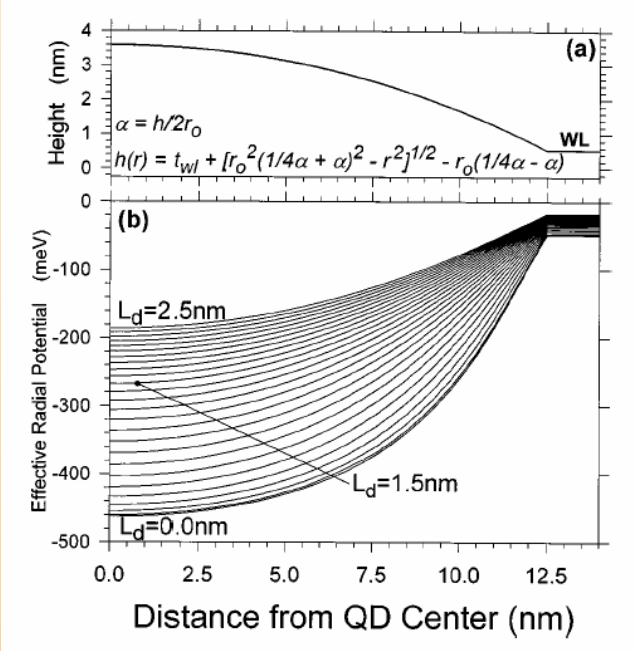

Annealed InAs QDs

Sample growth & annealing: V. Stavarache, D. Reuter, A. D.Wieck, University of Bochum, Germany

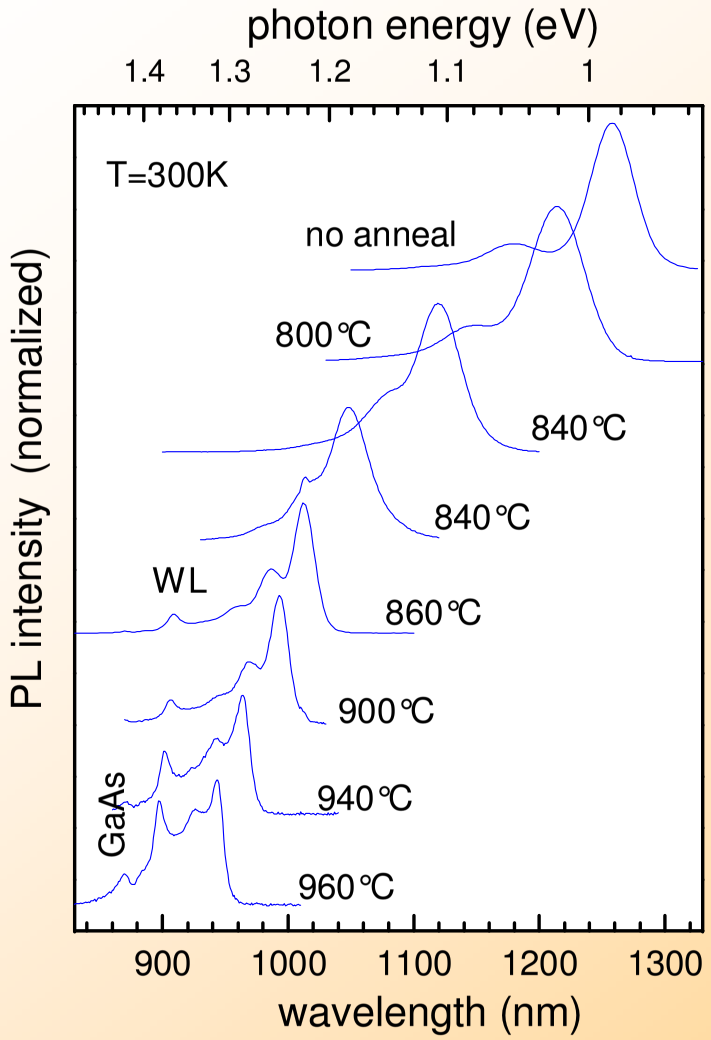

- 10 layers of InAs QDs in GaAs matrix, 100nm spacing between layers (no coupling)
- Rapid thermal annealing for 30 seconds
- Tuning of transition energy from 0.985 to 1.315 eV
- Tuning of confinement energy (QD ground state to wetting layer) from 340meV to 65meV
- Tuning of intersublevel spacing from 70meV to ~30 meV

Combination of directional and frequency selection

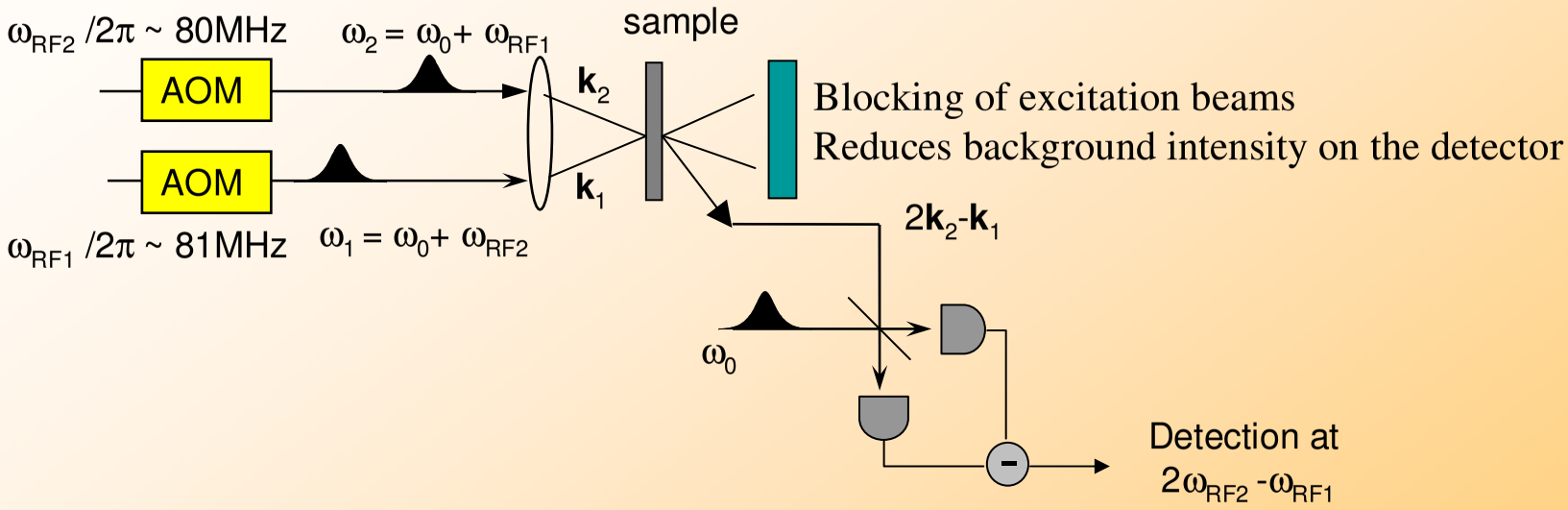

Experiments on single layers of self-organized InGaAs QDs:

- Input power ~1mW (third-order regime)
- Excitation spot size ~30μm
- Detection of coherent signal shot-noise limited (10^{-18} W/Hz$^{0.5}$)
- typical FWM intensity less than 10^{-10} of incident intensity
- excitation and detection polarizations freely adjustable

Langbein et al. Phys. Rev. B **69**, 161301R, and **70**, 033301 (2004); Borri et al. **71**, 115328 (2005)

Features visible in FWM dynamics

Polarization-dependent FWM:

polarization decay of phonon-assisted transitions

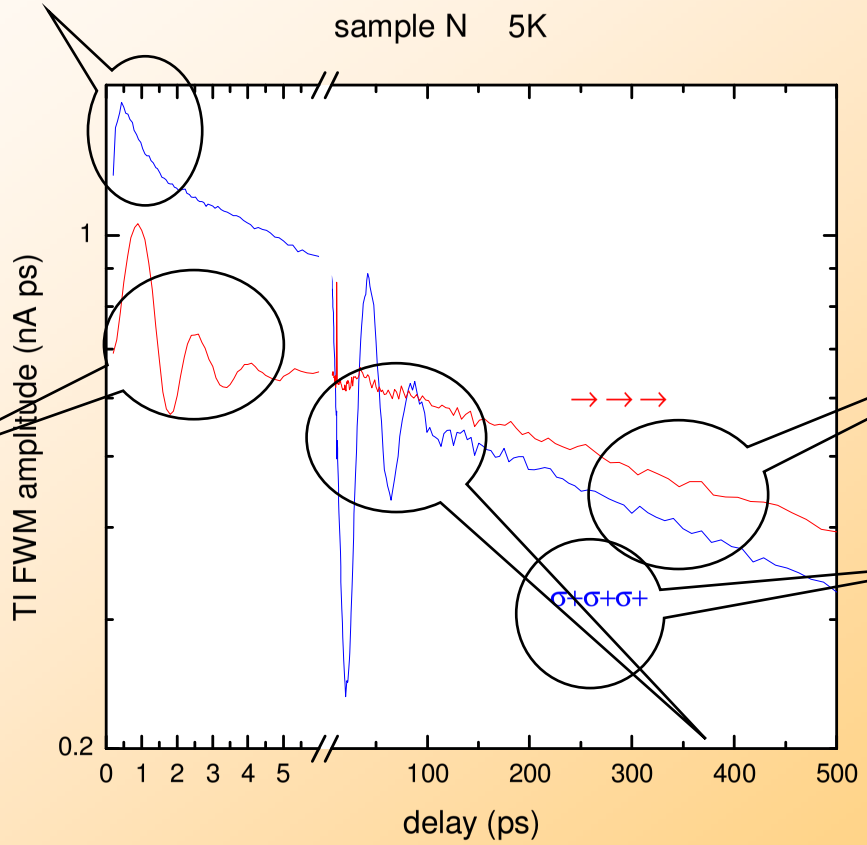

polarization decay of zero-phonon transition

exciton-biexciton polarization interference

Polarization configuration E_1, E_2, $E^{(3)}$

fine-structure quantum beats

Fine-structure splitting of excitons

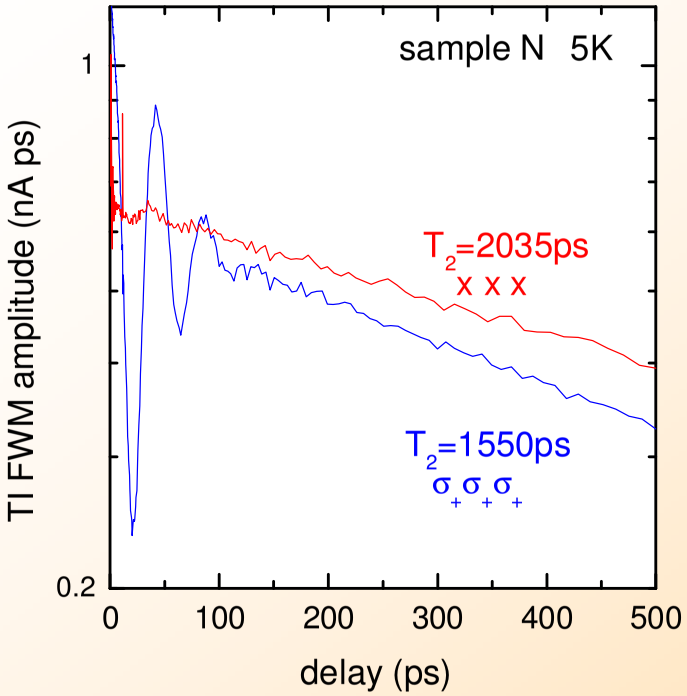

Polarization-dependence reveals exciton fine-structure:

- oscillations for circular polarization ($\sigma_+ \sigma_+ \sigma_+$)
- no oscillations for linear polarization (x x x)

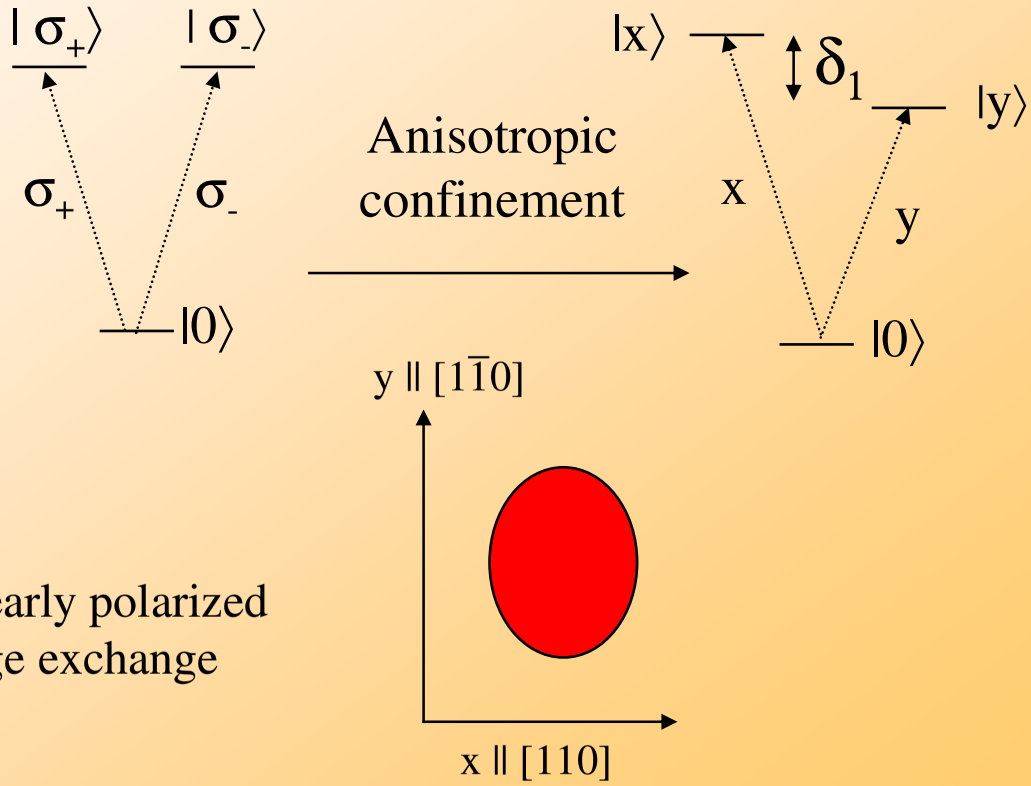

δ_1 : Splitting between two linearly polarized exciton states by long-range exchange

Fine-structure beat - circular excitation

Excitation: $|\sigma_+\rangle = \frac{1}{\sqrt{2}}(|x\rangle + i|y\rangle)$ Dynamics: $\frac{1}{\sqrt{2}}(e^{-i\omega t/2}|x\rangle + ie^{i\omega t/2}|y\rangle) = \cos(\omega t/2)|\sigma_+\rangle + i\sin(\omega t/2)|\sigma_-\rangle$ $\omega = \delta_1/\hbar$

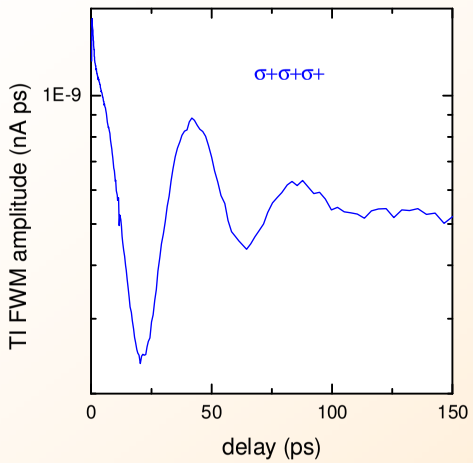

only $|\sigma_+\rangle$ creates FWM polarization, since pulse 2 is σ_+ polarized

$$P_{echo}^{(3)} \propto |\cos(\omega t/2)|^2 \propto 1+\cos(\omega t)$$

Damping of oscillations observed

$\Rightarrow$ QD ensemble exhibits a distribution p(ω) of ω

$$P_{echo}^{(3)} \propto 1+\int p(\omega)\cos(\omega t)d\omega$$

Consider $p(\omega) \propto \omega^{n-1}\exp(-n\omega/\omega_0)$ of average ω_0 and variance $\sigma = \omega_0/\sqrt{n}$

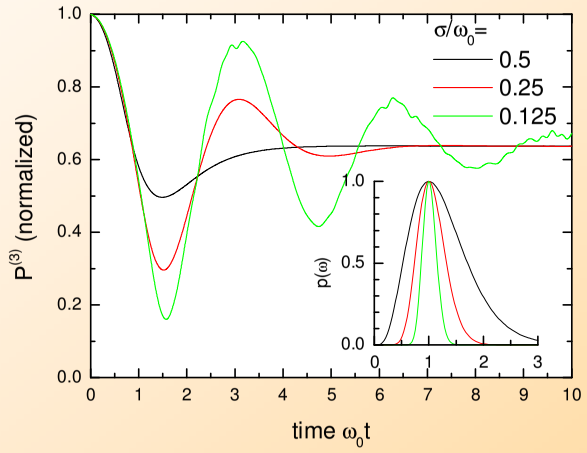

Fit to measured data determines average fine-structure splitting $\langle\delta_1\rangle$ and its variance $\sigma_1 = \sqrt{\langle\delta_1^2\rangle - \langle\delta_1\rangle^2}$

Observed oscillation amplitude smaller than model:
Charged QDs are present

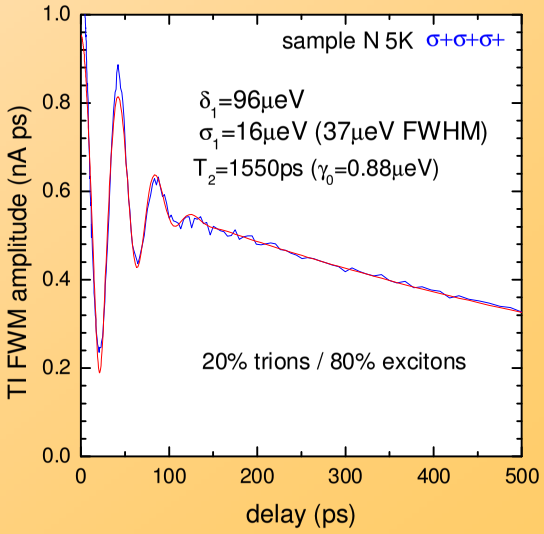

Fine-structure splitting versus annealing

W.Langbein, P. Borri, U.Woggon , V. Stavarache, D. Reuter, A. D. Wieck, Phys. Rev. **B** 69, 161301R (2004)

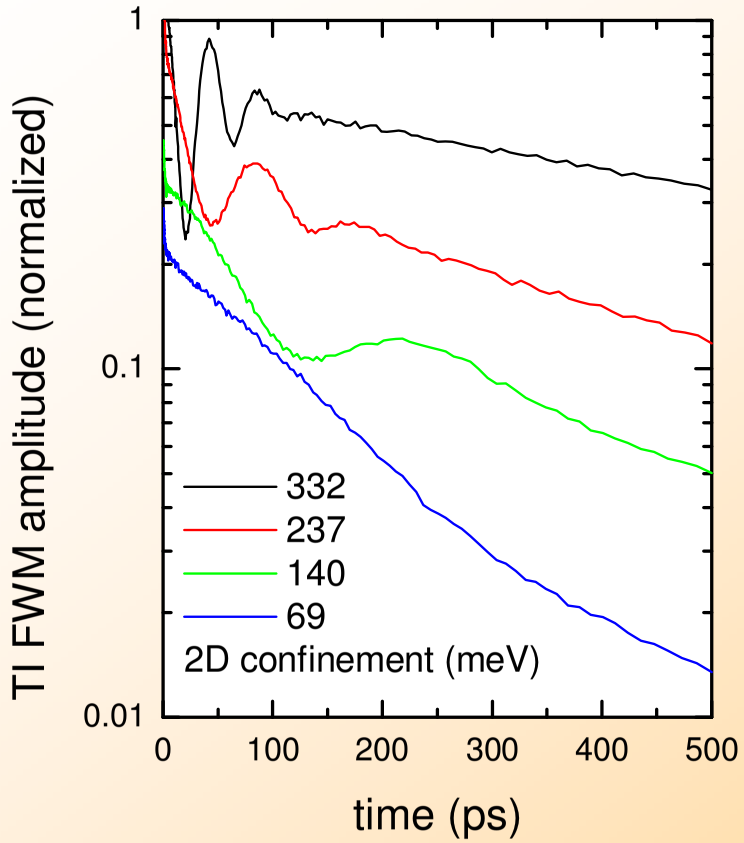

Strong dependence decrease of fine-structure splitting with annealing

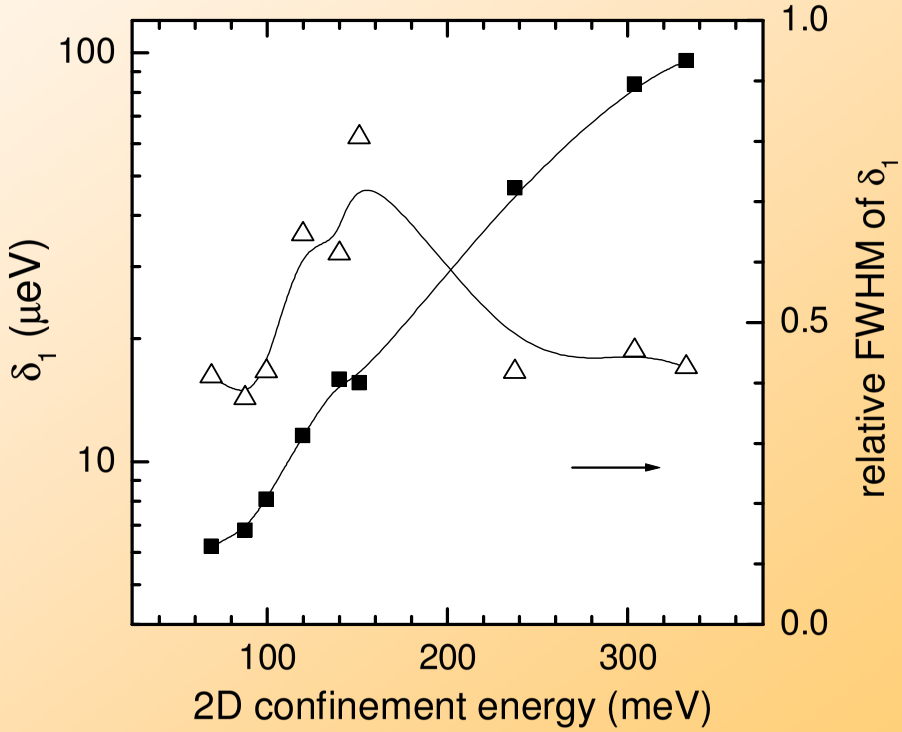

Relative width of inhomogeneous distribution rather constant

See also Tartakovskii et al. Phys. Rev. Lett. 93, 057401 (2004)

Dephasing of fine-structure split exciton states

W. Langbein, P. Borri, U. Woggon, V. Stavarache, D. Reuter, A. D. Wieck, Phys. Rev. **B**, 70, 033301 (2004)

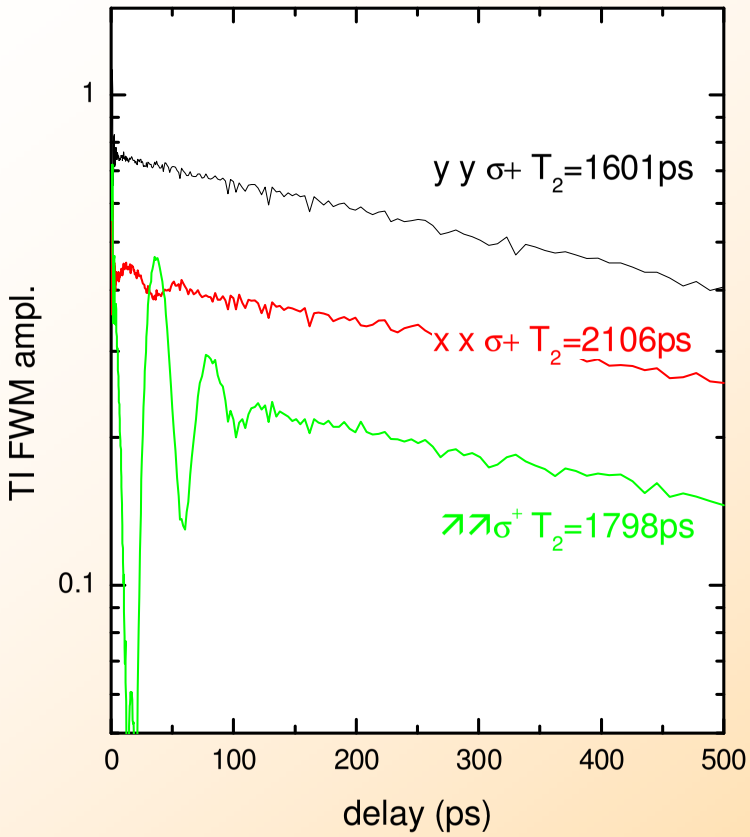

Fine-structure beat suppressed for [110] and [1-10] polarized excitation:

$\Rightarrow$ Dipole anisotropy of wavefunctions along (110)

Different polarizations show different decay rates.

Since $kT \gg \delta_1$ this is not spin relaxation

$\Rightarrow$ radiative lifetimes are different

$\Rightarrow$ oscillator strengths are different $\gamma_r \propto \mu^2$

$$\frac{\mu_y}{\mu_x} = \sqrt{\frac{\gamma_y}{\gamma_x}} = 1.147 \pm 0.005$$

This assumes radiatively limited dephasing

We can cross-check by the FWM signal strength

$$E^{(3)} \propto \mu^4$$

and we find

$$\frac{\mu_y}{\mu_x} = \sqrt[4]{\frac{E_y^{(3)}}{E_x^{(3)}}} = 1.149 \pm 0.01$$

Radiative lifetime limited dephasing

Biexciton binding energy

W. Langbein, P. Borri, U. Woggon, V. Stavarache, D. Reuter, A. D. Wieck, Phys. Rev. **B** 69, 161301R (2004)

δ_B : Difference between the sum of the two finestructure-split exciton energies and the biexciton energy $\delta_B = E_x + E_y - E_B$

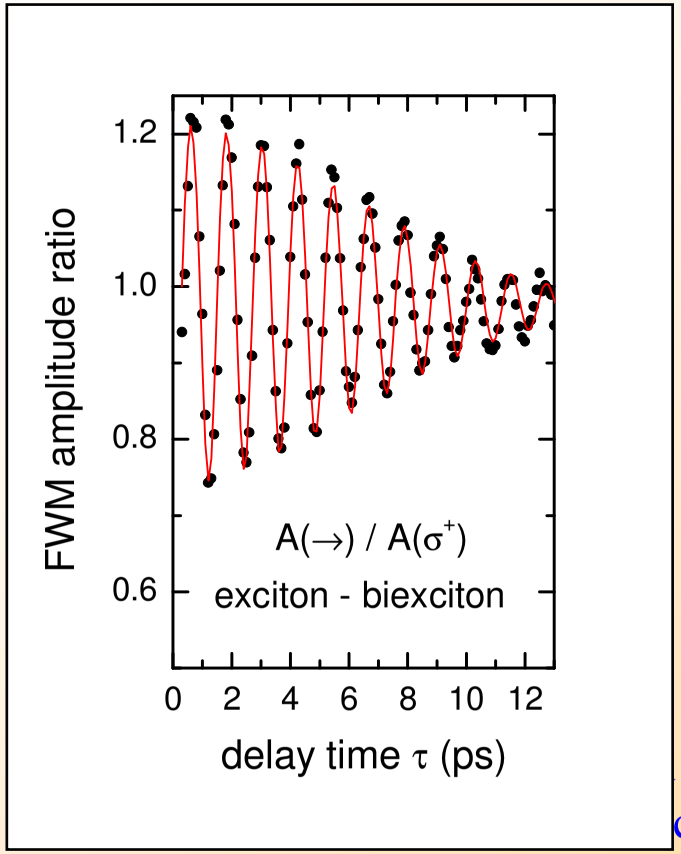

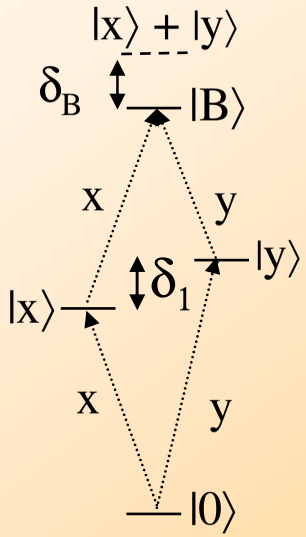

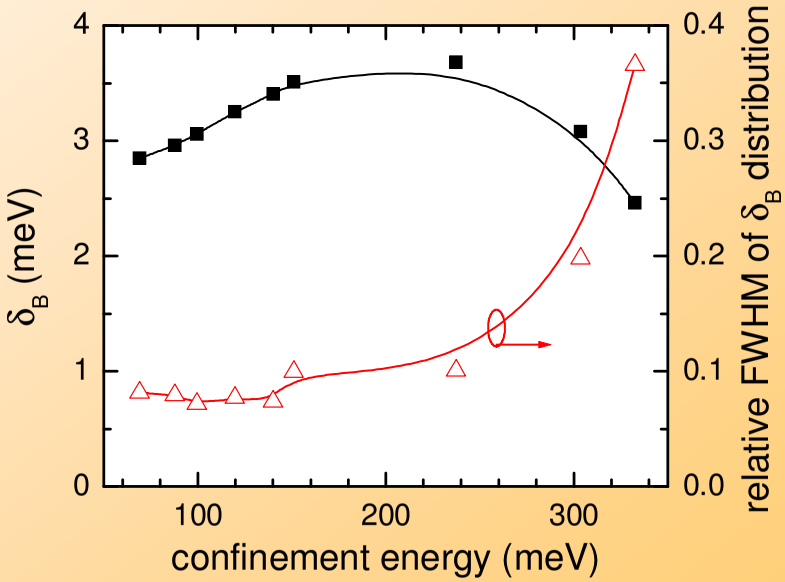

binding energy rather insensitive to annealing

creased and distribution decreased by initial annealing:

symmetrizing of the vertical confinement

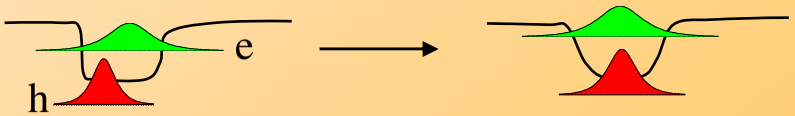

Acoustic-phonon assisted transitions in QDs

Small spatial extension of the electron-hole pair
⇒ Single pair creates a large local density (10^{19}cm^{-3})
⇒ electronic binding of atoms disturbed
⇒ lattice equilibrium position is shifted

⇒ phonon-assisted optical transitions exist, following the Franck-Condon principle for absorption/emission of acoustic phonons.
⇒ Each phonon mode creates a series of discrete lines on each side of the zero-phonon line (ZPL).

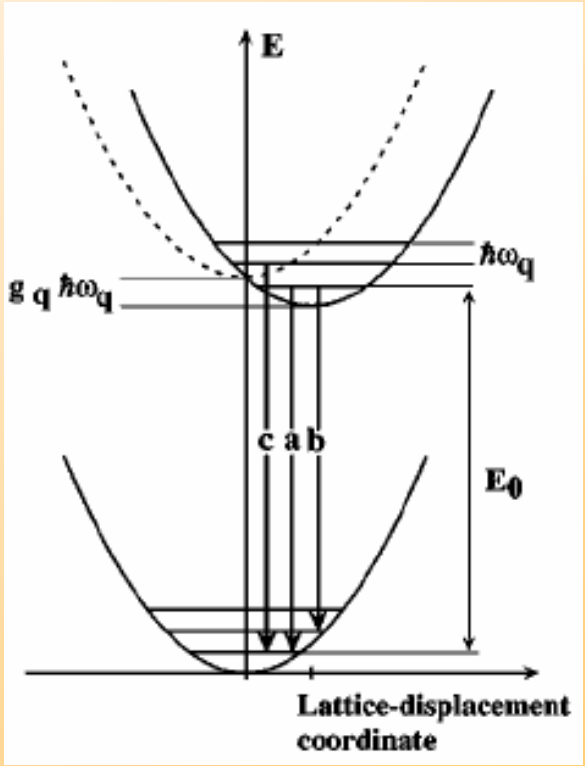

Compared to bi-atomic molecules:

- zero-phonon transition has relevant strength
- phonons are a continuum

Theoretical description: independent boson model:

$$H = \mathcal{E}_0 B^\dagger B + \sum_{\vec{q}} \hbar\omega_{\vec{q}} a_{\vec{q}}^\dagger a_{\vec{q}} + \sum_{\vec{q}} M_{\vec{q}} \left(a_{\vec{q}}^\dagger + a_{-\vec{q}}\right) B^\dagger B$$

H commutes with excitonic density $B^\dagger B$ (pure dephasing)

B. Krummheuer *et al.* PRB **65** 195313 (2002), R. Zimmermann and E. Runge ICPS26 (2002)

Exciton-acoustic phonon interaction in QDs

Deformation potential coupling with acoustic phonons of dispersion: $\omega_{\vec{q}} = qs$

$$M_{\vec{q}} = \sqrt{\frac{\hbar\omega_{\vec{q}}}{2s^2\rho V}} \int d\vec{r}_e d\vec{r}_h \left|\Psi(\vec{r}_e,\vec{r}_h)\right|^2 \left(D_c e^{i\vec{q}\vec{r}_e} - D_v e^{i\vec{q}\vec{r}_h}\right)$$

D_c,D_v: deformation potential coupling constants

Non-exponential decay of the first-order polarization:

$P^{(1)}(t) = i \exp(-i(\omega_0-\Delta)t + R(t) - S)$

Δ: polaron shift
R(t=0) = S : Huang-Rhys factor

$$R(t) = \sum_{\vec{q}} \frac{M_{\vec{q}}^2}{\hbar\omega_{\vec{q}}^2}\left[\left(2N_{\vec{q}}+1\right)\cos\left(\omega_{\vec{q}}t\right) - i\sin\left(\omega_{\vec{q}}t\right)\right]$$

$$N_{\vec{q}} = \frac{1}{e^{\hbar\omega_{\vec{q}}/k_BT}-1}$$

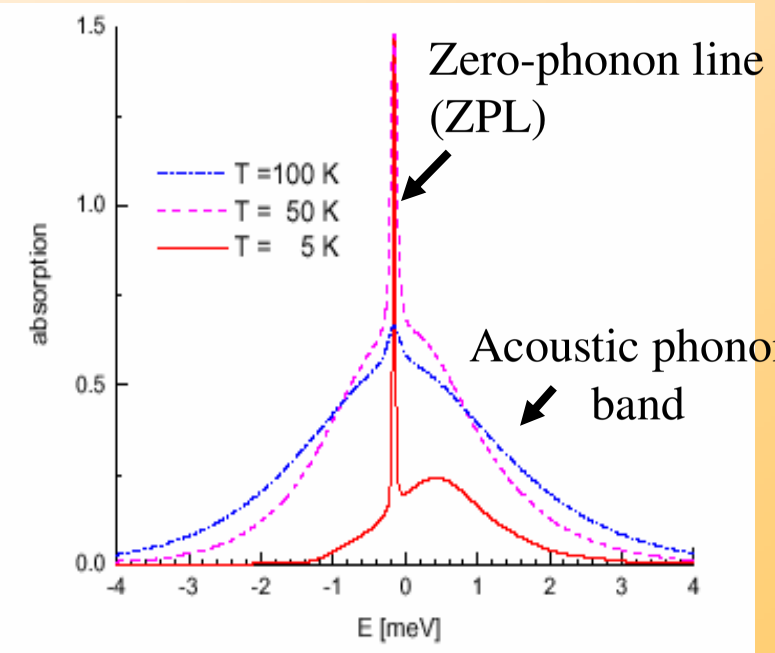

R. Zimmermann and E. Runge ICPS26 (2002)

Absorption spectrum: $a(\omega) \propto \mathrm{Im}\int_0^\infty dt P^{(1)}(t) e^{i\omega t}$

W.Langbein, Ultrafast nonlinear spectroscopy and control of semiconductor nanostructures

Phonon-assisted transitions: experiments

Fast initial decay of FWM due to dephasing of phonon-assisted transitions

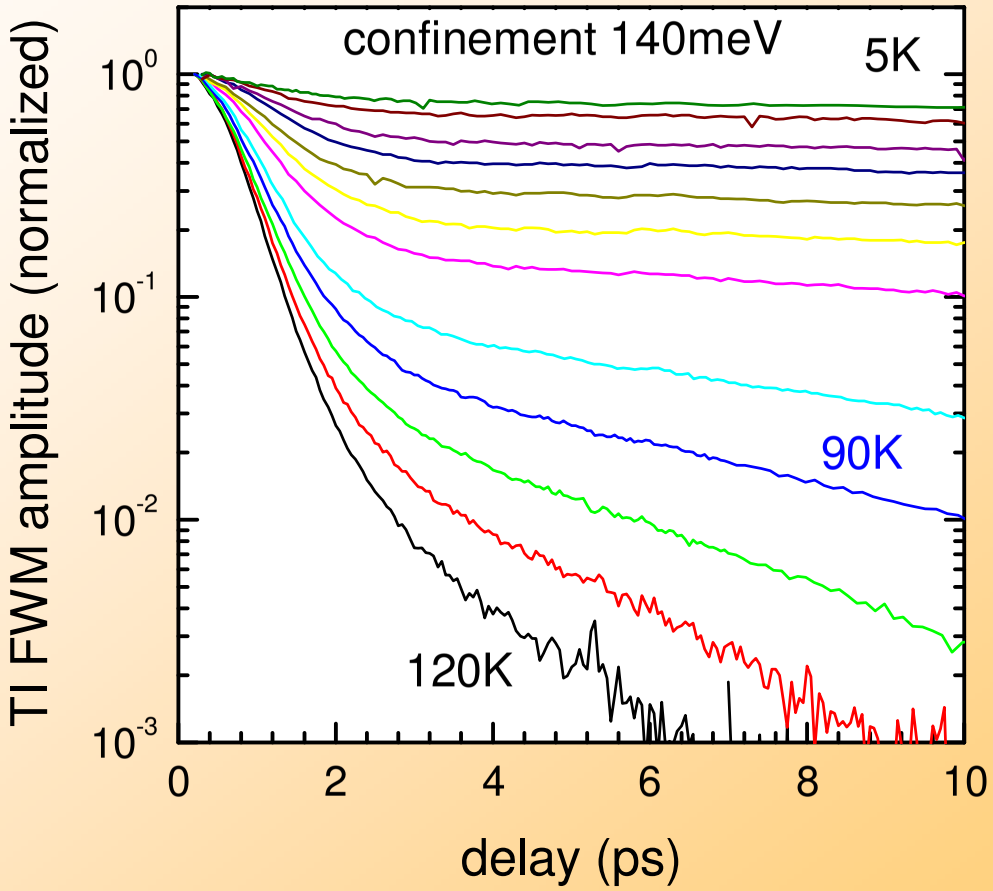

W.Langbein, Ultrafast nonlinear spectroscopy and control of semiconductor nanostructures

Weight of the zero-phonon line

Zero-phonon line weight: Area fraction of the ZPL in the absorption spectrum Z = exp(-S)
(For negligible ZPL dephasing: equal to the normalized polarization amplitude for t →∞)

The asymptotic value of the TI FWM photon echo is $Z^3 = \exp(-3S)$
A. Vagov *et al.* PRB **66** 165312 (2002)

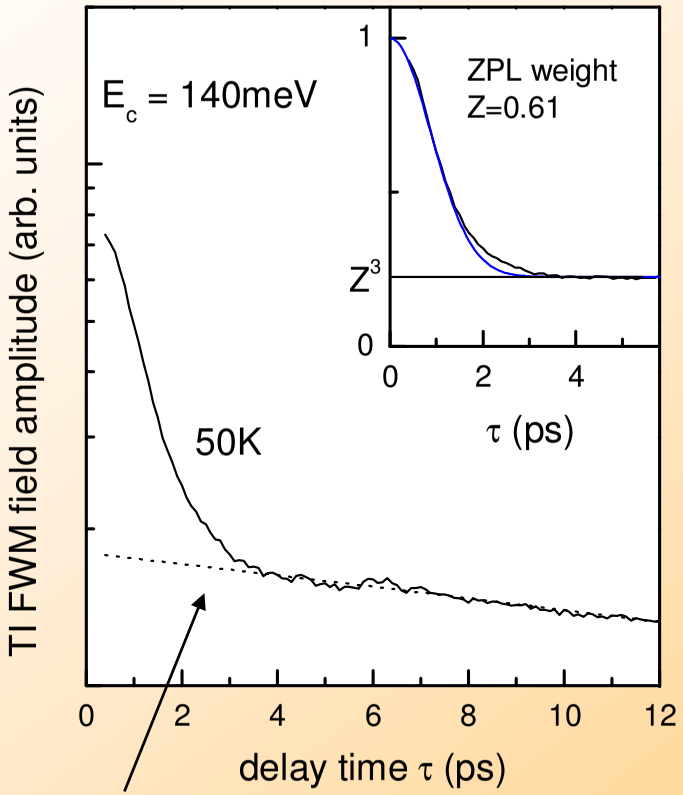

Correction for exponential ZPL decay

ZPL weight decreases with increasing temperature and decreasing extension of the exciton wavefunction, as expected by the model

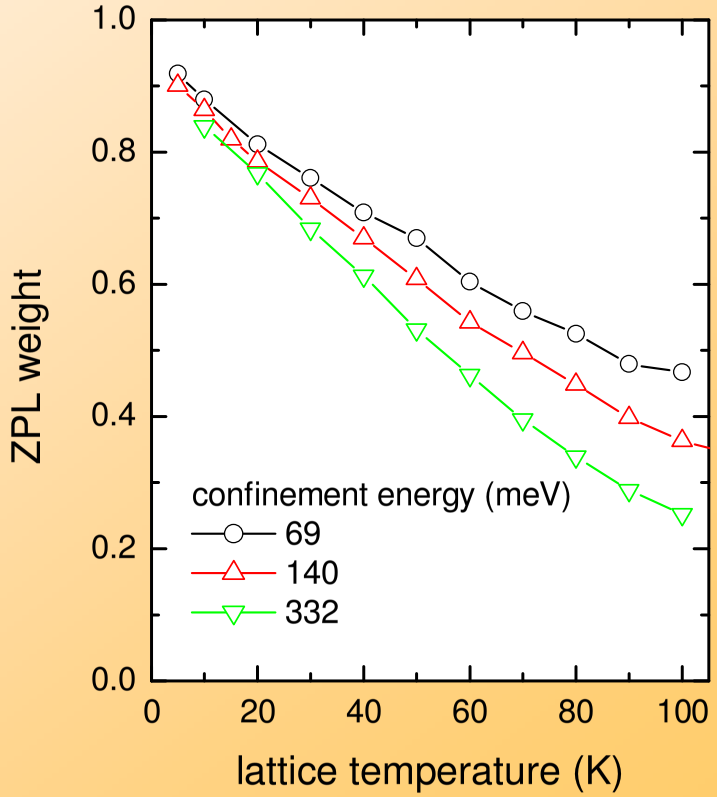

Dephasing of zero-phonon transition versus temperature

Zero-phonon line polarization:
exponential decay rate γ

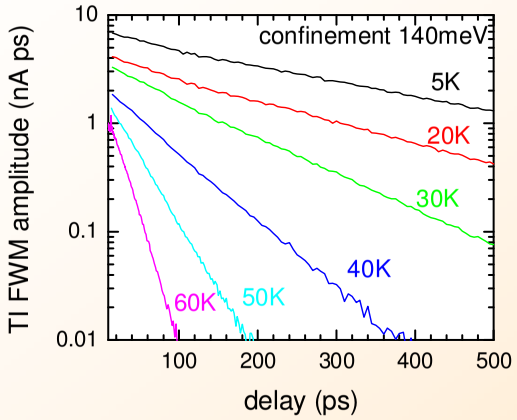

Temperature-dependence fitted by

$$\gamma(T) = \gamma_0 + \frac{b_1}{\exp\left(\frac{E_1}{kT}\right) - 1} + \frac{b_2}{\exp\left(\frac{E_2}{kT}\right) - 1}$$

natural (radiative) linewidth

acoustic phonons ?

optical phonons ?

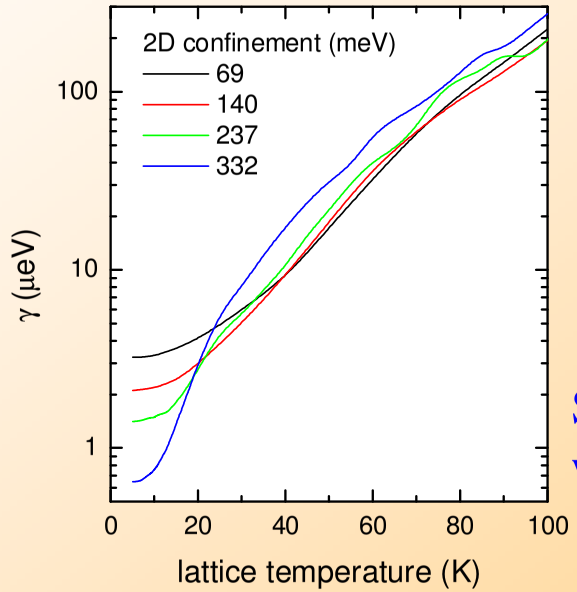

Systematic change
with annealing

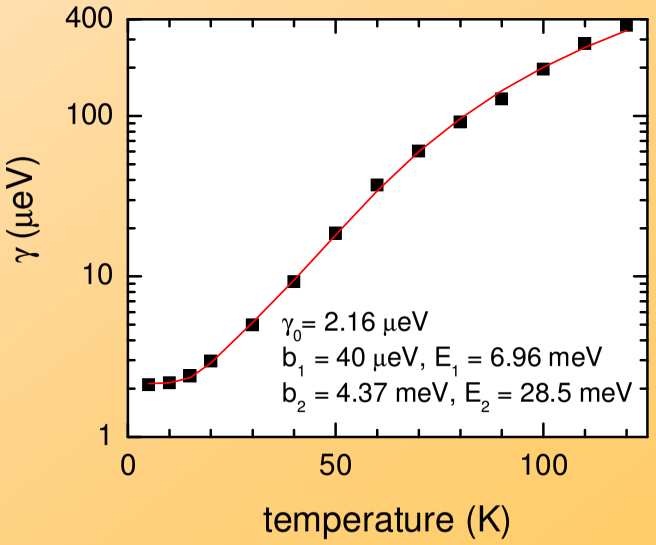

W.Langbein, Ultrafast nonlinear spectroscopy and control of semiconductor nanostructures

Low-temperatures: radiatively limited dephasing times

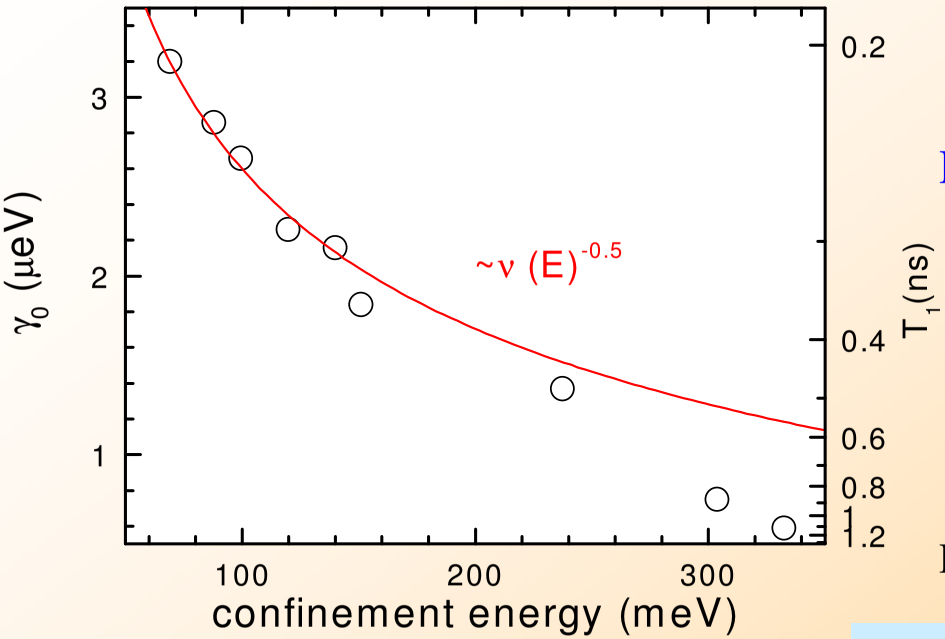

Decrease of dephasing rate with increasing confinement:
Radiative lifetime changes from 200ps to 1ns

Radiative rate is proportional to the coherence area *A*:

Parabolic in-plane confinement of „rigid“ exciton:

$$V(r) \propto \omega^2 \Rightarrow \omega \propto \sqrt{E_{\text{conf}}} \qquad A \propto l^2 \propto \omega^{-1} \propto 1/\sqrt{E_{\text{conf}}}$$

Deviation for weak annealing (i.e. large confinement):
Reduced e-h overlap by asymmetric vertical confinement of electron and hole in the exciton

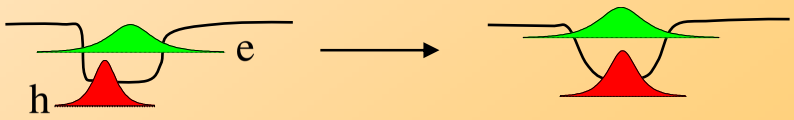

ZPL dephasing : phonon interaction parameters

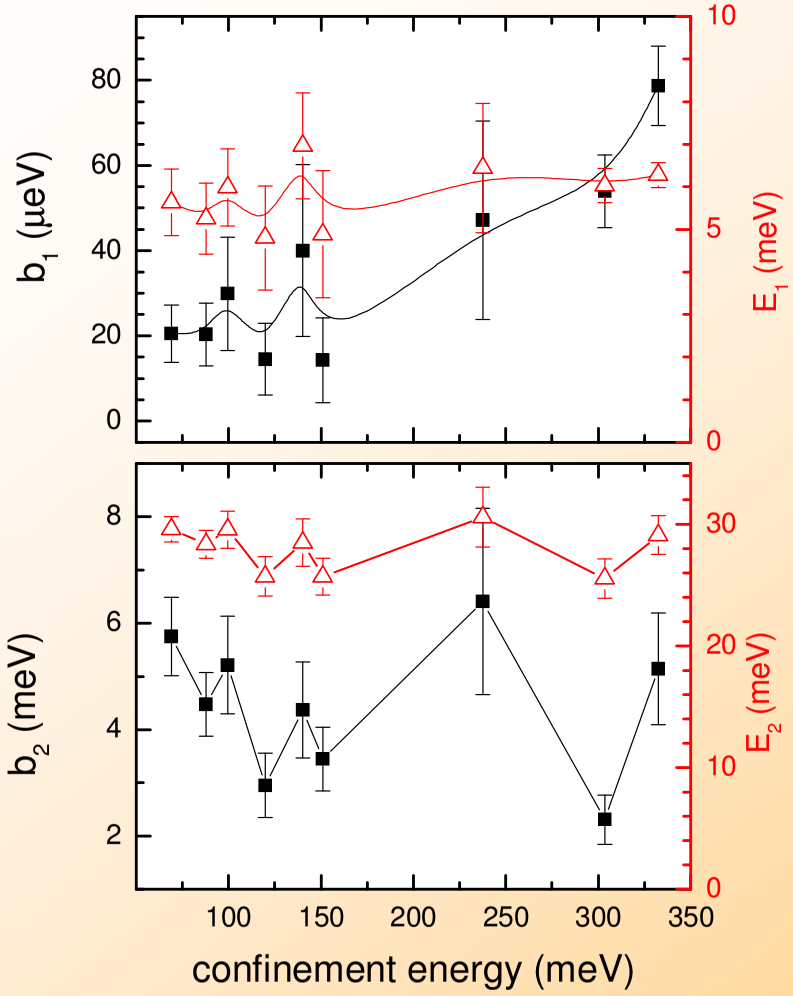

$$\gamma(T) = \gamma_0 + \frac{b_1}{\exp\left(\frac{E_1}{kT}\right) - 1} + \frac{b_2}{\exp\left(\frac{E_2}{kT}\right) - 1}$$

Both activated parts show an activation energy nearly independent of confinement energy !

Contradicts the importance of single phonon absorption to excited electronic levels for the dephasing !

W.Langbein, Ultrafast nonlinear spectroscopy and control of semiconductor nanostructures

ZPL dephasing : phonon interaction parameters

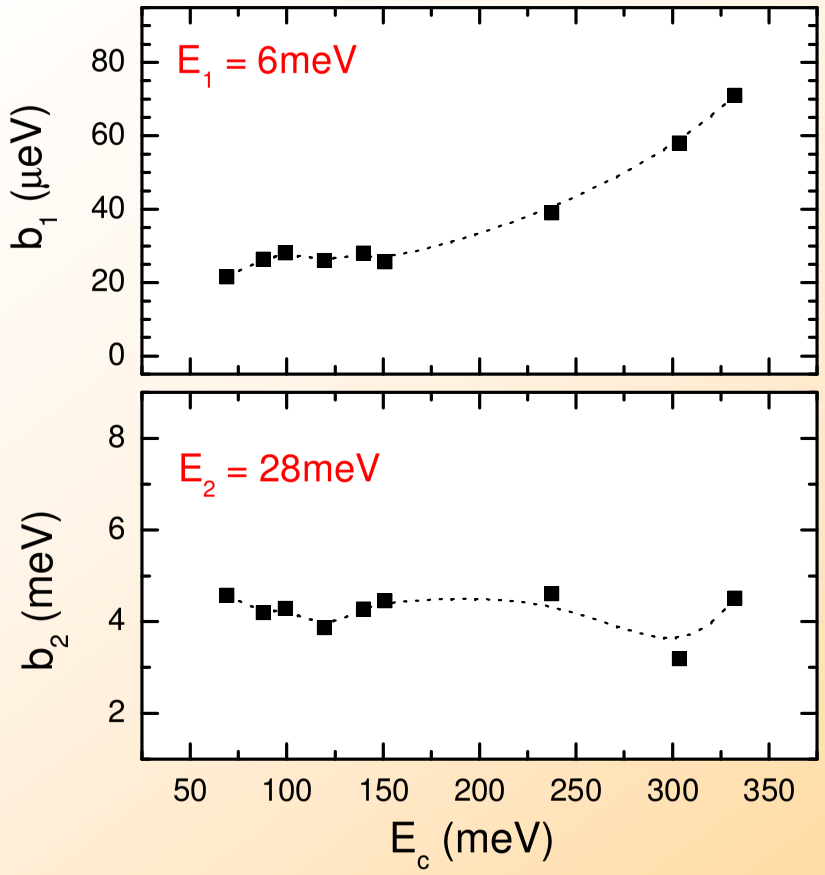

- Activation energies independent of E_c
  6meV: acoutical phonons
  28meV: optical phonons

No significant influence of electronic level spacing: phonon absorption is not the dominant process

- Systematic dependence of b_1 on E_c

Stronger coupling to acoustic phonons with decrasing size, similar to the behaviour of the ZPL weight

- Also ZPL dephasing is due to elastic phonon interaction ?

P. Borri *et al.*, Phys. Rev. B submitted

Optical Rabi oscillations

Two-level system in presence of a time-dependent electric field $\vec{E} = \Theta(t)\vec{E}_0 \cos \omega t$

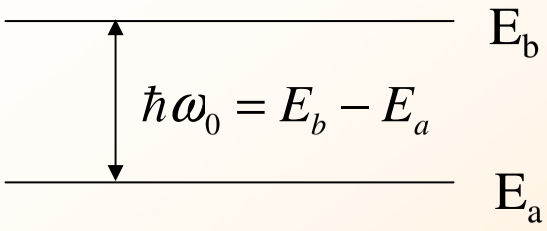

$\omega_R = \dfrac{\vec{\mu} \cdot \vec{E}_0}{\hbar}$: Rabi frequency

$|a|^2$ ($|b|^2$) : occupation probability of the ground (excited) state

$\vec{\mu}$: transition dipole moment

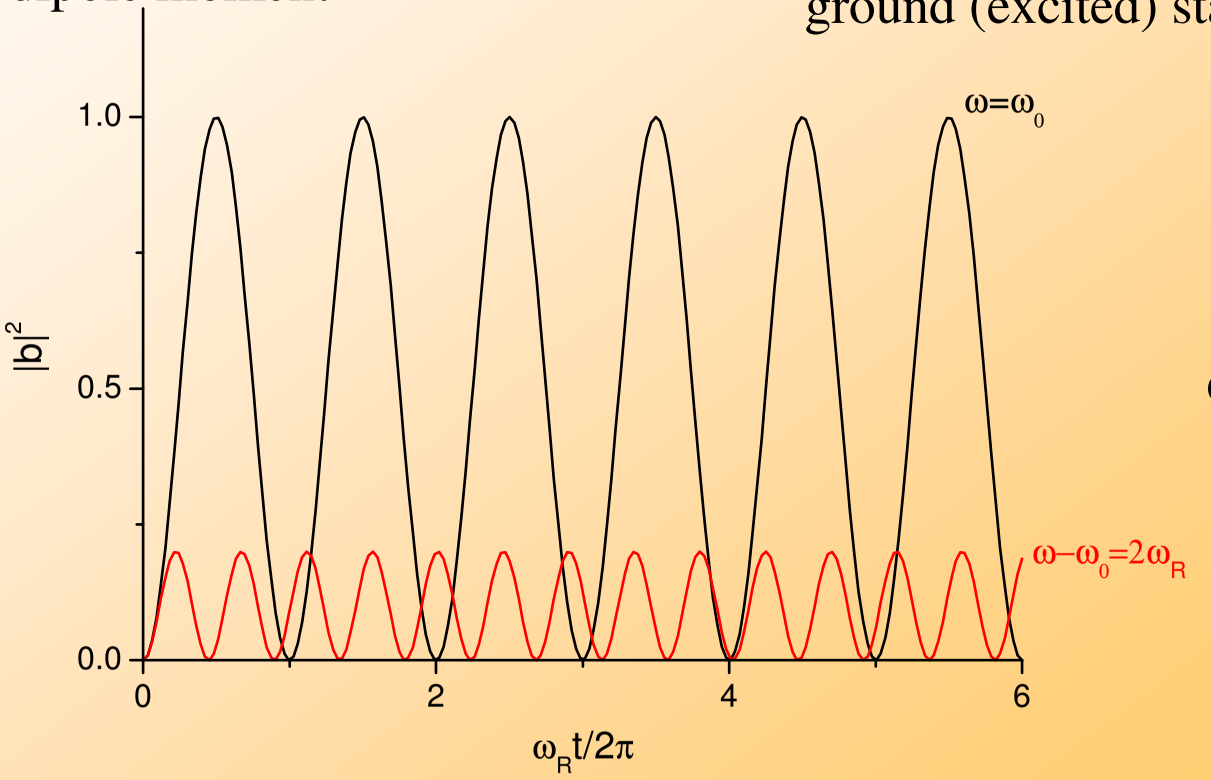

ω-ω_0=detuning

W.Langbein, Ultrafast nonlinear spectroscopy and control of semiconductor nanostructures

Optical Rabi oscillations

The effect of a radiative damping $\gamma=1/T_2$ of the polarization (T_2 dephasing time):

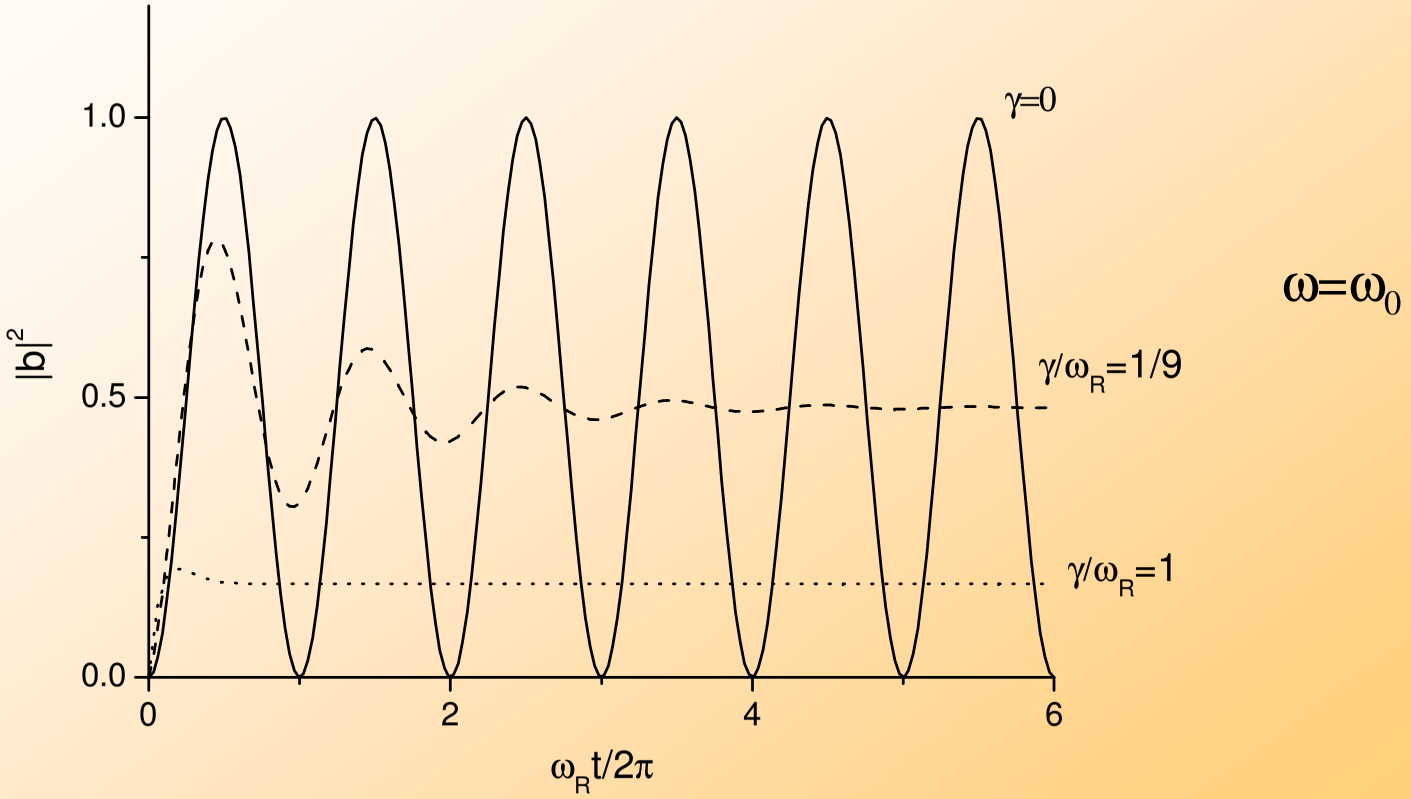

Population flopping over many periods is possible in systems with long dephasing times and large transition dipole moments: $\gamma/\omega_R<<1$.

Rabi oscillations versus pulse area

Pulsed excitation: e.g. $E_0=E_{00}\exp(-(t/t_0)^2)$

Pulse area: time-integrated Rabi frequency $\theta = \int_{-\infty}^{+\infty} \frac{\vec{\mu}\cdot\vec{E}_0}{\hbar} dt$

Population difference after pulse ($t >> t_0$)

$\Delta N = |b|^2 - |a|^2$

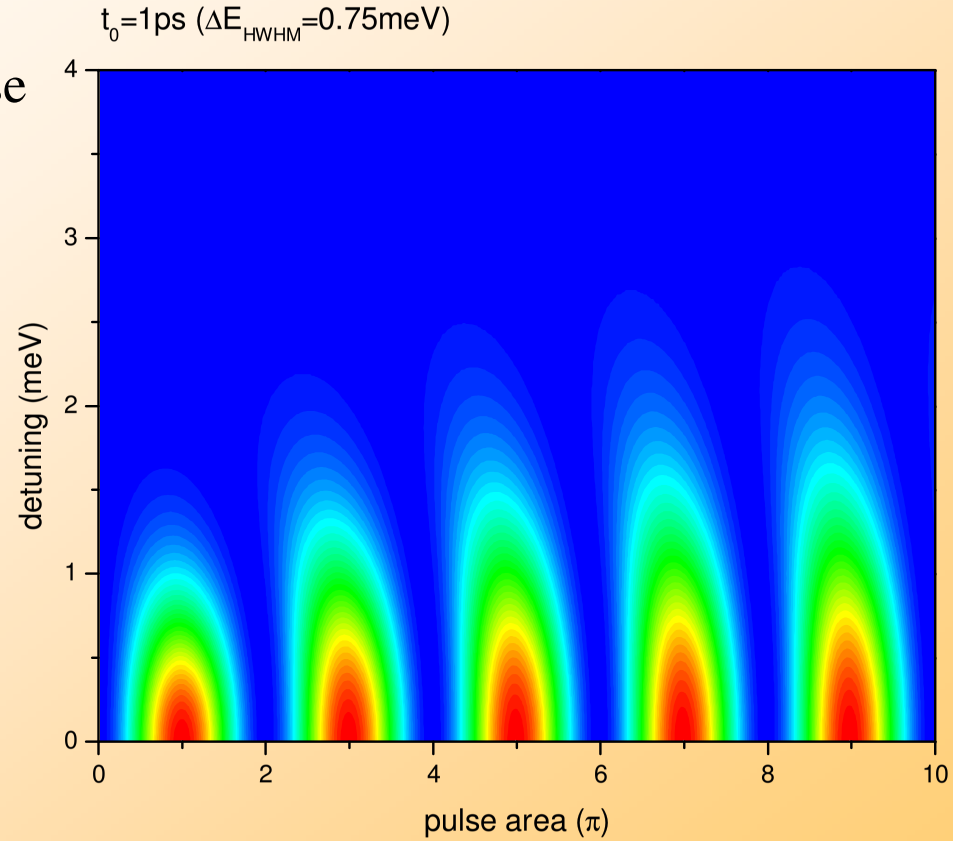

γ=0

blue = -1
red = +1

Initial conditions:

$\Delta N = -1$ ($t << -t_0$)

InGaAs quantum dots: investigated sample

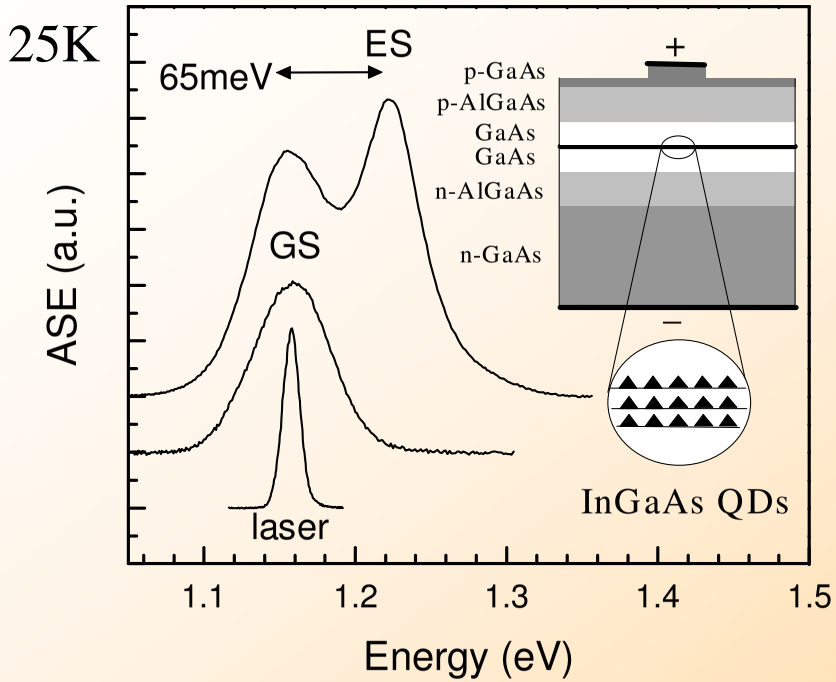

Inhomogeneous broadening: 60meV

GS-ES separation: 65meV

GS-WL separation ~220meV

ridge waveguide 5x500µm
3 stacked QD layers
35nm GaAs spacers
areal dot density ~$2x10^{10}cm^{-2}$

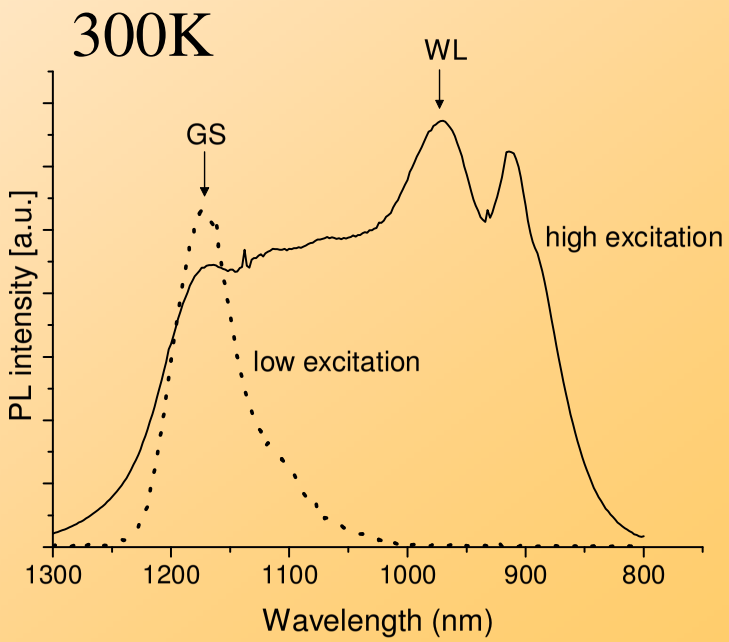

W.Langbein, Ultrafast nonlinear spectroscopy and control of semiconductor nanostructures

Differential transmission

Absorption coefficient of an inhomogeneously broadened ensemble:

$$\alpha(\omega) = \int_{-\infty}^{+\infty} \sigma_0 \frac{1/T_2}{(\omega-\omega_\xi)^2 + (1/T_2)^2} \Delta N(\omega_c - \omega_\xi, \theta_{pump}) f(\omega_\xi) d\omega_\xi \xrightarrow[T_2\to\infty]{} \sigma_0 \Delta N(\omega_c - \omega, \theta_{pump}) f(\omega)$$

Lorentz. pop. diff. inh. distrib.

α is probed by a weak probe pulse after the pump: differential transmission intensity of the probe

t_0=1ps

T=10K

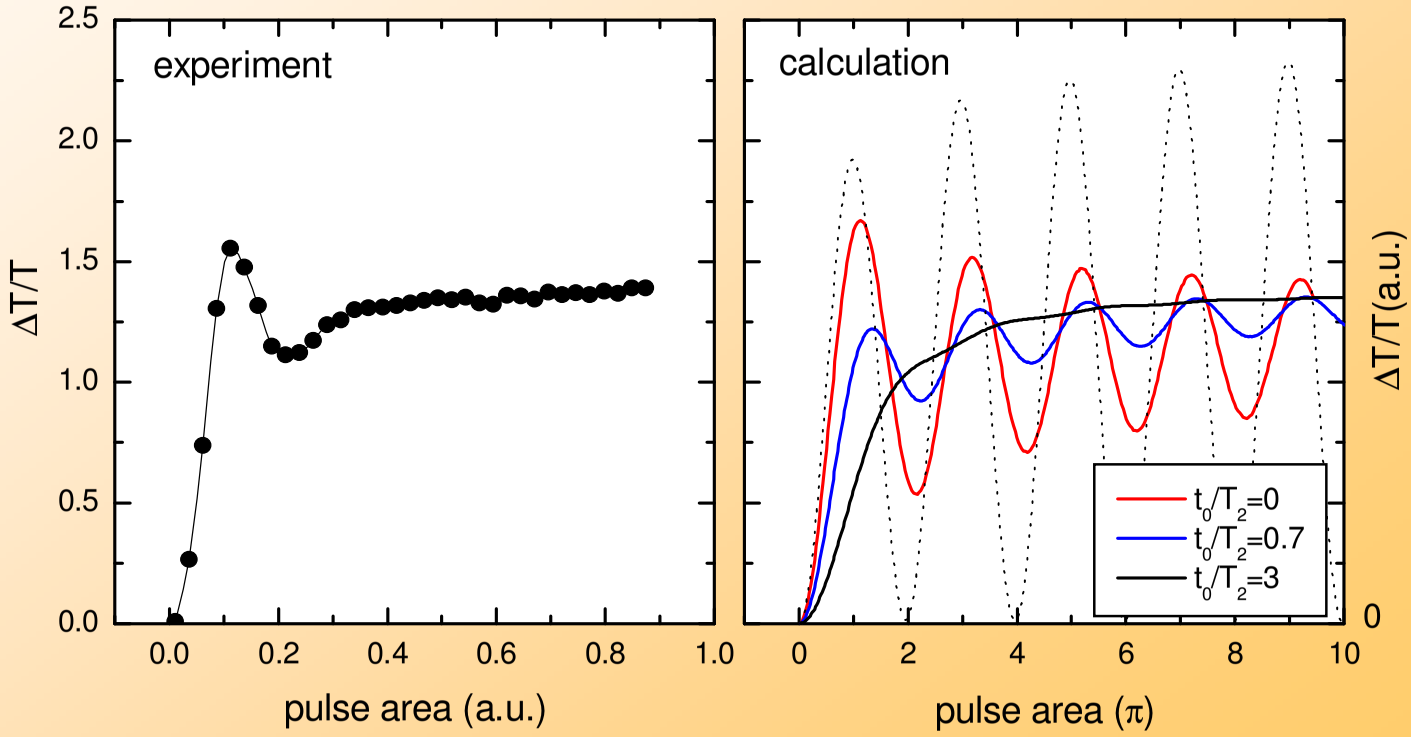

W.Langbein, Ultrafast nonlinear spectroscopy and control of semiconductor nanostructures

Study of the damping versus pulse area: Biexciton and dephasing

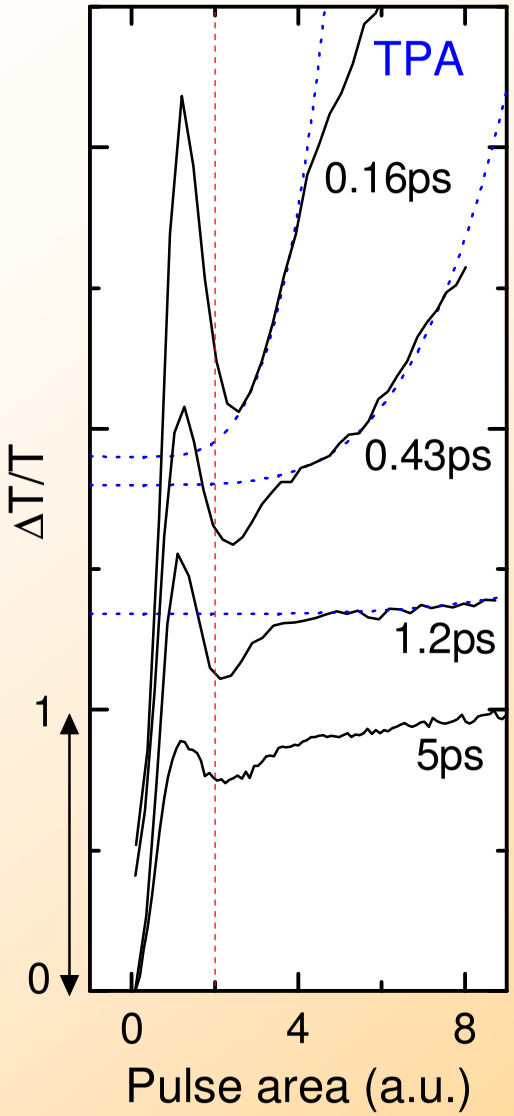

Differential transmission intensity using different pulse durations

We measured E_{XX}=3meV biexciton binding energy. If the pulse spectral width $\Delta E << E_{XX}$ the X-XX transition is out of resonance. However, for all pulses the damping of the oscillations remains. When $\Delta E \sim E_{XX}$ the oscillation changes period.

If $t_0 > T_2$ dephasing is important. We observe a quenching of the amplitude of the oscillations with increasing t_0. For short t_0 two-photon absorption (TPA density$\sim(\theta/t_0)^4 t_0$) in the waveguide covers the Rabi oscillations.

W.Langbein, Ultrafast nonlinear spectroscopy and control of semiconductor nanostructures

Calculations: Optical Bloch Equations

Basic equations:

$$i\hbar\frac{\partial\Psi}{\partial t} = (H_0 + V)\Psi$$

$$i\hbar\frac{\partial\Psi_i}{\partial t} = H_0\Psi_i = E_i\Psi_i$$

$$\Psi_i = \varphi_i e^{-\frac{iE_i t}{\hbar}}$$

$$\Psi = \sum_i a_i\Psi_i$$

$$\rho_{ij} = a_i^* a_j$$

$$\frac{d\rho_{ij}}{dt} = -\frac{i}{\hbar}\sum_k(\rho_{ik}V_{jk} - \rho_{jk}^* V_{ik}^*)$$

$$V_{ij} = e^{\frac{i}{\hbar}(E_i - E_j)t}\left(-\vec{\mu}_{ij}\vec{E}\right)$$

Considered 4-level system:

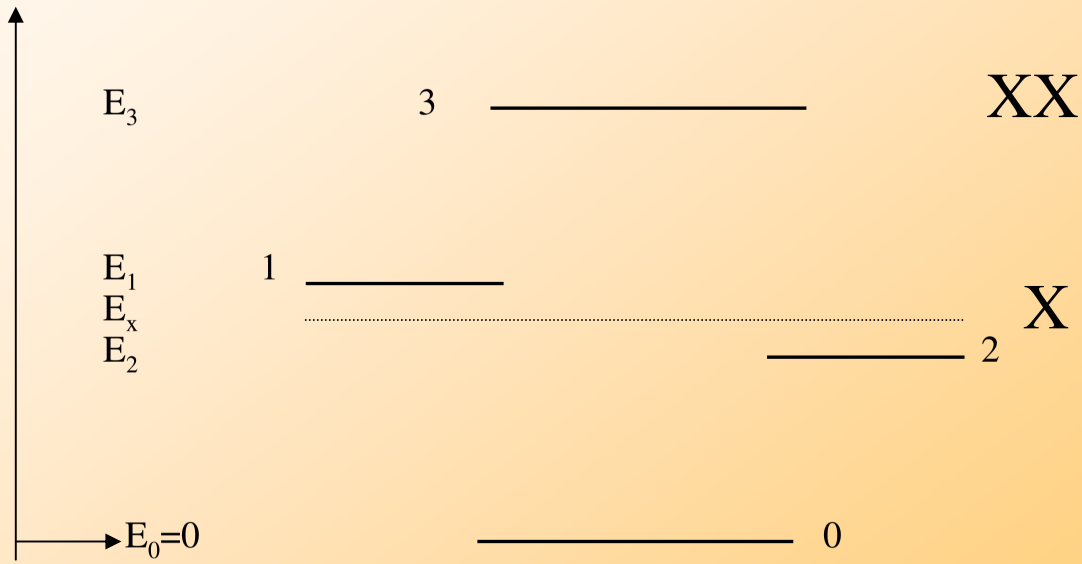

$\Delta = E_1 - E_2$ (exciton fine-structure splitting)
$-E_{XX} = E_3 - 2E_x$ (biexciton binding energy)

Dipole-allowed transitions:

Only $V_{10}, V_{20}, V_{32}, V_{31}$ (and c.c.) are different from zero.

Optical Bloch Equations with damping

Damping rates:

populations

$$\frac{d\rho_{00}}{dt} = ... + (\rho_{11} + \rho_{22})g_{1X}$$

$$\frac{d\rho_{11}}{dt} = ... + \rho_{33}\frac{g_{1XX}}{2} - \rho_{11}g_{1X}$$

$$\frac{d\rho_{22}}{dt} = ... + \rho_{33}\frac{g_{1XX}}{2} - \rho_{22}g_{1X}$$

$$\frac{d\rho_{33}}{dt} = ... - \rho_{33}g_{1XX}$$

coherences

$$\frac{d\rho_{10}}{dt} = ... - \rho_{10}g_{2X}$$

$$\frac{d\rho_{20}}{dt} = ... - \rho_{20}g_{2X}$$

$$\frac{d\rho_{31}}{dt} = ... - \rho_{31}g_{2XTXX}$$

$$\frac{d\rho_{32}}{dt} = ... - \rho_{32}g_{2XTXX}$$

$$\frac{d\rho_{30}}{dt} = ... - \rho_{30}g_{2XX}$$

$$\frac{d\rho_{21}}{dt} = ... - \rho_{21}g_{2XTX}$$

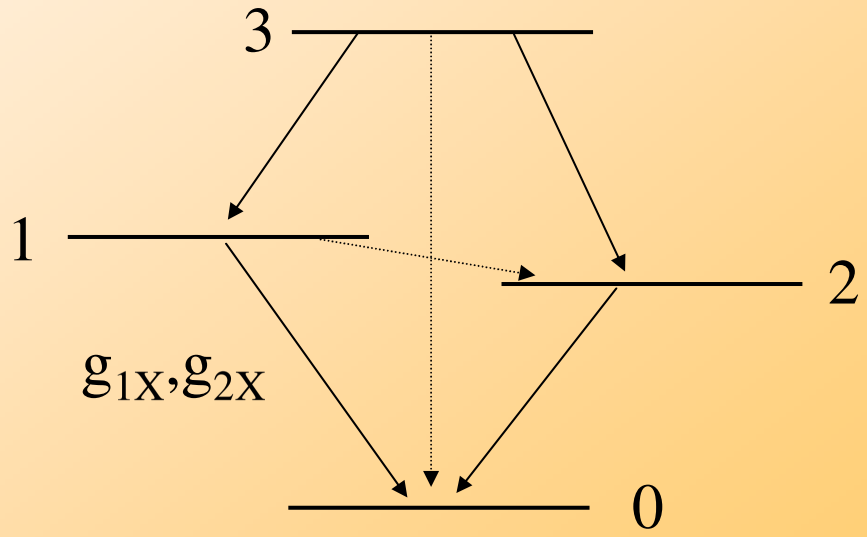

W.Langbein, Ultrafast nonlinear spectroscopy and control of semiconductor nanostructures

Chosen parameters for calculations

Fine structure splitting ~100μeV (important only for $t_0 \geq 5$ps)
Simplified calculation with Δ=0:

$\vec{\mu}_{01}\vec{E} = \vec{\mu}_{13}\vec{E}$
$\vec{\mu}_{02}\vec{E} = 0$
$\vec{\mu}_{23}\vec{E} = 0$
E_{XX}=3meV

Linearly polarized field along 0-1-3 transitions and same 0-X and X-XX dipole

Dephasing:

At 10K we measure $1/g_{2X}$=500ps>>t_0. However, the polarization decay is *non-exponential* with an initial fast dephasing time of ~1.5ps (non-Lorentzian lineshape).

Population lifetimes

$(g_{1X})^{-1}$ = 1ns>>t_0

are not important

Pulse field with TE_0 spatial profile:

$$E_0(t,r) = E_{00}e^{-(t/t_0)^2}\Psi_{TE_0}(r) = E_{00}e^{-(t/t_0)^2}\mathrm{sech}(r/r_0)$$

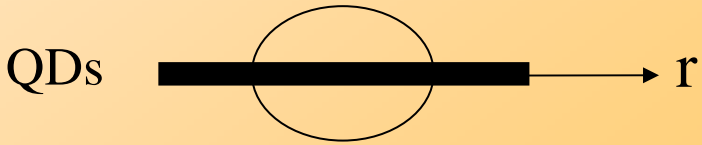

W.Langbein, Ultrafast nonlinear spectroscopy and control of semiconductor nanostructures

Calculations

$$\frac{\Delta T}{T} \propto \int_{-\infty}^{+\infty} d\omega \left|E_{probe}(\omega)\right|^2 \int_{0}^{+\infty} \Psi_{TE_0}^2(r) dr \int_{-\infty}^{+\infty} \left[L(\omega-\omega_\xi)(n_X - n_0) + L(\omega-(\omega_\xi-\omega_{XX}))(n_{XX}-n_X)\right] f(\omega_\xi) d\omega_\xi$$

Solutions of OBE at t >> t_0: functions of $\omega_c - \omega_\xi, \theta_{pump}(r)$

Example: t_0=1ps

The biexciton population oscillates with a different period compared to the exciton population.

The dephasing reduces the amplitude of the oscillations.

Many oscillation periods are present, even when the averaging over the inhomogeneous broadening and the spatial mode profile are included.

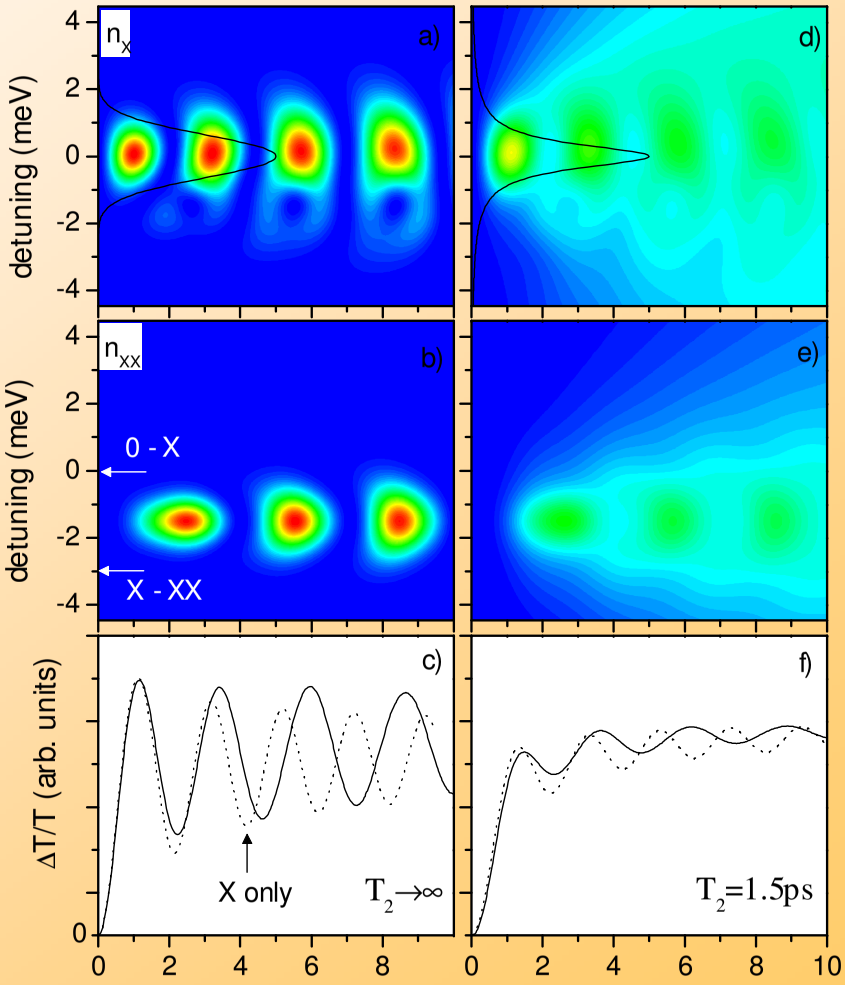

Distribution of transition dipole moments

$$\frac{\Delta T}{T} \propto \int_{-\infty}^{+\infty} d\omega \left|E_{probe}(\omega)\right|^2 \int_{0}^{+\infty} \Psi_{TE_0}^2(r) dr \int_{-\infty}^{+\infty} P(\mu) d\mu \int_{-\infty}^{+\infty} \alpha\left(\omega, \omega_\xi, \mu, \theta\left(E_{pump}, \mu\right)\right) f\left(\omega_\xi\right) d\omega_\xi$$

$$P(\mu)\mu^2 = \frac{1}{\sigma\sqrt{2\pi}} e^{-\frac{(\mu-\mu_0)^2}{2\sigma^2}}$$

$$\alpha \propto \sigma_0 \propto \mu^2$$

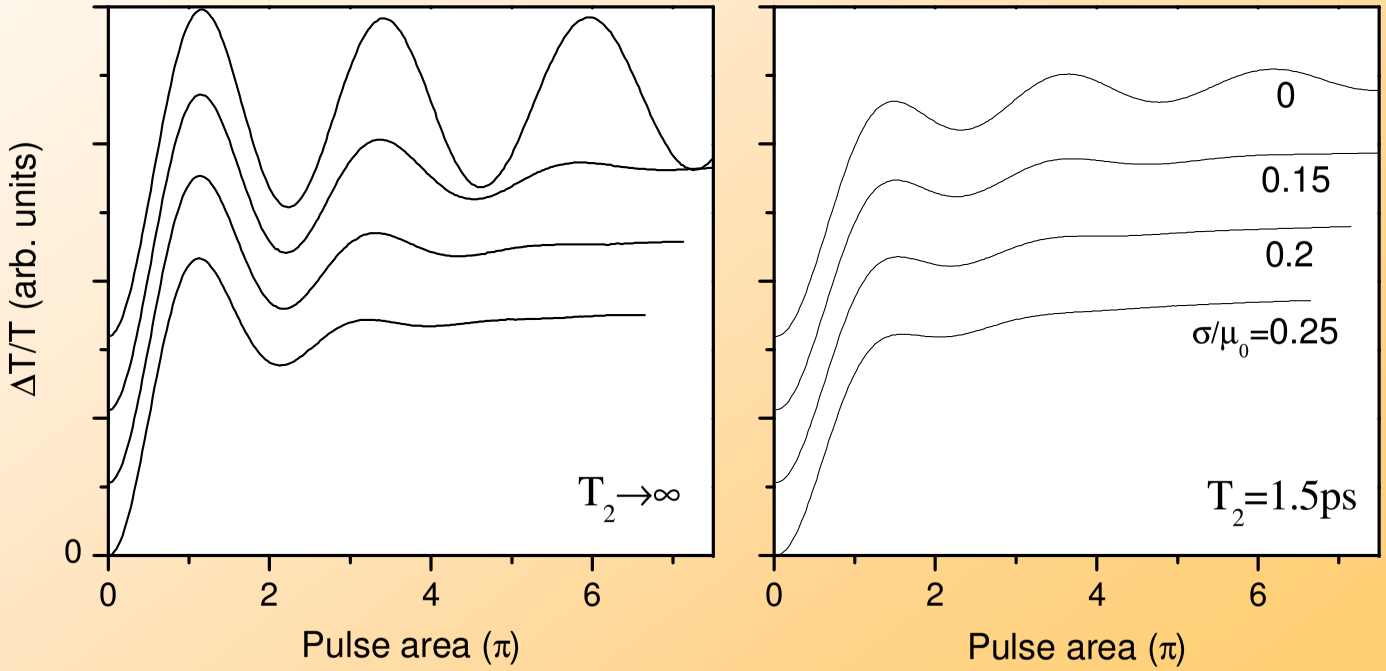

W.Langbein, Ultrafast nonlinear spectroscopy and control of semiconductor nanostructures

How to measure FWM from individual localized states ?

States are typically much smaller than light wavelength : k is undefined

FWM consist of several sharp resonances: Single channel detection is inefficient

Solution:

- Use time-invariance for FWM selection
- Upgrade the balanced detection to multichannel

Heterodyne spectral interferometry (HSI)

- Frequency shift of excitations pulses 1,2 by radio-frequencies $\Omega_{1,2}$
- Interference of signal with reference in an AOM under a frequency shift Ω_d
- Measurement of spectrally resolved mixed intensities containing the interference terms

$$2I_{a,b}(\omega,t) = |E_r|^2 + |E_s|^2 \pm 2\Re(E_r E_s^* e^{i\Omega_d t})$$

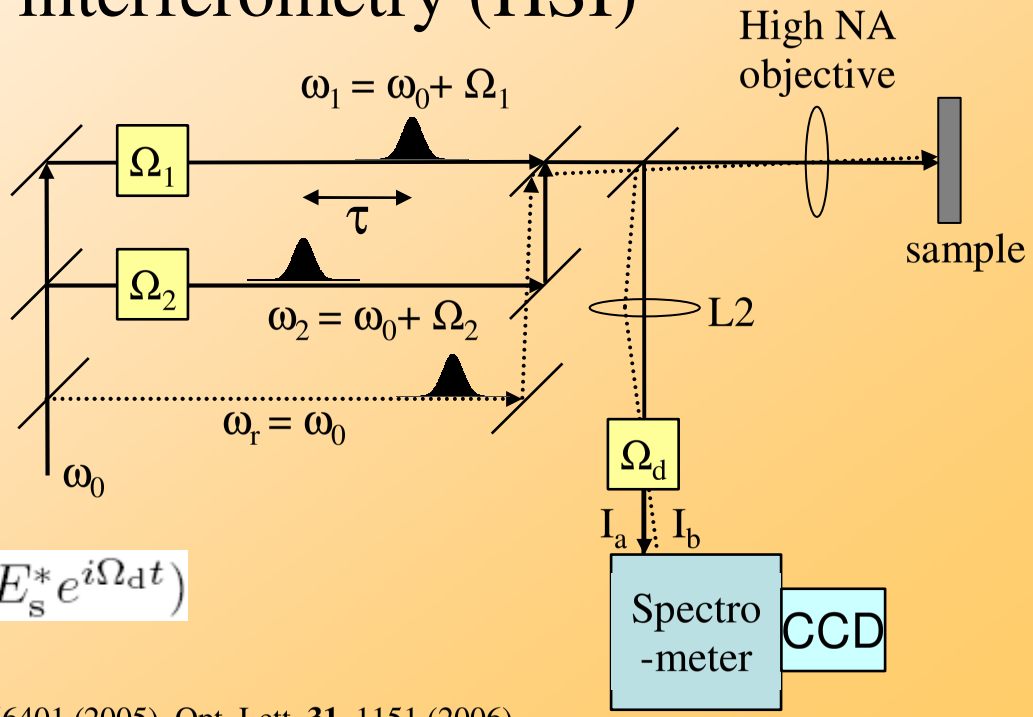

W.Langbein, B.Patton et al., Phys. Rev. Lett. **95**, 017403 ; 266401 (2005), Opt. Lett. **31**, 1151 (2006)

How to measure FWM from individual localized states ?

- Balanced measurement of interference

$$I_{\mathrm{d}}(\omega) = I_{\mathrm{a}} - I_{\mathrm{b}} = 2\int_0^T \Re(E_{\mathrm{r}}E_{\mathrm{s}}^{*}e^{i\Omega_{\mathrm{d}}t})dt$$

filters the signal of frequency-shift Ω_d with a bandwidth 4/T

Choice of Ω_d determines measured field: for $\Omega_d = \Omega_{1,2}$ Pulse 1,2 , for $\Omega_d = 2\Omega_2 - \Omega_1$ FWM

- Retrieval of signal field in phase and amplitude using spectral interferometry

$$F(\Theta(t)F^{-1}(I_{\mathrm{d}}(\omega))) = E_{\mathrm{r}}^{*}(\omega)E_{\mathrm{s}}(\omega)e^{i\Omega_{\mathrm{d}}t}$$

- Balanced detection eliminates classical reference noise
- Multichannel detection enables measurement of all signal components at once

This setup offers the best possible detection sensitivity and background supression

W.Langbein, B.Patton et al., Phys. Rev. Lett. **95**, 017403 ; 266401 (2005), Opt. Lett. **31**, 1151 (2006)

Localized Excitons in GaAs quantum wells

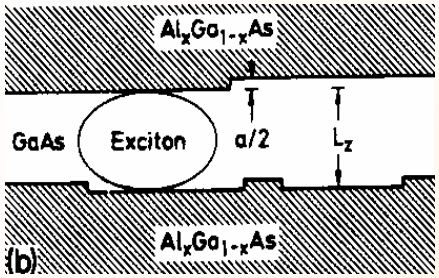

Large islands form on the AlAs and GaAs surfaces
when a growth interruption is applied.
Excitons can be localized in these islands

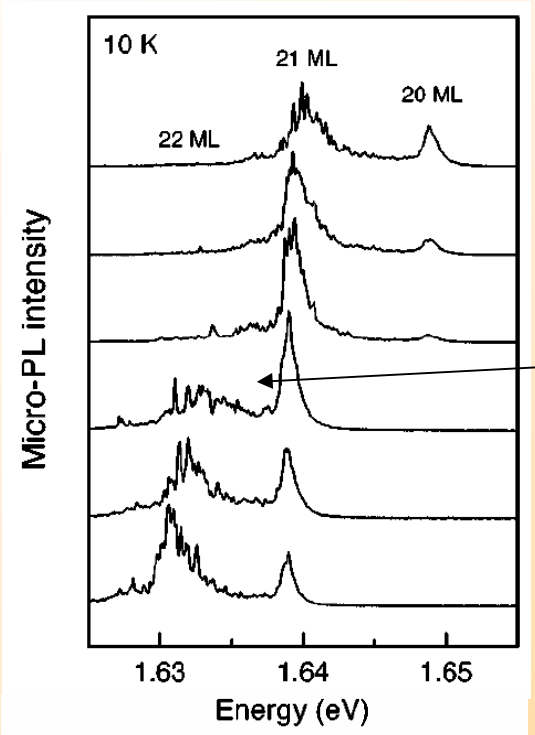

Thickness of the QW determines the spatial distribution
of the localization potential due to the monolayer islands

At the onset of a new monolayer,
few and small islands are present,
creating a small density of localized exciton states

Spectrally resolved FWM from a few-state ensemble

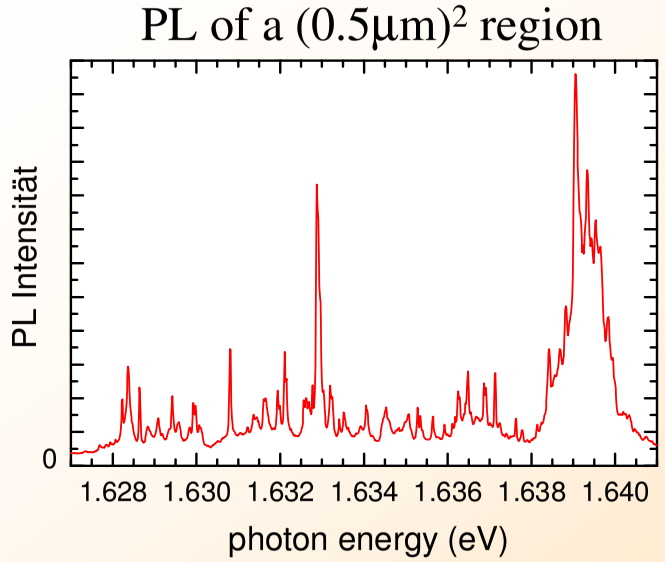

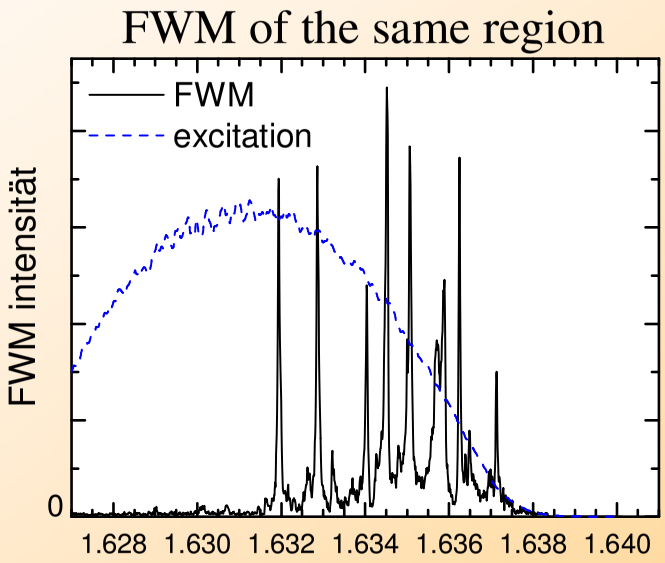

- Selection of the investigated region using a confocal excitation/detection (500nm resolution)
- Few localized exciton states emit in the range of the larger monolayer thickness
- Exciting laser selects only strongly localized states
- FWM intensities of states are not related to the PL intensities: Phonon-assisted relaxation efficiency determines the PL while the oscillator strength determines the FWM intensities & higher spatial resolution in FWM (~I^4)
- Narrow linewidth of single states (20-50µeV FWHM)

FWM imaging

Imaging of non-linear reponse by scanning the optical focus over the sample surface:

Identification of spatial positions and distances of the excitonic states with 100nm accuracy

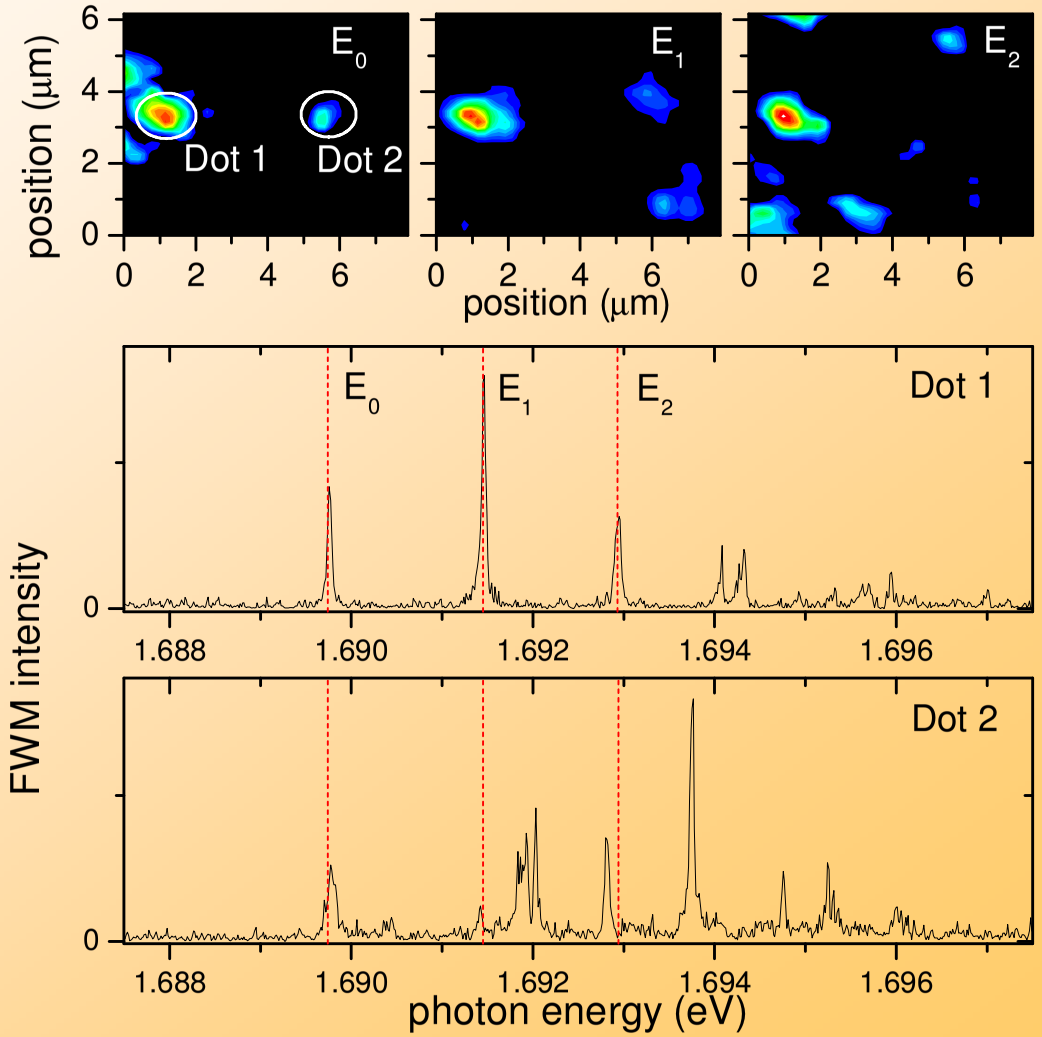

W.Langbein, Ultrafast nonlinear spectroscopy and control of semiconductor nanostructures

XY mapping: FWM vs. PL

FWM

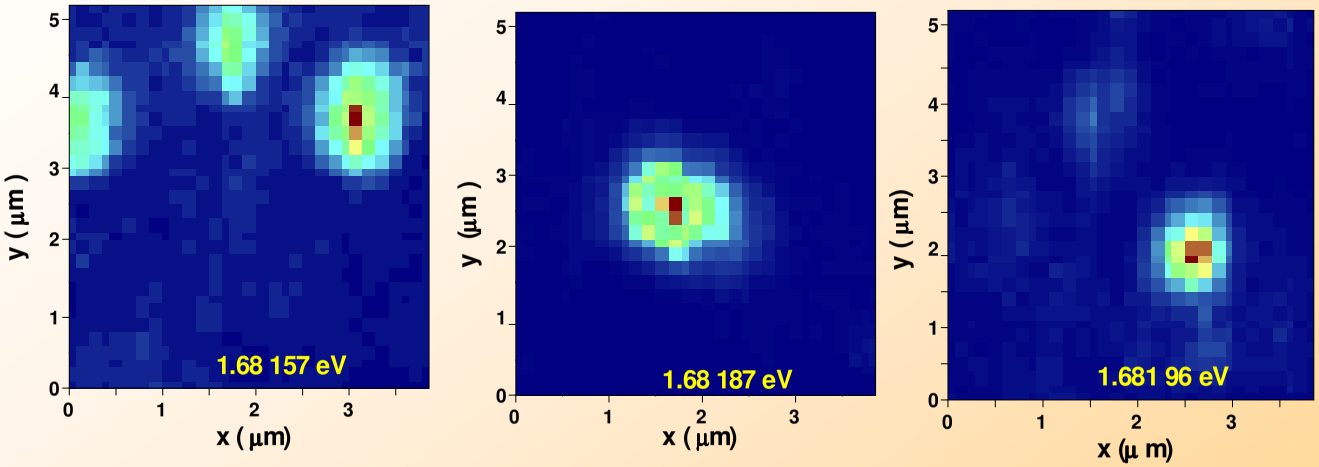

PL

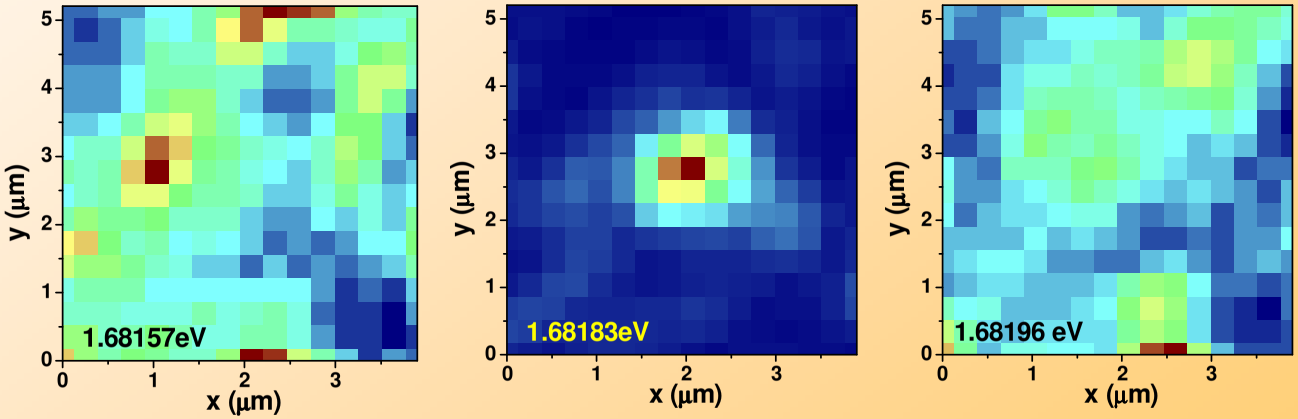

PL and FWM show mostly different states – as in spectral comparison

QDs in 5 nm QWs, T=7K

Intensity-scaling: third-order regime and above

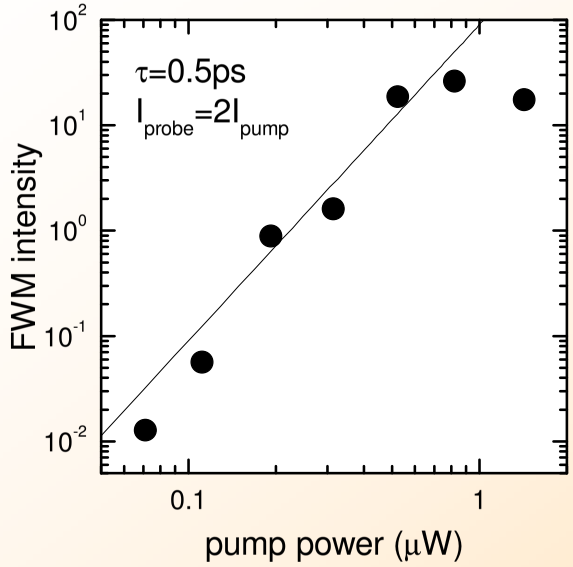

- Detected FWM intensity scales with the third power of ecitation intensity up to saturation
- FWM spectra do not change significantly
- Spatial resolution is improved by the nonlinearity, but deteriorates once saturation is reached

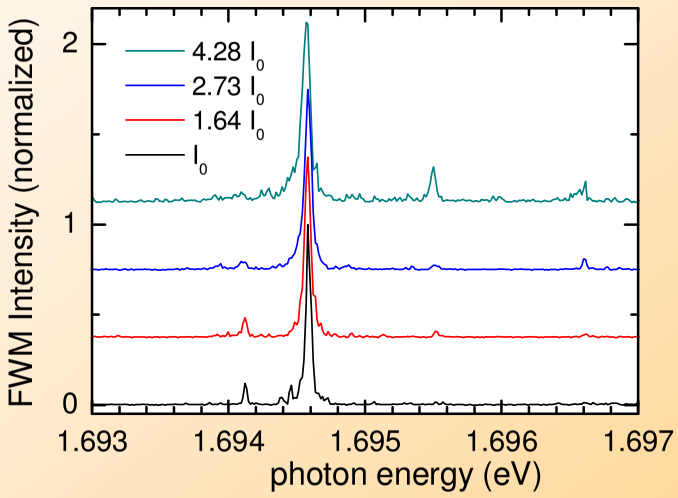

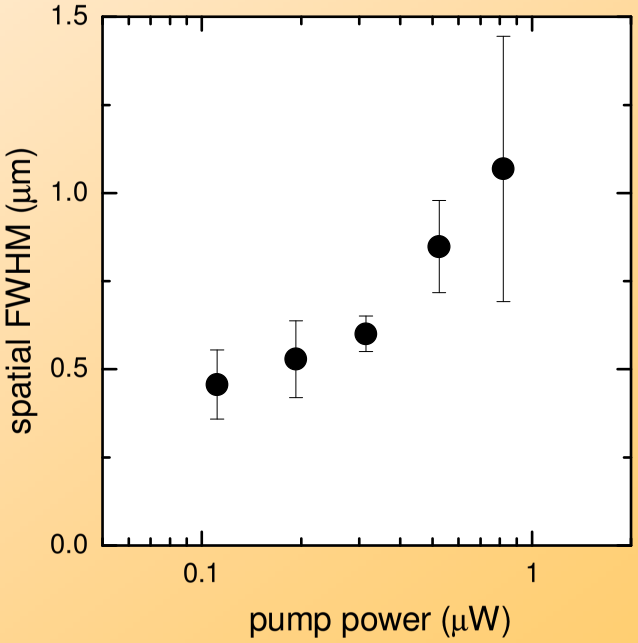

Simulation of photon echo in small ensembles

Photon echo formation of finite ensembles (size N) of frequency variance σ for τσ=50

$$E^{(3)}(t,\tau) = \sum_{k=1}^{N} \mu_k^4 E_1(\omega_k) E_2^2(\omega_k) e^{i\omega_k(t-\tau)-\gamma_k(t+\tau)}$$

In phase (e.g. at t=τ): $E_{sum} = NE_0$

random phases: $E_{sum} \approx \sqrt{N} E_0$

Intensity enhancement by a factor of N by superradiance

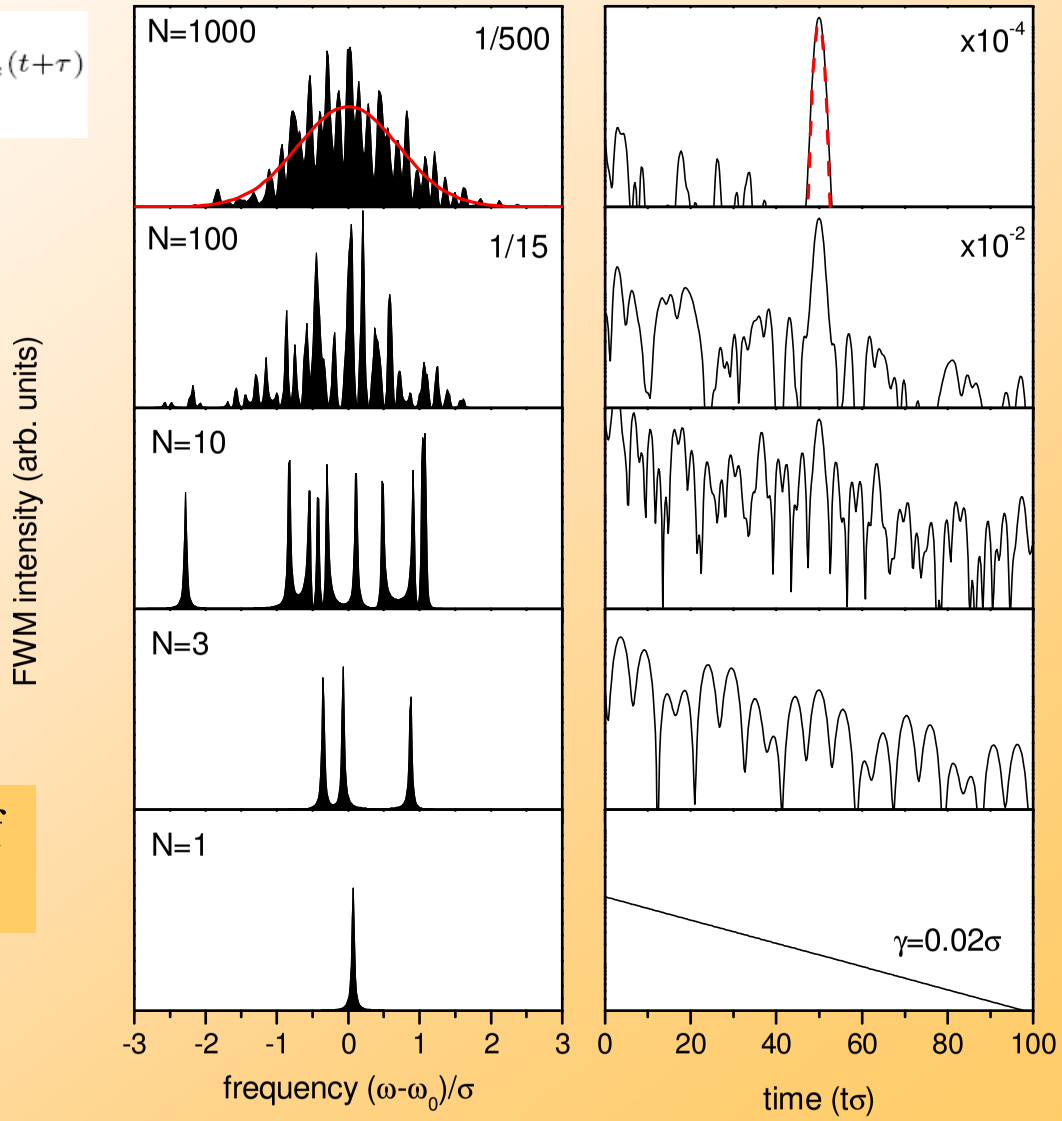

W.Langbein, Ultrafast nonlinear spectroscopy and control of semiconductor nanostructures

Time-resolved FWM from a few-state ensemble

Photon echo formation of a finite ensemble at τ=20ps

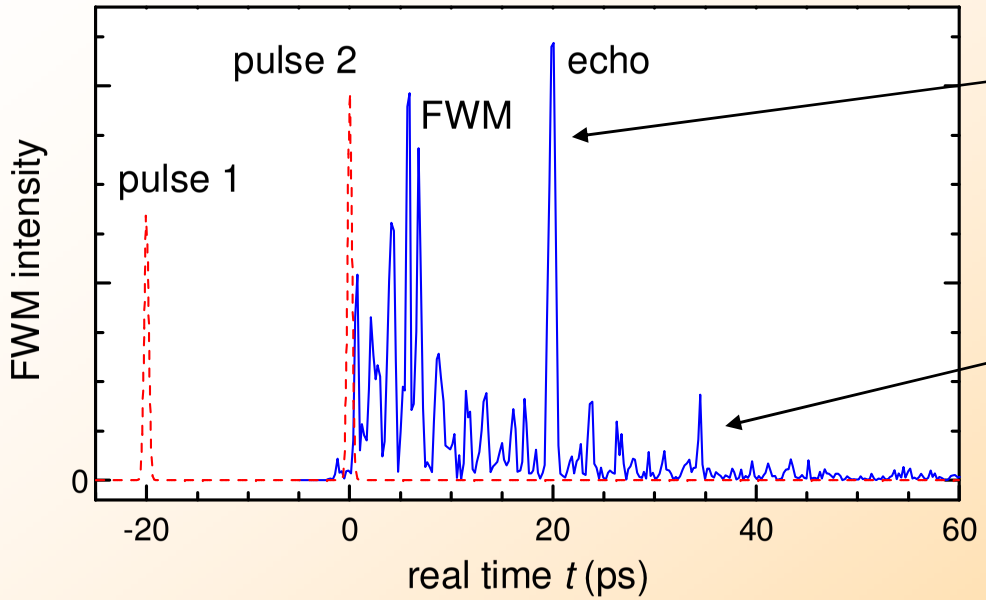

In phase: $E_{sum} = NE_0$

random phases: $E_{sum} \approx \sqrt{N} E_0$

Measured phase evolution of the 4 contributing states: Direct observation of rephasing

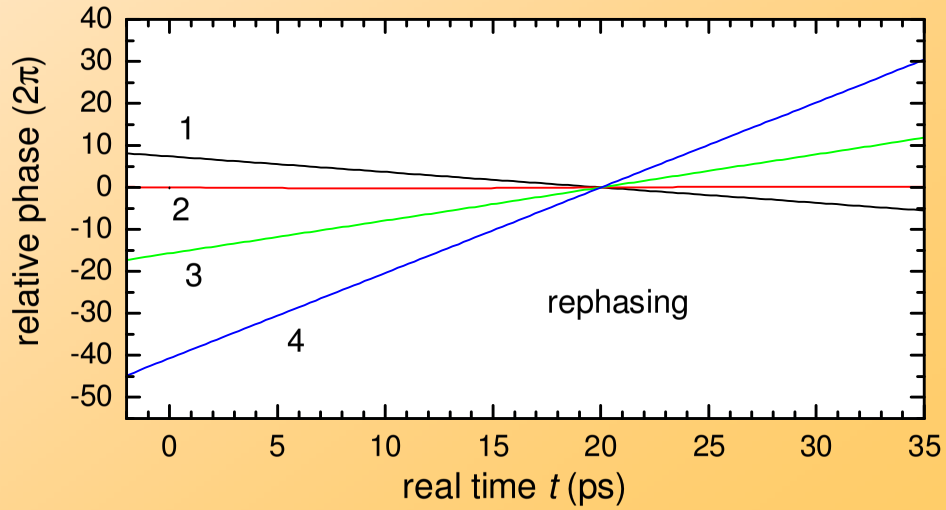

W.Langbein, Ultrafast nonlinear spectroscopy and control of semiconductor nanostructures

Measured echo formation versus N

- Select ensemble size using different sample positions
- Count number of contributing states in spectrally resolved FWM
- Observe photon echo formation in time-resolved FWM

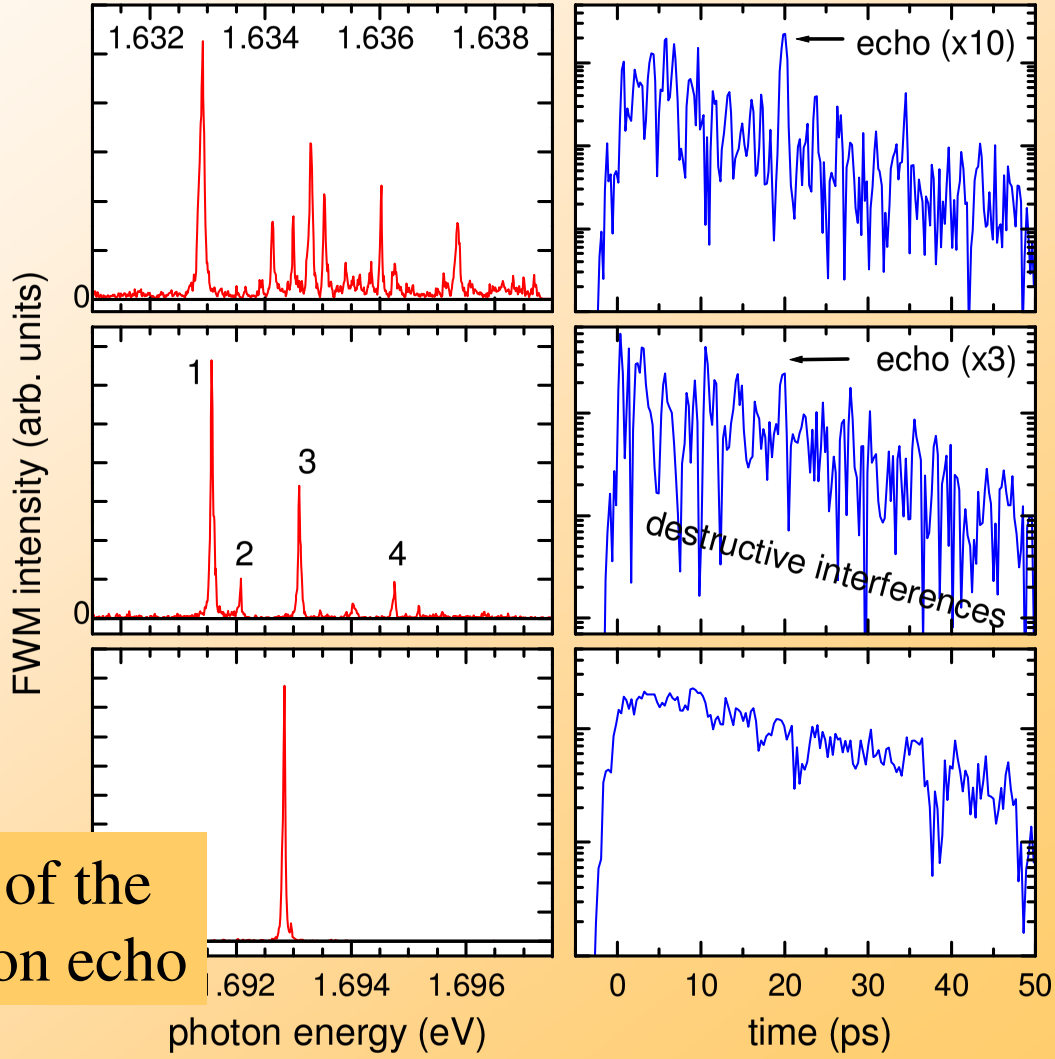

Experimental demonstration of the microscopic origin of a photon echo

W.Langbein and B.Patton, Phys. Rev. Lett. **95**, 017403 (2005)

Photon-echo from a single transition

Also a single exciton resonance can exhibit inhomogeneous broadening by slow spectral diffusion:

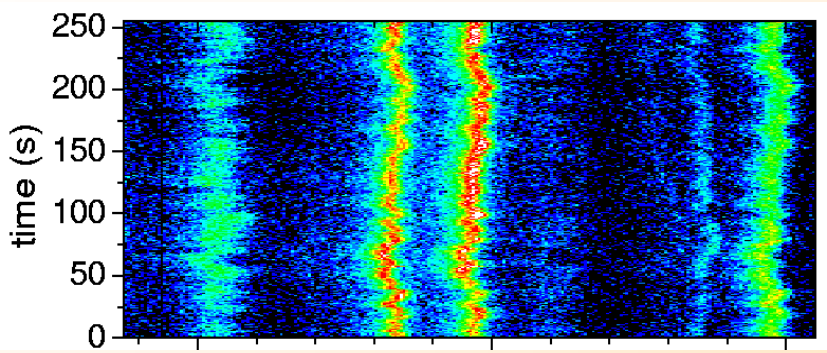

Time-ensemble of eigenenergies

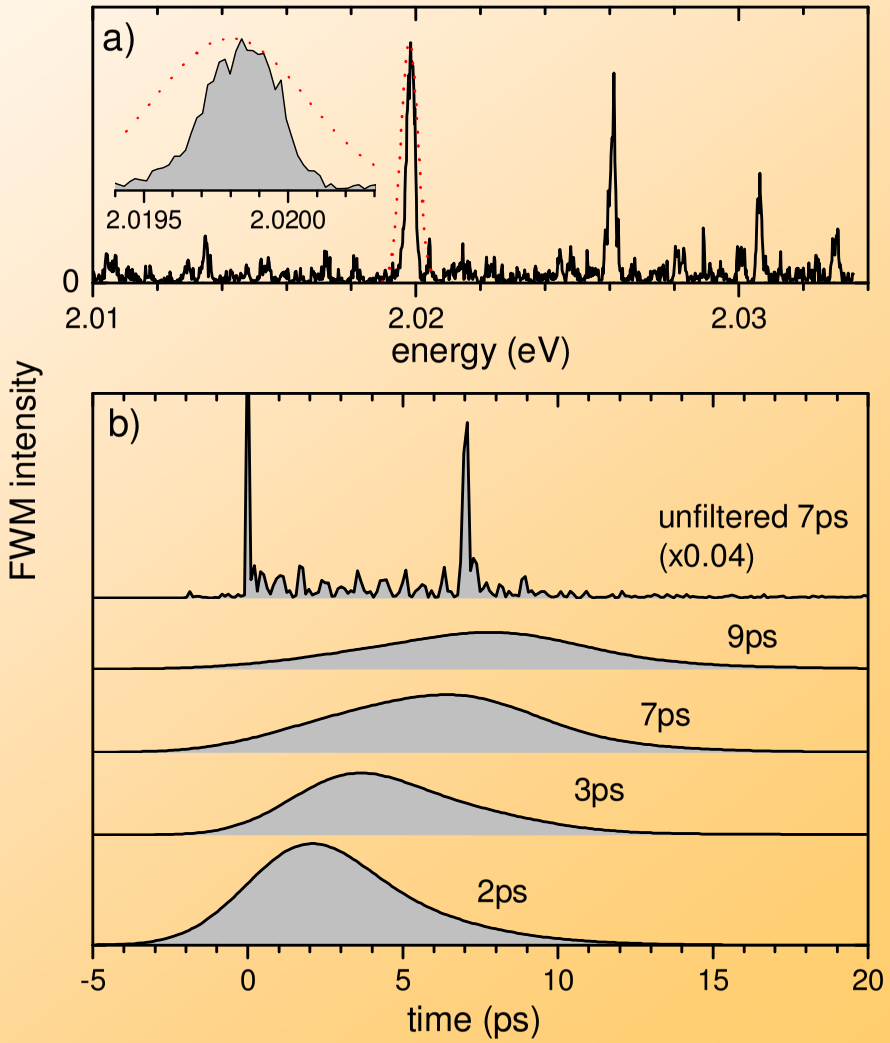

Measurements on epitaxial
CdTe/ZnTe quantum dots
(grown in the group of H. Mariette, Grenoble)

B.Patton et al, submitted to Phys. Rev. B

Rabi Oscillations

Represent the state-vector of a two level system as a position on a unitary sphere:
Bloch Sphere

n: Population Inversion
p: Polarisation

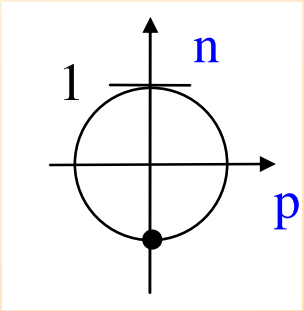

For resonant excitation, the rotation angle θ (also called pulse area) is proportional to electric field ε and transition dipole moment μ

$$\theta = \frac{1}{\hbar}\int_{-\infty}^{\infty} \mu\varepsilon(t)dt$$

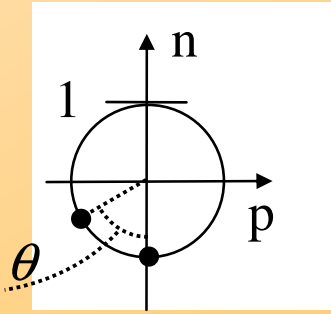

FWM measures the projection of the state vector onto the polarisation-plane:
Rabi oscillations have period of π

Selection of an individual transition

τ=30ps

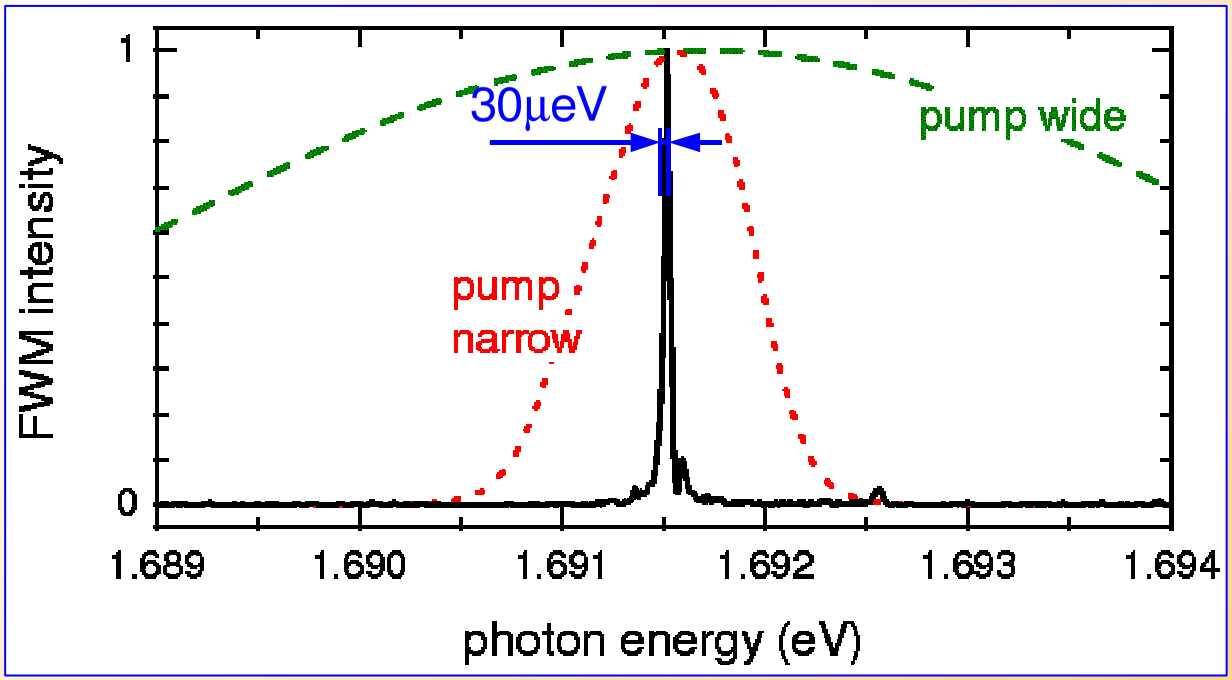

- Identify region with isolated exciton transition using a spectrally wide pump
- Narrow spectrum down centered to transition.

Rabi oscillations of a single transition

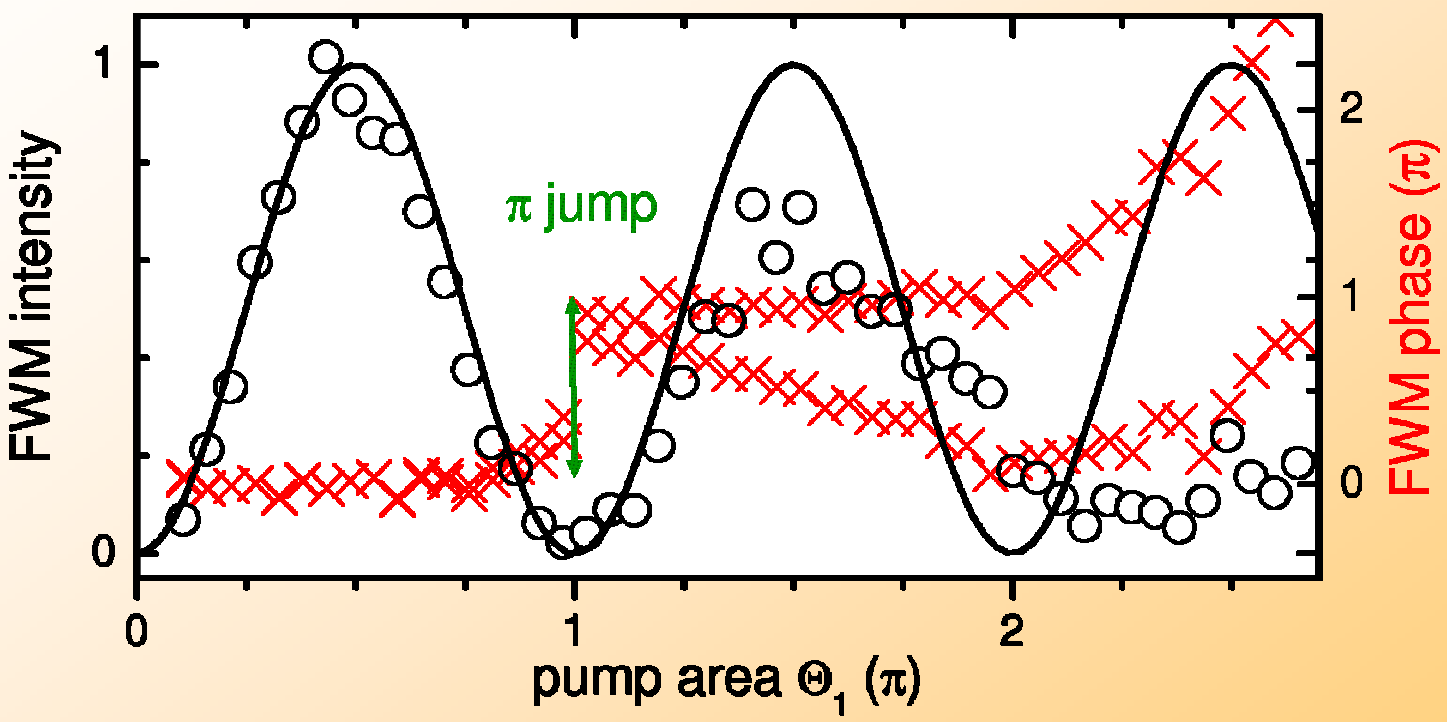

- Observed Rabi oscillations in the FWM intensity versus pump area
- Observed phase shows π-jump at top of Bloch sphere
- Deviations from ideal two-level system at higher pulse areas

Damping by Excitation Induced Dephasing ?

Deviations from the expected two-level behaviour are observed at large pulse areas.
Excitation-Induced Dephasing has been suggested as a source for such effects

• linewidth of third-order polarisation quantifies EID:

Negligible EID observed

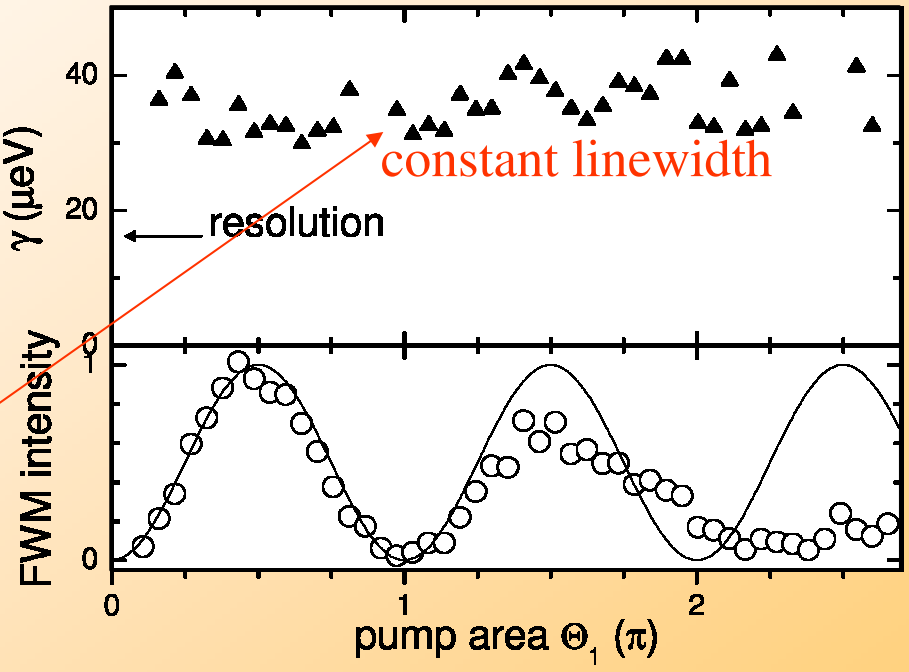

Interpretation: Presence of energetically close multiexcitonic transitions, to which the polarisation is transferred

Polarisation Transfer

Interpretation of observed polarization dynamics:
Nearly resonant multiexcitonic resonances

⇒ transferral of polarisation to coherently coupled multiexcitonic states

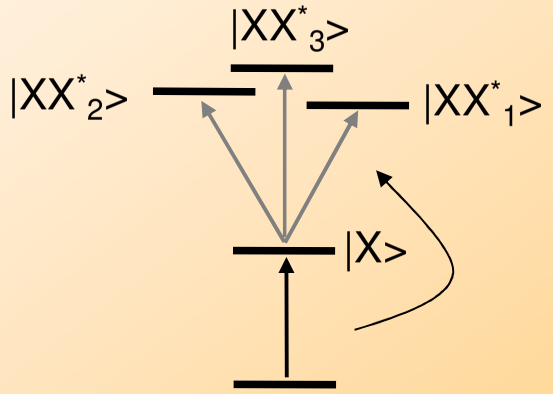

Model calculation of FWM response:

- No dephasing
- 3 nearly resonant biexciton states with
- 0.5, -0.6, -0.8meV binding energy and
- 30% of the exciton transition dipole moment (i.e. 9% oscillator strength)

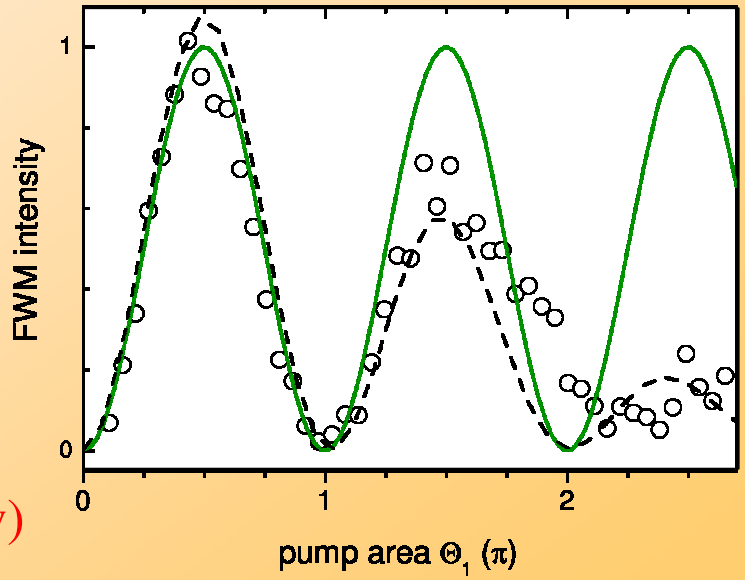

shows qualitative agreement (dashed line)
Biexcitonic FWM to weak to be detected (for now)

Instead of EID, discrete non-resonant multiexcitonic states explain the observed polarization decay without line broadening

Off-resonant Rabi Oscillations

Spectral detuning between excitation pulses and transition

Precession no longer purely about p-axis

Bloch-sphere picture:

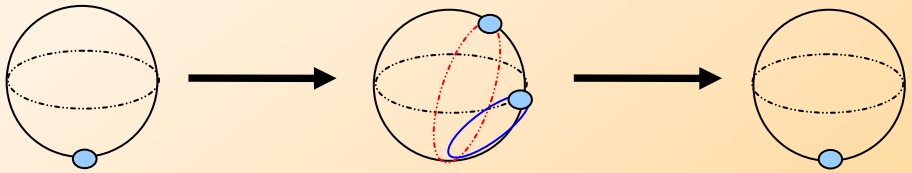

Numerically calculated polarization for a two-level system (no dephasing)

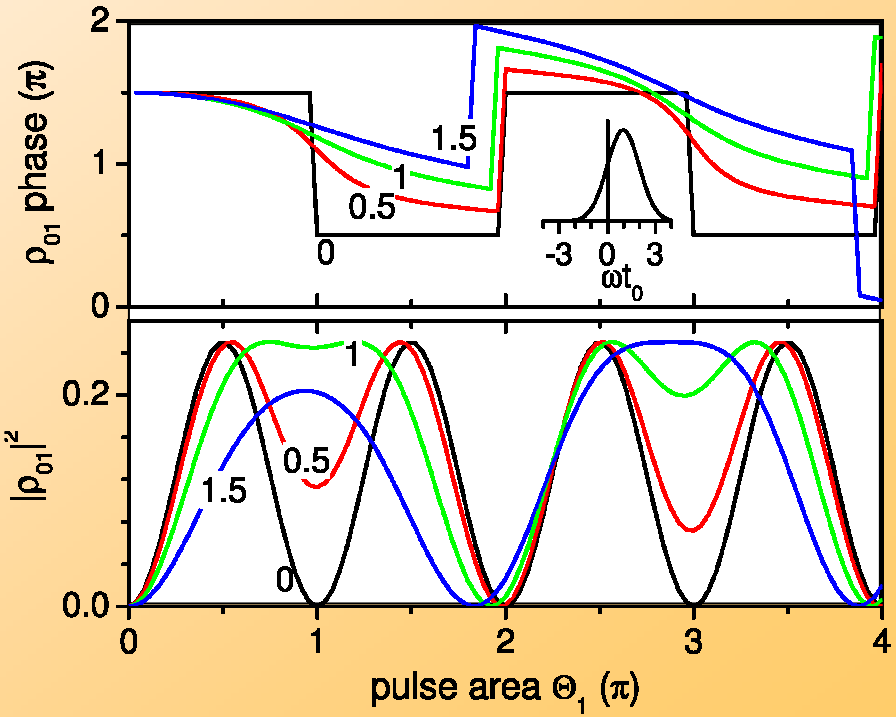

W.Langbein, Ultrafast nonlinear spectroscopy and control of semiconductor nanostructures

Off-resonant Rabi oscillations: Experiment

Measured FWM intensity and phase for different excitation detunings

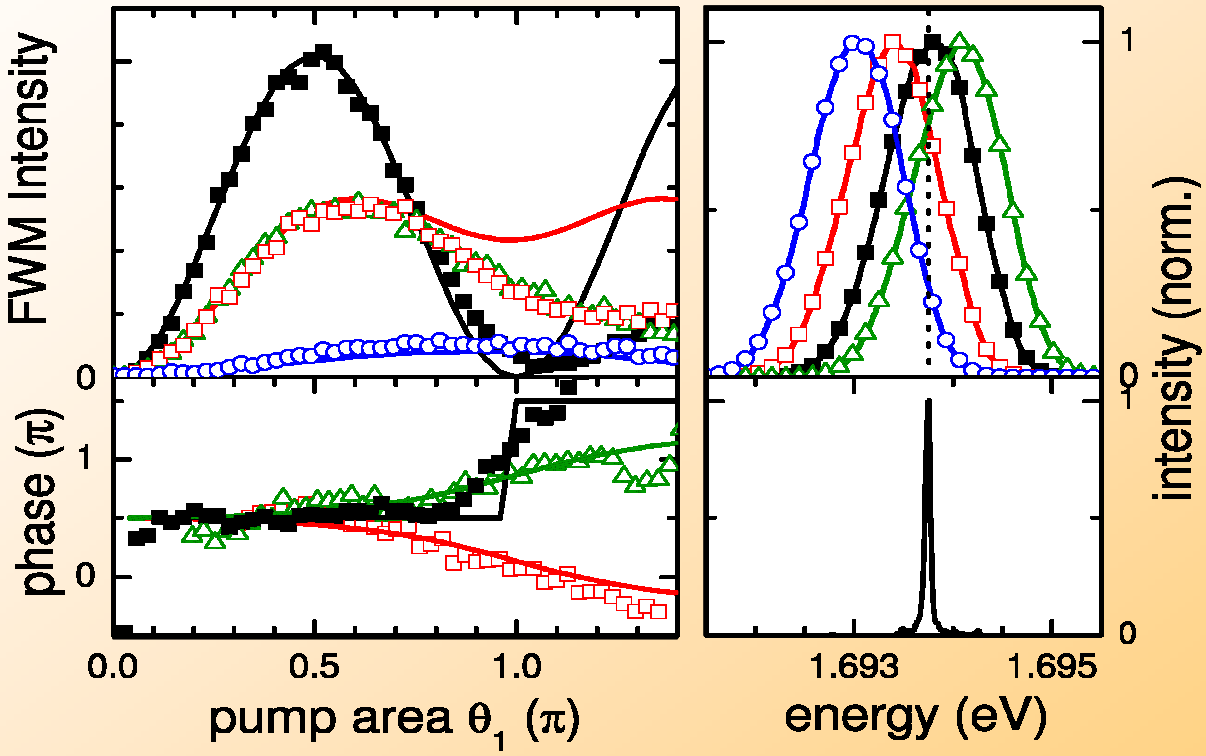

- FWM Intensity & Phase evolution in agreement with two-level calculation (lines)
- Deviations for large pulse areas, as discussed previously

Phase control via detuning demonstrated

Coherent manipulation in FWM

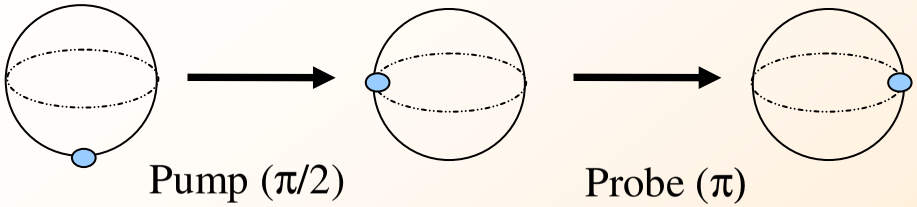

Pump area π/2 : maximum polarization
Probe area π : full phase conjugation

⇒ maximum FWM signal

$$\vec{P}^{(3)} \propto \vec{\vec{\chi}}^{(3)} \vec{E}_2 \vec{E}_2 \vec{E}_1^{\,*}$$

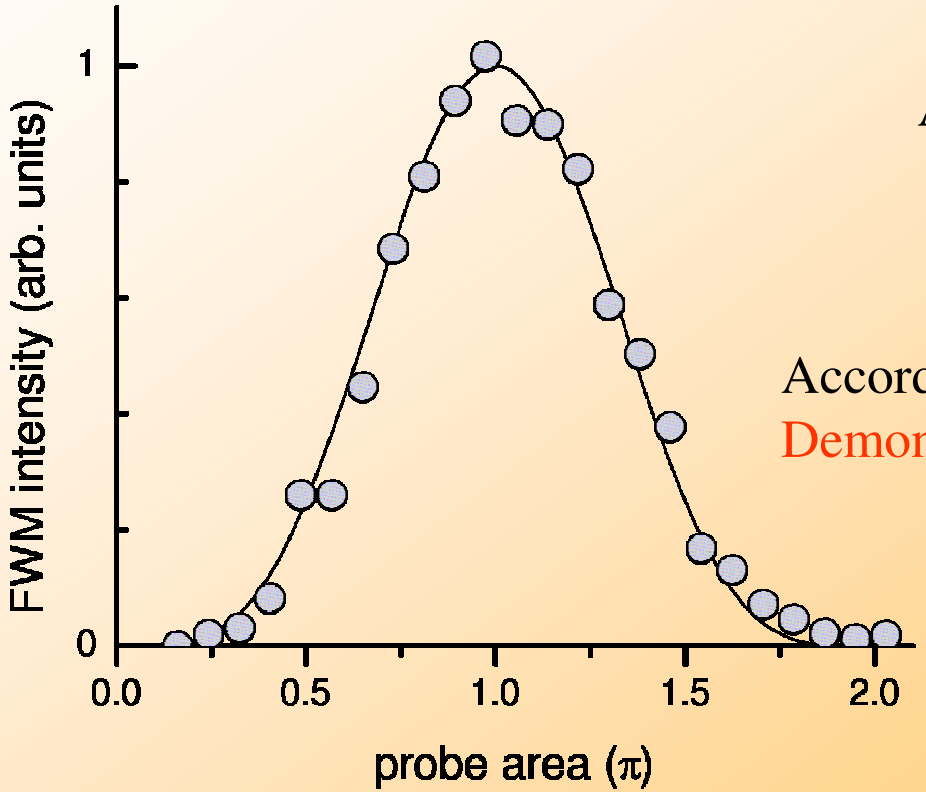

Analogous to π/2 - π spin flip in NMR

According response observed in experiment:
Demonstration of two pulse coherent control

W.Langbein, Ultrafast nonlinear spectroscopy and control of semiconductor nanostructures

Multi-state Rabi oscillations

Excitation of a small exciton ensemble by spectrally wide pulses:

- Observation of Rabi-Oscillations for all resonances
- Coherent coupling between resonances is weak (inferred from 2D FWM)
- Since the FWM intensity ~μ^8, different FWM intensities result from only small differences in the dipole moment μ and thus in the pulse area

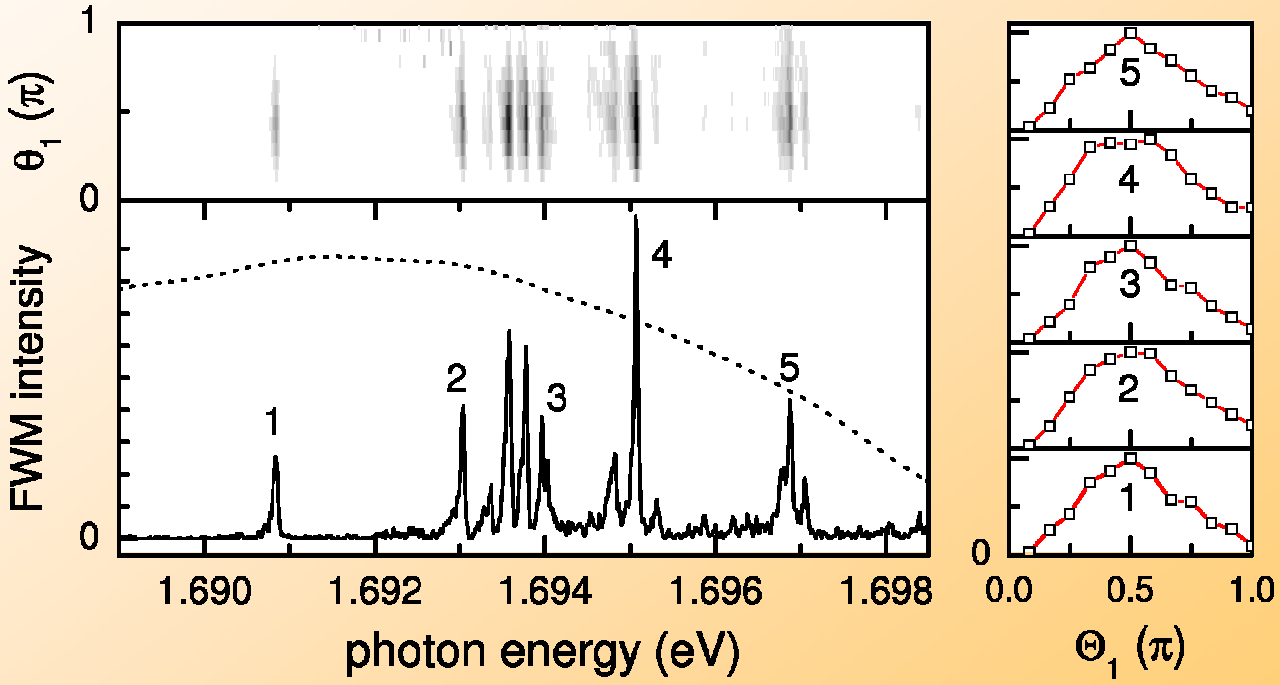

This observation shows the possibility of a simultaneous application of a gate operation on a set of two-level systems

CARDIFF UNIVERSITY
PRIFYSGOL CAERDYDD

Two-dimensional spectroscopy

$\vec{P}^{(3)}(t,\tau)$ Measured by HSI

$$\vec{P}^{(3)}(\omega,\tau)=\int e^{i\omega t}\vec{P}^{(3)}(t,\tau)\,dt$$

$$I(\omega,\tau)=\left|\vec{P}^{(3)}(\omega,\tau)\right|^2$$

Transform delay time to first-order frequency ω_1

$$\vec{P}^{(3)}(\omega,\omega_1)=\int e^{i\omega_1\tau}\vec{P}^{(3)}(\omega,\tau)\,d\tau$$

$$I(\omega,\omega_1)=\left|\vec{P}^{(3)}(\omega,\omega_1)\right|^2$$

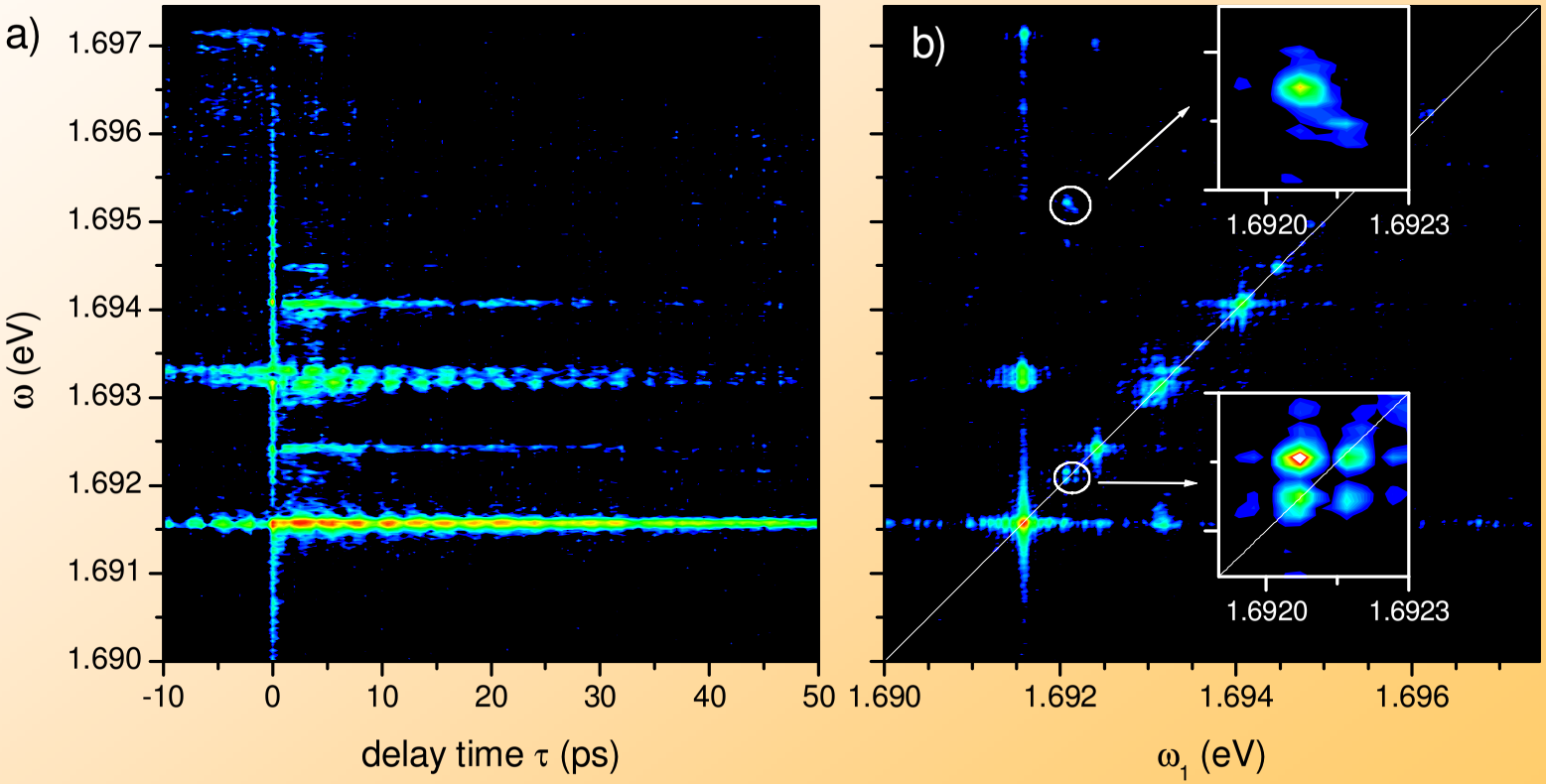

W.Langbein, Ultrafast nonlinear spectroscopy and control of semiconductor nanostructures

Conceptually similar to 2-dimensional nuclear magnetic resonance (NMR)

" The invention of multidimensional spectra was the major leap in NMR spectroscopy apart from the introduction of FT-NMR. Both techniques were acknowledged by a nobel prize"

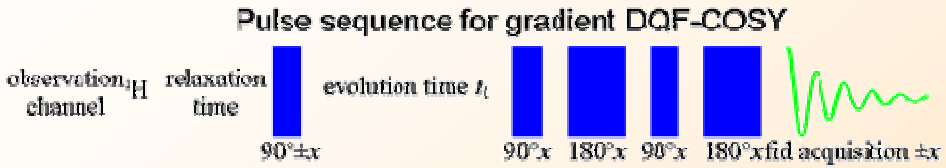

Aromatic part of the 2D COSY spectrum:
- protons at different positions in the molecule have different chemical shift
- coherent coupling between protons ~ distance^{-6} (magnetic dipole-dipole coupling)

Structure of 12,14-dibutylbenzo[g]chrysene

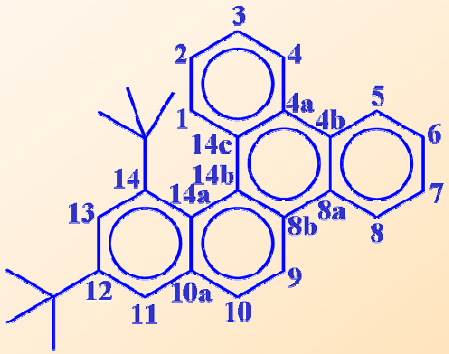

blue group of four protons is connected in the order 8.62 ppm to 7.55 to 7.59 to 8.56
green group of four protons in the order 8.54 to 7.34 to 7.44 to 8.17
red group or two protons, that correspond to H9 and 10 because they are the only group of two protons expected to have a three-bond coupling constant (8.9 Hz), are at 7.76 and 8.32 ppm.
yellow group of two protons correspond to H11 and 13 because the coupling constant is small (1.9 Hz) and consistent with a four bond correlation.

http://drx.ch.huji.ac.il/nmr/techniques/2d/cosy/cosy.html

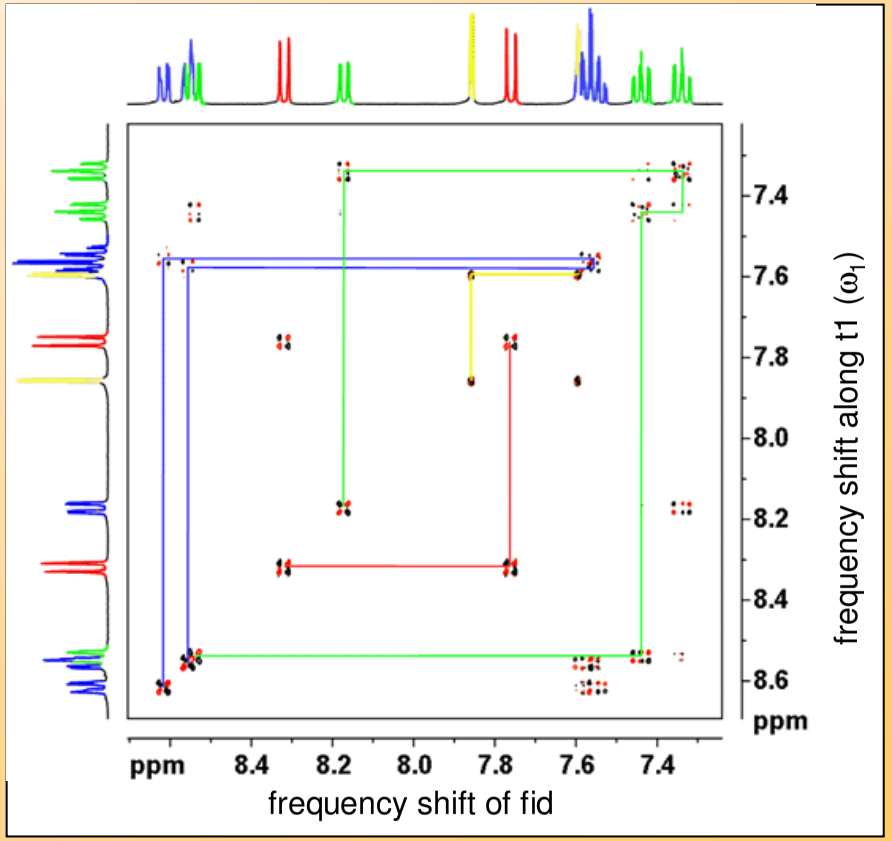

W.Langbein, Ultrafast nonlinear spectroscopy and control of semiconductor nanostructures

Two-dimensional spectroscopy

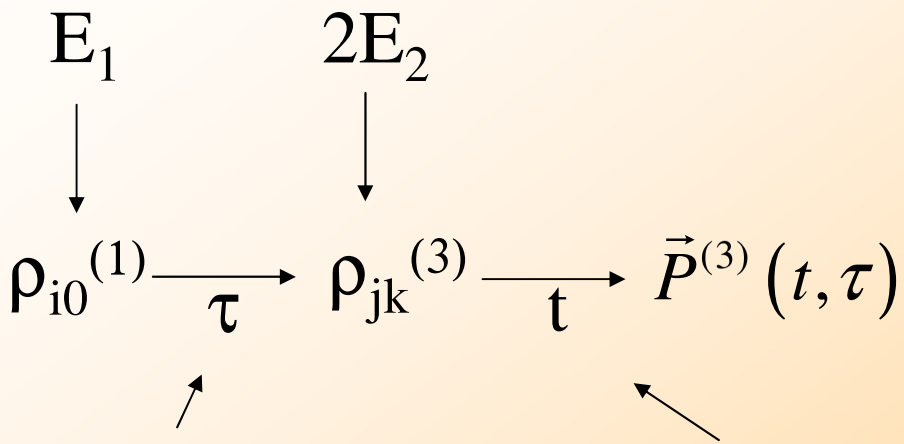

$$\rho_{i0}^{(1)} \propto \exp\left(\left(i\tilde{\omega}_{i0} - \gamma_i\right)\tau\right) \qquad \rho_{jk}^{(3)} \propto \exp\left(\left(i\tilde{\omega}_{jk} - \gamma_{jk}\right)t\right)$$

neglect damping γ for the moment

$$\vec{P}^{(3)}(\omega,\omega_1) = \sum_{i>0} \mu_{i0}\delta(\omega_1 + \omega_{i0}) \sum_{j>k} \mu_{jk} A_{i0,jk}\delta(\omega - \omega_{jk})$$

$A_{i0,jk}$: Polarization coupling coefficient for the FWM process

Uncoupled two-level systems: $A_{i0,jk} = \mu_{i0}\mu_{jk}\delta_{i0,jk}$ is diagonal

Uncoupled two level systems

Two uncoupled two-level systems

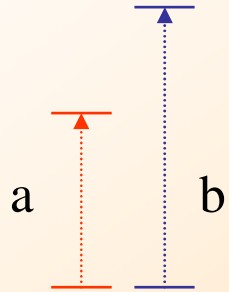

Four-level picture

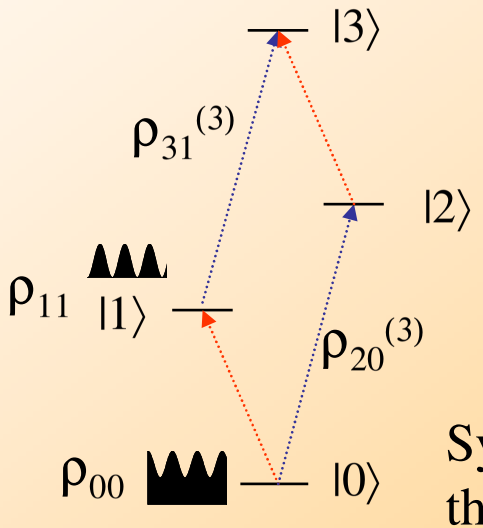

System initially in the ground state

2D FWM signature

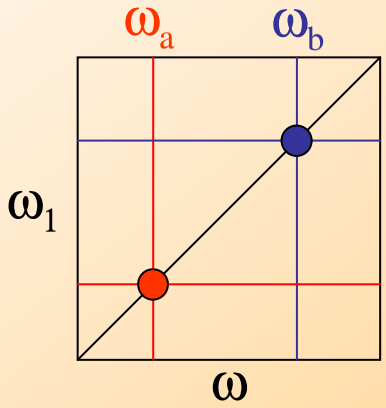

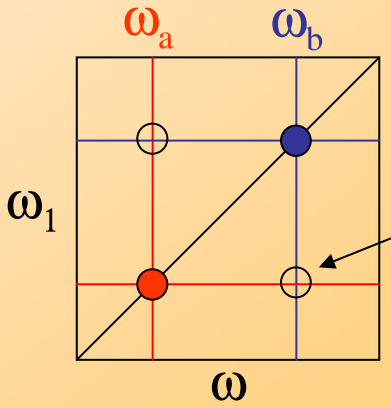

Cancellation of $\rho_{20}^{(3)}$ and $\rho_{20}^{(3)}$ (out of phase)

Coupled two level systems

Renormalization δ of two-exciton state
(Static dipole-dipole, exchange)

$$\omega'_{a,b} = \omega_{a,b} - \delta$$

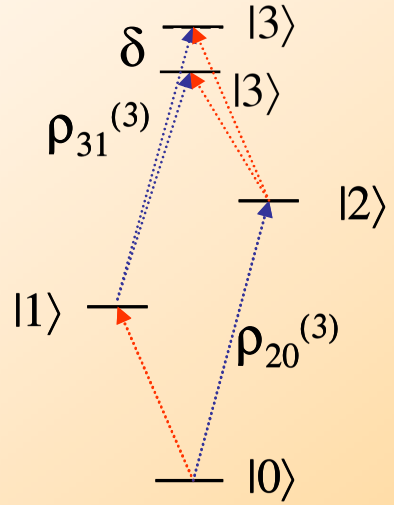

two-exciton states visible
only in 3rd order frequencies

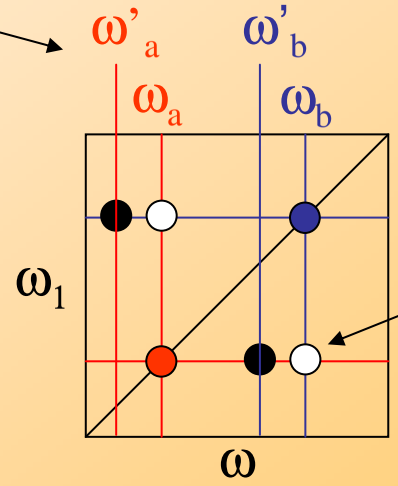

2D FWM signature

$\rho_{31}^{(3)}$ and $\rho_{20}^{(3)}$
out of phase but
spectrally separated

Coupled two level systems

Coupling of exciton states by δ_2
(transition dipole, Förster coupling)

$$\omega_{1,2} = \frac{\omega_a + \omega_b}{2} \pm \sqrt{(\omega_a - \omega_b)^2 + \delta_2^{\,2}}$$

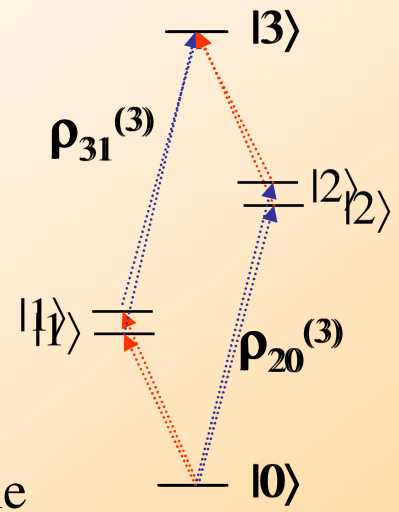

After coupling: different transition dipole moments of the states (super/subradiant superpositions)

2D FWM signature

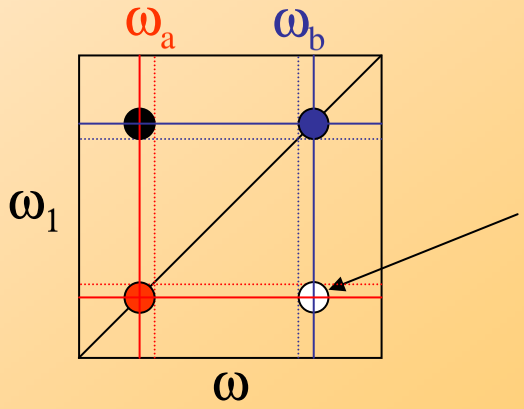

$\rho_{20}^{(3)}$ and $\rho_{20}^{(3)}$ out of phase but different amplitude

CARDIFF UNIVERSITY
PRIFYSGOL CAERDYDD

Experimental data

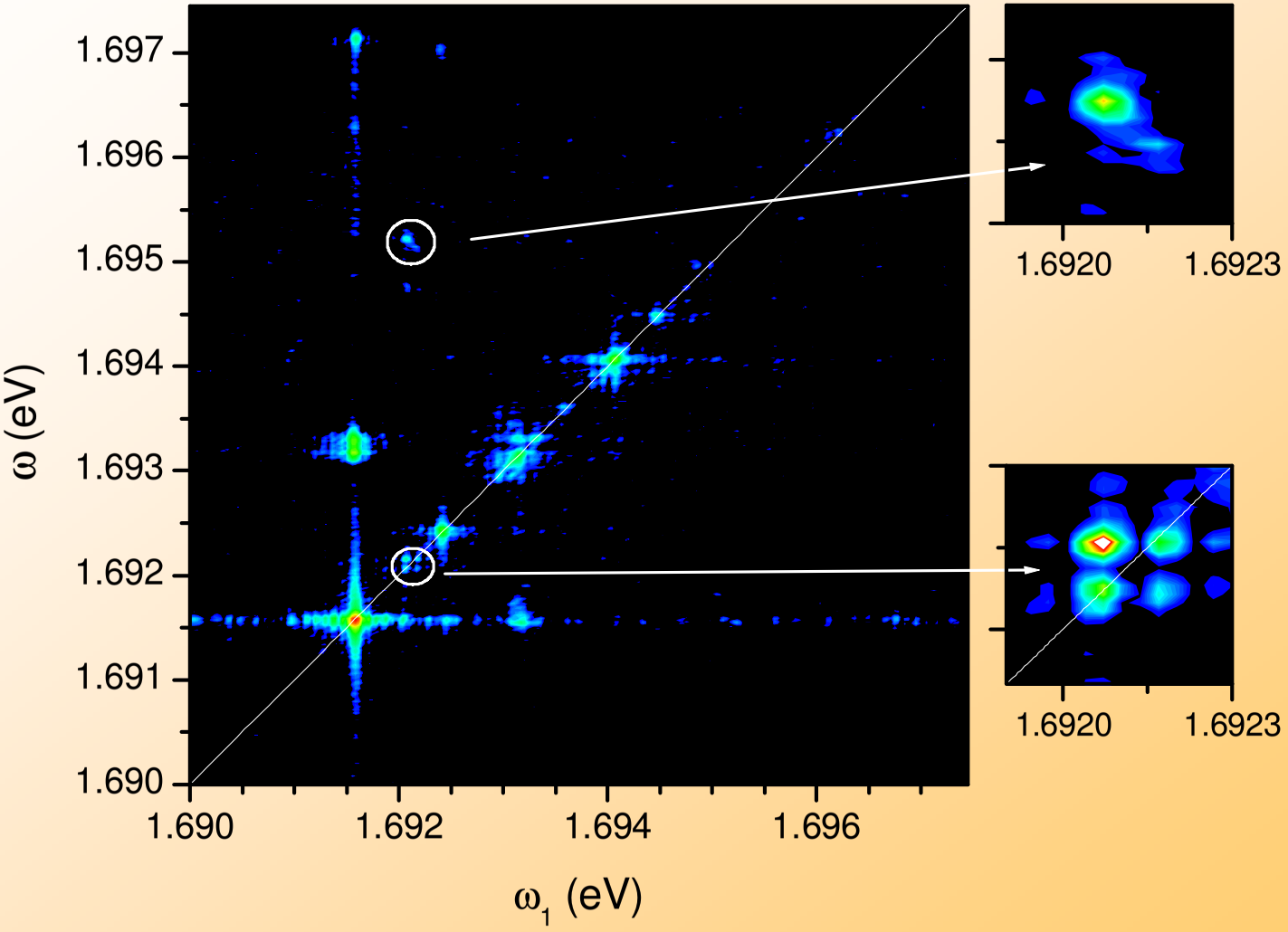

W.Langbein, Ultrafast nonlinear spectroscopy and control of semiconductor nanostructures

CARDIFF UNIVERSITY
PRIFYSGOL CAERDYDD

Analysis of coherent coupling

green lines indicate diagonal position in each plot

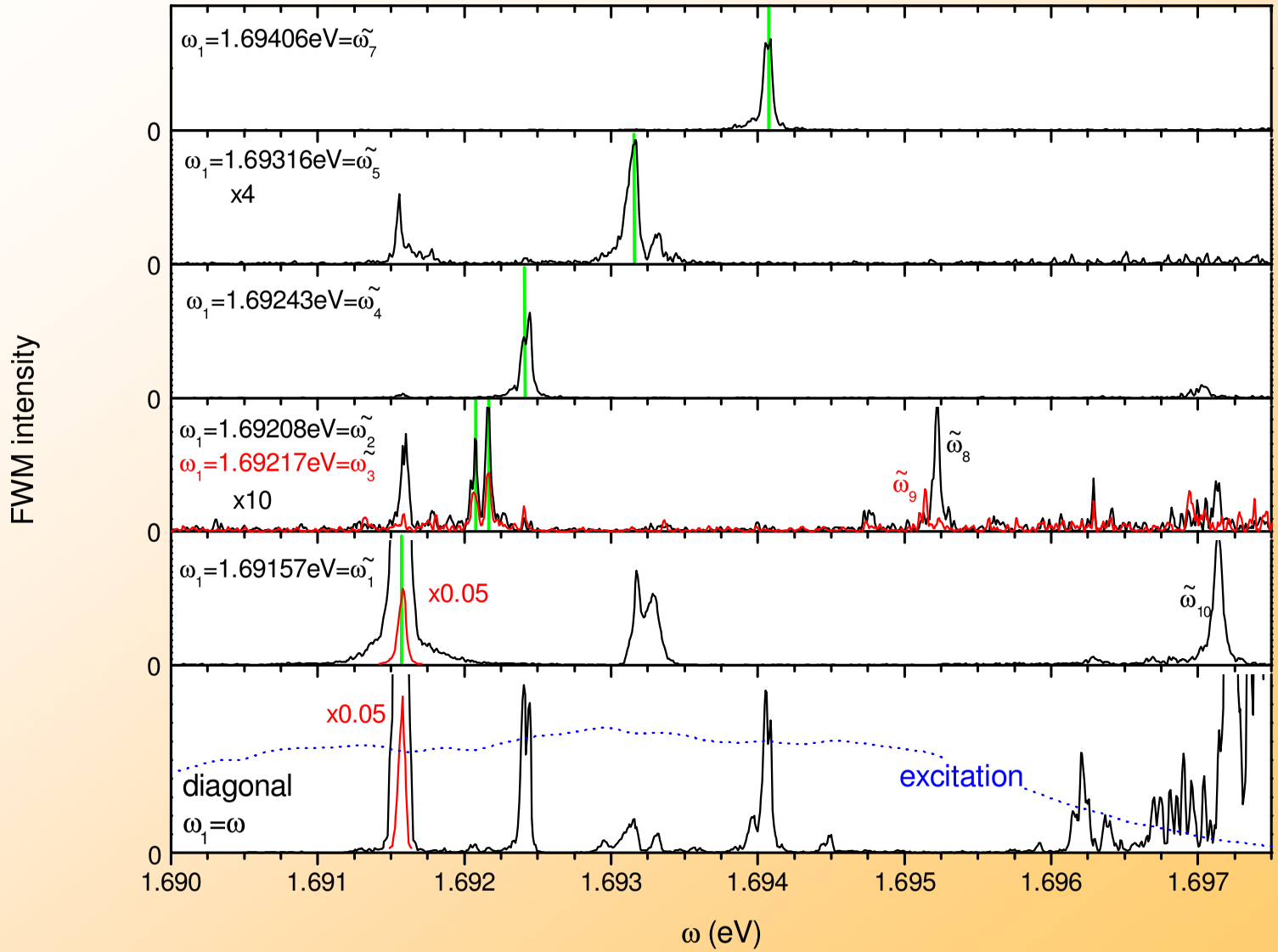

W.Langbein, Ultrafast nonlinear spectroscopy and control of semiconductor nanostructures

Exciton-Biexciton system

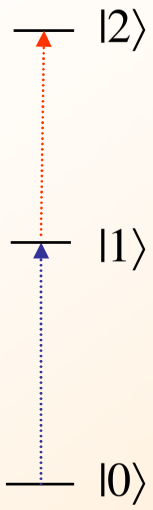

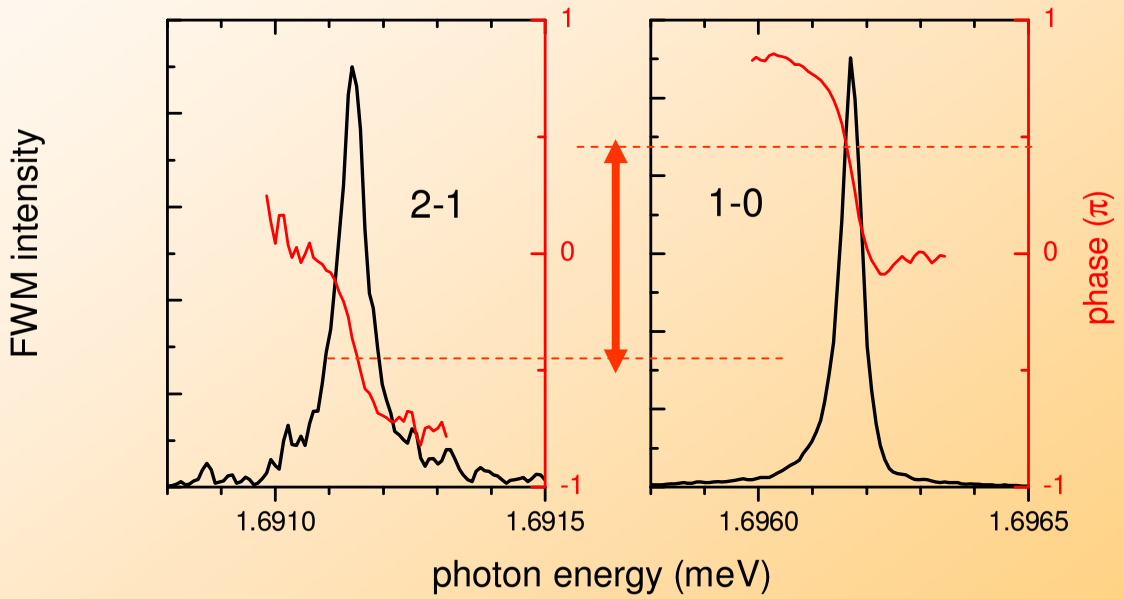

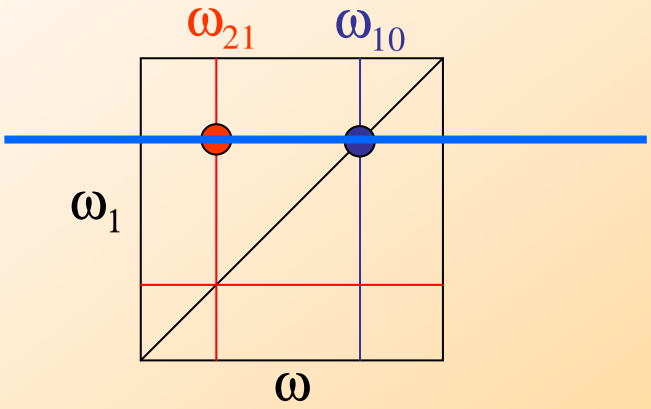

$$\vec{P}^{(3)}\left(\omega, \omega_1 = \omega_{10}\right)$$

π phase shift observed

Acknowledgements

Collaboration with

G.Kocherscheidt, B.Patton, S.Schneider, Ch.Mann, F.Gindele, U. Woggon, M.Bayer. *University Dortmund*
V.Cesari, B. Patton, P.Borri, *Cardiff University*
K.Leosson, J.R.Jensen, J.Erland, D.Birkedal, H.Gislason, J.M.Hvam *Danish Technical University*
N.LeThomas, A.Fiore *EPFL Lausanne*
A.Smirl, University of Iowa
H.P.Wagner, *University of Cincinatti*
M.Umlauff, M.Hetterich, D.Gerthsen, H.Kalt, C.Klingshirn, *Universität Karlsruhe*
H.Giessen, *University Stuttgart*
D.Bimberg, *TU Berlin*
D.Hommel, *University Bremen*
D.Reuter, A.D.Wieck *University Bochum*
M.Heuken, *TH Aachen*

N.N. Ledentsov, *Ioffe Insitute, Russia*
M.V.Artemyev, *Belarussian State University*
S. Fafard, P.Hawrylak, *Institute for Microstructural Science, Canada*
Le Si Dang, H.Mariette, *Universite Fourier, Grenoble*
A.Kavokin *University Southampton*
G.Malpuech, *Blaise Pascal Universite*
V.Savona, *EPFL Lausanne*
M.Axt, T.Kuhn, *Unversity Münster*
T.Meier, S.W.Koch, *UniversityMarburg*
A.Esser, G.Mannarini, E.Runge, E.Muljarov, R.Zimmermann, *HU Berlin*
A.Vagov, *University of Antwerp*
S. Savasta, O. Di Stefano, *Università di Messina*
A.Ivanov, *Cardiff University*
J. Mørk, *Danish Technical University*

Funding from

Deutsche Forschungsgemeinschaft DFG

EU RTN

Marie Curie Actions Human resources and mobility

EPSRC Engineering and Physical Sciences Research Council

bbsrc biotechnology and biological sciences research council

THE ROYAL SOCIETY

CARDIFF UNIVERSITY
PRIFYSGOL CAERDYDD

PhD positions available

Biophotonics and Quantum Optoelectronics Group
School of Physics and Astronomy and School of Biosciences
Cardiff, Wales UK
http://langsrv.astro.cf.ac.uk/

PhD positions are available starting from September 2007 on the following subjects:
Coherent Antistokes Raman Scattering microscopy for non-invasive imaging of living cells
Coherent light-matter interaction in semiconductor quantum dots using transient nonlinear spectroscopy

Fully-funded studentships are available for UK/EU candidates.

To apply and for further information please contact:
Dr. Wolfgang Langbein: LangbeinWW@Cardiff.ac.uk
Dr. Paola Borri: BorriP@Cardiff.ac.uk